Phenomenology of Diffractive Higgs Production and Large Extra Dimensions

Malin Sjödahl

Department of Theoretical Physics
Lund University, Sweden

Thesis for the degree of Doctor of Philosophy

Thesis Advisor: Leif Lönnblad

Faculty Opponent: Peter Richardson

To be presented, with the permission of the Faculty of Natural Sciences of Lund University, for public criticism in Lecture Hall F of the Department of Theoretical Physics on Friday, Sep 29th, 2006, at 10.15 a.m.

Organization **LUND UNIVERSITY** Department of Theoretical Physics Sölvegatan 14 A 223 62 LUND	**Document Name** **DOCTORAL DISSERTATION** **Date of issue** August 2006 **CODEN:** ISBN 91-628-6915-9
Author(s) Malin Sjödahl	**Sponsoring organization**

Title and subtitle

Phenomenology of Diffractive Higgs Production and Large Extra Dimensions

Abstract

This thesis is based on phenomenological predictions for high energy particle collisions from two different theoretical models. The first two papers deal with uncertainties in exclusive reactions of type
proton + proton → proton + proton + Higgs.

The other four papers concern gravitational scattering and black hole production in the scenario of large extra dimensions.

Summary in Swedish

Denna avhandling baseras på fenomenologiska förutsägelser för högenergetiska partikelkollisioner från två olika teoretiska modeller. De två första artiklarna handlar om osäkerheter i exklusiva reaktioner av typen
proton + proton → proton + proton + Higgs.

De fyra andra artiklarna behandlar gravitationell spridning och produktion av svarta hål i modeller med stora extra dimensioner.

Key words

Diffractive, Higgs, large extra dimensions, ADD, black holes, gravitational scattering, LHC

Classification system and/or index terms (if any)

Supplementary bibliographical information | **Language** English

ISSN and key title | **ISBN** 91-628-6915-9

Recipient's notes | **Number of pages** 155 | **Price**

Security classification

Distribution by (name and address)
Malin Sjödahl, Dept. of Theoretical Physics
Sölvegatan 14 A, SE-223 62 LUND

This thesis is based on the following publications:

I L. Lönnblad and M. Sjödahl
Central Exclusive Scalar Luminosities from the Linked Dipole Chain Model Gluon Densities
Journal of High Energy Physics **02**, 042 (2004).

II L. Lönnblad and M. Sjödahl
Uncertainties on Central Exclusive Scalar Luminosities from the Unintegrated Gluon Distributions
Journal of High Energy Physics **05**, 038 (2005).

III L. Lönnblad, M. Sjödahl and T. Åkesson
QCD-Supression by Black Hole Production at the LHC
Journal of High Energy Physics **09**, 019 (2005).

IV M. Sjödahl
Gravitational Scattering in the ADD Model Revisited
Submitted to European Physical Journal C.

V G. Gustafson and M. Sjödahl
Gravitational Scattering in the ADD Model at High and Low Energies
Submitted to Journal of High Energy Physics.

VI L. Lönnblad and M. Sjödahl
Classical and Non-Classical ADD Phenomenology with High-$E_\perp$ Jet Observables at Collider Experiments
Submitted to Journal of High Energy Physics.

Contents

Introduction

Our universe is quite a complex and interesting place to live in. Consider for example a straw of grass. With the resolution of the human eye it does not look too exciting. Still, it is too complicated to be understood by present day science. It seems however, that inside the cells and molecules, in the atoms, the description becomes simple again – in principle. This is the electromagnetic domain, habitated by electrons and atomic nuclei. Almost anything going on here can be described in terms of some relatively short equations,

$$\partial_\mu F^{\mu\nu} = ej^\nu. \tag{1}$$

(The notation here is illusive, this is actually four equations since ν has four different values.) The only problem is that we cannot really solve them, it requires too much work. Zooming in inside the nucleus, the simple equations are no longer enough, another force has entered the stage. It is called the strong force, or the color force, or QCD. Never mind what it is called. What is important is that it is more complicated than electromagnetism, it is stronger, and it keeps nuclei and their constituents, the protons and neutrons, together. These entities are themselves not fundamental, they consist of still smaller objects called quarks, but the quarks are – as far as is known – elementary and contain no smaller parts. This is also the case for the electron.

In fact, at distances which are roughly 1/100 of the proton size, the electromagnetic force seems to change nature, become more complex and similar to the strong force, it transforms into the electroweak force. But this is not particularly important for the straw of grass. Neither does it matter that the quarks and the electrons have heavier cousin particles. Nature, for some reason, made (at least) three kinds of "electrons": one light (the ordinary), one heavier and one which outweights a proton. Similarly, the quarks have heavier cousins. As if this was not enough there are oppositely charged "electrons" and "quarks", the antiparticles. But none of these are major inhabitants of grass. There is also a set of three extremely light, and extremely weakly interacting, particles called the neutrinos. These are frequent visitors not only of grass, but

also of our own bodies, but, since they fly through the universe almost without interacting, we do not notice.

These are all the particles that have been discovered. As for the forces we have the strong force, the short distance version of the electromagnetic force called electroweak force (alternatively described as the "weak" and the electromagnetic forces), and last, and often least, the gravitational force.

All in all there are thus a few players on the stage; but imagine, from expressions not much more complicated than eq. (1), grass, with all its complexity, seems to grow. To a non-physicist the equations may look horrible, but if they are to be read as the main recipe for grass and all other living things on earth, anyone must agree that it looks simple, very much more simple than a cell or a protein or even an atom. This is a triumph of science. There may be many steps in the growth of grass which are not understood, but it seems that fundamentally it all looks quite simple. Complexity grows from simplicity.

All pieces in the puzzle have, however, not been laid. Gravity is a troublesome piece, not easily fitted with the other pieces. Furthermore, for the fundamental particles, it is ridiculously weak. This may also seem a bit strange. The strong force, and the electroweak force are, despite their names, fairly equal in strength, the strong force is only something like 10 times stronger. For any two fundamental particles gravity is however many orders of magnitude weaker.

There are also problems with the electroweak model and particles having masses at all. For this fact to fit in, special treatment is needed. The standard solution is to introduce a new kind of field and an associated particle, named the Higgs boson, after one of it's inventors.

Further simplifying, and, if possible, making all pieces fit into one theory, is the goal of fundamental theoretical physics. But theories that have been constructed must make predictions and ultimately be confronted with experimental data. This is in itself a complex and tedious work and here phenomenological descriptions are important.

This thesis deals mainly with predicting observables for attempts to solve two different theoretical problems. The first papers (paper I and II) deal with a special way of detecting the Higgs boson. The other papers deal with predictions from the so called ADD model (after Arkani-Hamed, Dvali and Dimopoulos) which is an attempt to explain why the known particles interact so weakly gravitationally.

Whereas the papers and the specific paper introductions are necessarily written for physicists, the more general introduction is intended for a much wider audience. It does contain equations and special words, and to understand it completely a few years of physics university education is needed. I hope however, that interested readers without this background should get a taste of theoretical physics by simply skipping all the non-understood equations (this may well be all equations) and strange words.

Some Principles of Physics

It is a too little stressed fact that much of what is known in physics can actually be obtained from the simple concept of invariance. I would have liked to know this in high school.

The intuitively most obvious invariance is probably the translational invariance. Things work the same way if we move them to another place in space. Indeed it would be utterly surprising if the kitchen clock started to turn backwards just because it was moved to another kitchen wall!

But translational invariance in fact implies that momentum is conserved. This is not too hard to get a feeling for. Imagine that momentum was not conserved, such that cups of coffee could start flying around on the table as they pleased. As cups change speed only if a force is acting on them, this would mean that some force would push the coffee cups around. But then (in a sense to be strictly defined later) the force would break translational invariance. So, as there is translational invariance along the table surface, cups stand still. Cups of coffee do occasionally end up on the floor. This is because there is a force pulling them downwards since translational invariance *is* broken by the gravitational field we live in. Gravity on the surface of the earth does, however, only break translational invariance vertically, giving vertical forces and vertically falling coffee cups. It does not break translational invariance horizontally and cups do not fall horizontally.

The above argument is incomplete since it pre-assumes that things change speed when a force is acting them. This observation, originally due to Newton, can in fact be derived by instead postulating that objects follow trajectories which minimizes something called an *action*. The action is the time integral of an object called a Lagrangian, which for a particle of mass m at position x moving around with some velocity $\dot{x}$ in a potential $V(x)$ is given by

$$L = \frac{m\dot{x}^2}{2} - V(x). \tag{2}$$

Actions and Lagrangians are extremely important creatures in theoretical physics. It is, strictly speaking, the Lagrangian which should stay the same (be invariant) for physicists to say that there is translational invariance. The action for the above Lagrangian is

$$S = \int_{t_1}^{t_2} L dt = \int_{t_1}^{t_2} \left(\frac{m\dot{x}^2}{2} - V(x) \right) dt \tag{3}$$

and all non-relativistic and non-quantum mechanical things in the world move between any two times t_1 and t_2 in a way which minimizes the action. Since the action has the property that it changes only a little if the path taken changes only a little, the special paths, minimizing the action, are given by those paths

which do not change (to first approximation) the action when they are varied slightly. This turns out to give the equations

$$\frac{d}{dt}\frac{\partial L}{\partial \dot{x}} - \frac{\partial L}{\partial x} = 0. \tag{4}$$

As $L = m\dot{x}^2/2 - V(x)$ we have

$$\frac{d}{dt}m\dot{x} + \frac{\partial}{\partial x}V(x) = 0 \tag{5}$$

and since the force is precisely $-dV(x)/dx$ this is just Newton's second law, stating that the mass times the acceleration is the force.

So, we have seen that from minimizing a combination of kinetic ($m\dot{x}^2/2$) and potential ($V(x)$) energy called action we can find the trajectories that particles follow, or, alternatively formulated, we have derive Newton's second law.

Now we can also see from eq. (5) that when the action is translationally invariant, such that it does not depend on position, momentum is conserved (since then $\partial V(x)/\partial x = 0$).

If x is the height of a falling cup of coffee, $\partial L/\partial x = \partial V/\partial x$ is however not 0, so the momentum is changed, but if x describes the position on the table surface $\partial L/\partial x$ is 0, so the cup is not moving around on the table surface.

The implication of momentum conservation from translational invariance is only one example of a general principle called Noether's theorem, which states that for each symmetry the Lagrangian has, there is a corresponding conserved quantity. Time invariance (that things function the same today as yesterday) turns out to imply energy conservation. If a system is rotationally invariant, then angular momentum is conserved.

There are also other "non-spatial" – or internal – invariances. Electric charge conservation (that no net electric charges can be created from uncharged material) can be thought of as arising from a kind of "rotational" or *phase* invariance in a space which has nothing to do with our ordinary dimensions. The strong color force also comes with conserved quantities associated with (more complex) internal rotational-like invariances.

Even the unification of the electromagnetic and the weak force is thought of in terms of invariances, which in this case, are broken in a special way. This special breaking, called *spontaneous symmetry breaking* is the cause of the Higgs boson and will be discussed in the next section, since the first papers in this thesis deals with a special way of detecting it. Gravity however, is not associated with internal invariances but with invariances in space-time itself. In this respect it differs from all the other known forces.

To understand anything about the fundamental forces it is necessary to also introduce the concept of a *field*. A field is something which exists in space with different values in different points, like the gravitational field which is weaker on

the moon surface than on the earth surface. As a field exists in many points it can have contributions to the Lagrangian from the whole space. Furthermore, fields are often relativistic, meaning that the simple time derivative squared $\dot{x}^2$, has to be replaced by a more complicated combination of derivatives

$$\dot{\phi}^2 = \left(\frac{\partial\phi}{\partial t}\right)^2 \to \left(\frac{\partial\phi}{\partial t}\right)^2 - \left(\frac{\partial\phi}{\partial x}\right)^2 \equiv (\partial^\mu\phi\partial_\mu\phi). \tag{6}$$

The combination $(\partial^\mu\phi\partial_\mu\phi)$ means $(\partial\phi/\partial t)^2 - (\partial\phi/\partial x)^2$, this is just a way of writing. The reason for the replacement is that the Lagrangian has to be relativistically invariant, again illustrating the importance of invariances. In fact Einstein preferred the name "theory of invariance" rather than "theory of relativity". For a simple field ϕ with just one value in each point (fields in nature often have many values in each point) and a mass m, we then have the Lagrangian

$$L = \int \left(\frac{1}{2}(\partial^\mu\phi\partial_\mu\phi - m^2\phi^2) - V\right) dx. \tag{7}$$

For the electroweak and the color fields, there are additional complications since the internal (non-spatial) degrees of freedom must be taken into account as will be seen in the following section.

To postulate that things should move along paths which minimizes the action may seem like a fairly simple but arbitrary assumption. But, it turns out that this can actually be obtained as a special case of the more fundamental quantum mechanics. Quantum mechanics is much like wave mechanics (apart from the troublesome and confusing issue of measurements) and waves, such as on a sea, are present everywhere, sometimes bulging upwards and sometimes downwards. Quantum mechanics is very exciting because you never know what will happen! The only thing that can be calculated is the probability with which something will happen. This probability turns out to be something like the height of the wave (the amplitude) squared. A quantum mechanical electron takes all paths through space. The probability for a particle to go from a place x_1 to a place x_2 in the time $t_2 - t_1$ is something like

$$\left|\int_{\text{paths}} e^{iS(\text{path})}\right|^2. \tag{8}$$

The notation here is somewhat unusual, what is meant is that $e^{iS(\text{path})}$ should be computed for each path, starting in (t_1, x_1) and ending in (t_2, x_2), and the results should be summed (each point in space is therefore summed over many times as it is passed by many paths). For most choices of space-time points (t_1, x_1) and (t_2, x_2) the contribution from different paths will cancel since their contributions have different phases. If the action S is very large,

such that the phase in the exponent is rapidly oscillating, this cancellation will typically be even worse. There are, however, some paths through space with the property that if you vary them slightly, the action S(path) does not change to first approximation. If the action is large these will be the important paths. But these are just the classical paths! We have just found, by assuming that quantum mechanical particles take *all* paths, that when the action is large, particles do indeed follow paths which minimize (actually extremize) the action, what we postulated before. So, what happens is that "everything happens", all paths are taken, and in the special case of large non-relativistic objects, this gives Newton's second law.

If nature takes all paths, does it also obey all possible invariances? Here the answer is no. There is, for example, no such thing as size invariance. If the chestnut trees outside my window grew twice as large, the branches would have 4 times as large cross sections, and be something like be 4 times as strong, but they would be 8 times as heavy. These would be fragile trees. Looking at the equation eq. (2) we also see that the first terms does in itself break size invariance (since it does change if make all distances twice as large).

If the potential $V(r)$ is a gravitational potential

$$V(r) = -G_N \frac{m_1 m_2}{r} \tag{9}$$

this terms would also break size invariance in the Lagrangian. Rescaling space would give 8 times as heavy masses, giving a factor 64 for both masses. This would only be compensated by a factor 2 from doubling r. From this we conclude that if the diameter of the earth was twice as large the trees would probably not be twice as large as well. It is more likely that they would be a half as large!

It is often claimed that gravity is an extremely weak force. This statement is unfortunate, since the mass at which gravity should be compared to the other forces, has to be specified in order for the statement to be meaningful, as gravity gets stronger with increasing mass. Gravity is certainly not weak for earthly trees (compared to other forces acting on typical earthly trees), but it is weak for two electrons interacting with each other (compared to the electro-magnetic force).

In a sense gravity is actually about as strong as the other forces. This is because a special mass, at which the gravitational strength could be measured, does exist. This is the mass for which the corresponding black hole radius r_{Sch} equals the quantum mechanical uncertainty in position, $r_{Sch} = \Delta x$. (In quantum mechanics the place where a particle occurs can not be predicted, but one can say that it is likely that the particle appears within the length interval Δx.) For this special mass (which obviously does not depend on the electromagnetic force) the gravitational force is about as strong as the electromagnetic force, or the strong force. In physics language, this is because $\alpha_{\text{em}} \sim \alpha_{\text{strong}} \sim 1$.

A better formulation of the weakness of gravity is to say that the fundamental particles are extremely light compared to the mass at which gravity becomes as strong as the other forces. In this sense gravity is extremely weak, and this is known as (a version of) the *hierarchy problem* as it seems so unnatural. (Having very light particles is not forbidden in any sense, it just seems strange that the particle masses are such that fundamental particles interact much less gravitationally than via the other known forces.) The ADD model, to be discussed later, is an attempt to solve this problem, and the papers (III-VI) in this thesis deal with various observational effects of the ADD model.

The Higgs Mechanism

In the previous section the role played by symmetries, or invariances, in physics was stressed. It was mentioned than there are non-spatial, or internal, symmetries which are essential for the fundamental forces (except gravity). These are symmetries in the particles or fields themselves. Imagine a completely round white ball, it looks the same regardless of how it is rotated. If we paint a round red dot on it this is no longer true. Now, when the ball is rotated the red dot will (typically) move around, such that the rotational invariance is broken, see fig. 1. It is, however, possible to rotate the ball in such a way that the red dot is kept still, so the rotational invariance is not completely gone, only mostly. To be more specific, without the dot, it is possible to rotate the ball around three completely different axes, but with the dot, the ball only looks the same while rotated around the axis which goes through the red dot, and the center of the ball.

These rotational invariances are properties of the ball itself, and not of the space in which it lives. Of course a ball has a spatial extension, and here the analogy is incomplete. For the fundamental particles the internal symmetries live in completely different spaces which have nothing to do with

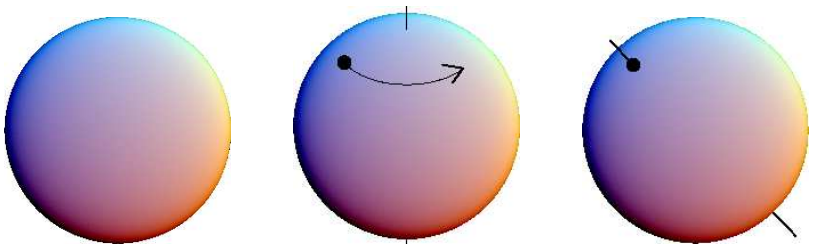

Figure 1: Without a dot the rotational symmetry is perfect, but with the dot only one rotational invariance remains.

our 3-dimensional space.

The strong force lives in a space in which eight (completely) different rotations can be made. This space has, in a sense, more than three dimensions, and is complex (in literate and pictorial meaning). To be precise, it is an SU(3)-space. The strong force "has no red dots" meaning that all rotational symmetries are perfect, there is no special direction. If the fields in the Lagrangian of the strong force are rotated, the Lagrangian does not change, and the equations governing the motion, corresponding to equation eq. (5), do not change either.

For the combination of the electromagnetic and the weak force, the electroweak force, the situation is more complex. Here the internal space is a combination of a space in which only one rotation can be made (a U(1)-space), and a space in which three different rotations can be made (an SU(2)-space). For a field ϕ, living in this space, its rotated version can be written

$$e^{i\alpha^a \tau^a} e^{i\beta/2}\phi \tag{10}$$

where the first exponent performs the rotation in the SU(2)-space, and the second generates the simpler U(1) rotation. The field ϕ is really a 2-component complex field (it has $2 * 2$ values in each point) and the τ:s (there are three of them corresponding to three different rotations) are really 2×2 complex matrices. A factor $1 + i\epsilon\tau$ (for a small ϵ) "multiplied" with ϕ generates a small rotation of ϕ. When many infinitesimal rotations are put together, the expression turn into an exponent and it results in a finite "large" rotation.

Since the Lagrangian is supposed to be unchanged by all of these rotations, it must, in particular, be unchanged by every infinitesimally small rotation. Furthermore, the rotations in the internal $(SU(2) \times U(1))$ space can differ from point to point in ordinary space, or be *local*. In order to ensure that the Lagrangian stays constant under local transformation the derivative ∂_μ has to be replaced,

$$\partial_\mu \to D_\mu = \partial_\mu - igA^a_\mu \tau^a - \frac{i}{2} g' B_\mu, \tag{11}$$

by the *covariant* derivative D_μ. Here the τ:s are again the generators of rotation in $SU(2)$-space, the A:s and the B are combinations of physical fields and the constants g and g' are coupling constants.

With this replacement the variation under rotation in $\partial_\mu\phi$ is compensated for by the variation in the A:s and the B such that the Lagrangian density containing the pieces

$$\frac{1}{2}(D_\mu\phi)^\dagger(D^\mu\phi) + \mu^2\phi^\dagger\phi - \lambda(\phi^\dagger\phi)^2, \tag{12}$$

stays invariant. In this Lagrangian density, the first terms $(D_\mu\phi)^\dagger(D^\mu\phi)$ is just the replacement of $\partial^\mu\phi\partial_\mu\phi$ in eq. (7) and is fixed as soon as the invariances

are chosen, whereas the other terms, $\mu^2\phi^\dagger\phi - \lambda(\phi^\dagger\phi)^2$, correspond to the potential $V(x)$. The choice $V(x) = -\mu^2\phi^\dagger\phi + \lambda(\phi^\dagger\phi)^2$ may seem arbitrary, but for believers in renormalizable quantum field theory it is completely general. Comparing eq. (12) to eq. (7), it is tempting to interpret the constant μ^2 in front of the (field)^2-term as a (mass)^2, but it comes with the wrong sign (if $\mu^2 > 0$), this would correspond to a negative mass squared.

As opposed to the $(SU(3))$ symmetry of the strong force, the $(U(1)\times SU(2))$ symmetry of the electroweak force is broken. It is broken by the field ϕ which tries to minimize the potential $V(x) = -\mu^2\phi^\dagger\phi+\lambda(\phi^\dagger\phi)^2$ in eq. (12) (much like a ball rolling down a slope minimizes the gravitational potential). To understand this, consider the potential as a function of ϕ. ϕ has $2*2$ components, $\phi = (\phi_1 + i\phi_2, \phi_3 + i\phi_4)$, and in terms of these four components the potential can be written

$$-\mu^2(\phi_1^2 + \phi_2^2 + \phi_3^2 + \phi_4^2) + \lambda(\phi_1^2 + \phi_2^2 + \phi_3^2 + \phi_4^2)^2. \tag{13}$$

If all ϕ:s except ϕ_3 are 0 and $\lambda > 0$, the potential, as a function of ϕ_3 has the shape shown in fig. 2.

This means that (if all other fields are 0) there are two minimal values of the potential as a function of ϕ_3. The other ϕ:s enter the potential in the same way, and the total potential only depends on the length of ϕ. Viewed in the $(\phi_1, \phi_2, \phi_3, \phi_4)$-space, the potential is therefore minimal at a certain length $v = \sqrt{\mu^2/(2\lambda)}$ of ϕ. As things, and fields, tend to stay at the places with lowest potential (since they are pulled there), ϕ will have approximately this absolute value. But there are many possible ϕ:s with the same length, as ϕ can point in many directions. Which direction should nature choose? Well, no direction is better than any other, so it just has to choose one spontaneously, hence *spontaneous symmetry breaking*.

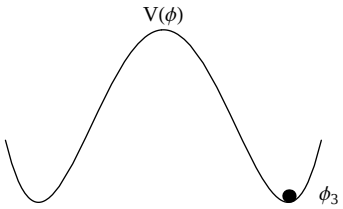

Figure 2: The potential as a function of ϕ_3. Nature spontaneously have to choose one of the ϕ:s which minimizes the potential.

This spontaneous choice of direction is much like the spontaneous choice of magnetization direction in a piece of iron. Initially no direction is special, but by accident a few more atoms start pointing in one direction, and then it is favorable for the other atoms choose this direction as well. The symmetry is spontaneously broken and the piece of iron turns into a magnet.

So, nature accidentally chooses a direction. This can be $\phi_1 = v$, $\phi_2 = v$, $\phi_3 = v$, $\phi_4 = v$, or any combination of ϕ_1, ϕ_2, ϕ_3 and ϕ_4 which satisfy $|\phi| = v$. Let us consider $\phi_3 = v$.

It is now straightforward to take the expression eq. (11) and plug it in in

eq. (12) using $\phi = (0, v)$. From the $(D_\mu\phi)^\dagger(D^\mu\phi)$ term we have the piece

$$\frac{1}{2}(0,v)\left(gA^a_\mu\tau^a + \frac{1}{2}g'B_\mu\right)\left(gA^{b\mu}\tau^b + \frac{1}{2}g'B^\mu\right)\begin{pmatrix}0\\v\end{pmatrix} \tag{14}$$

from the extra terms in the covariant derivative. If we use the standard representation of the generators ($\tau^i = \sigma^i/2$ where σ^i are the Pauli matrices) some matrix calculations turn this into

$$\frac{1}{2}\frac{v^2}{4}\left(g^2A^1_\mu A^{1\mu} + g^2A^2_\mu A^{2\mu} + (-gA^3_\mu + g'B_\mu)(-gA^{3\mu} + g'B^\mu)\right). \tag{15}$$

Using the definitions

$$W^\pm_\mu \equiv \frac{1}{\sqrt{2}}(A^1_\mu \mp iA^2_\mu), \qquad Z^0_\mu \equiv \frac{1}{\sqrt{g^2+g'^2}}(gA^3_\mu - g'B_\mu) \tag{16}$$

it can also be expressed

$$\frac{1}{2}\frac{v^2}{4}\left(g^2|W^+|^2 + g^2|W^-|^2 + (g^2+g'^2)|Z^0|^2\right). \tag{17}$$

If we interpret $W^\pm$ and Z^0 as physical fields, we see, by comparing to eq. (7), that (field)^2-terms, $|W^+|^2$, $|W^-|^2$ and $|Z^0|^2$, are just mass terms (and the spatial components have a positive (mass)^2 as desired), so, there seems to be three physical massive fields, W^+, W^- and Z^0. But we started out with four fields (three A:s and one B), there should be one more. There is, but this field,

$$A_\mu \equiv \frac{1}{\sqrt{g^2+g'^2}}(g'A^3_\mu + gB_\mu) \tag{18}$$

has no mass. It is interpreted as the photon (light) field. The massive $W^\pm$ and Z_0 are "interaction fields" much like the photon, but since they are heavy (as 100 protons roughly), much energy is needed to produce them and they were not discovered until 1983. As seen from the constants in front of $|W^\pm|^2$ and $|Z^0|^2$ in eq. (17) the masses of W^+ and W^- differ from the mass of Z^0 in a way which depends on the coupling constants g and g'. This means that once these constants are determined, the mass ratio between $W^\pm$ and Z^0 is a prediction of the theory. This prediction has been tested to about 1% accuracy, and it agrees well with experiments. This way of giving masses to $W^\pm$ and Z^0 is called the Higgs mechanism.

So far large parts of the presentation of the Higgs mechanism has been way above the head of several of my imagined readers. But the mechanism can partially be quite well understood pictorially as well.

The ϕ-field has four different values (components), and can be imagined in a four dimensional space. It is hard to imagine a four-dimensional space, and

hard to try to draw it on a two dimensional paper, so instead imagine a two dimensional space. In fig. 3 two of the components of ϕ are therefore shown, and the potential as a function of them.

The favorable ϕ:s are the ϕ:s in the valley, but there are many combinations of ϕ_3 and ϕ_2 which lie in the valley. Nature can not choose all ϕ:s in the valley, but spontaneously chooses one, in this case ϕ_3. ϕ_3 is the "ground state" of nature, corresponding the magnetization direction in a magnetic piece of iron. There are however small fluctuations around the ground state. If the field is "sitting" in the point $\phi_3 = v$, $\phi_2 = 0$, and changes slightly by "walking up hill" it would cost energy, so this *excitation* is associated with a massive field, it is in fact associated with the famous Higgs boson. Similarly, "walking" in the ϕ_2 direction, along the minimum, does not cost energy, so it is tempting to think of this as corresponding to a massless excitation. Before the symmetry breaking, there where four different rotational directions (one B and three A:s). With the choice $\phi = \phi_3$, three rotational invariances are gone, the only rotational symmetry being left is rotation around the ϕ_3-axis. Each destroyed invariance gives a massless excitation. (This is a famous theorem, the Goldstone theorem.) But in this case the massless excitation is (for reasons which I can not explain pictorially) associated with the $W^{\pm}$ and Z^0 masses rather than fields in themselves.

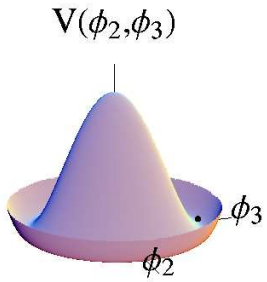

Figure 3: The potential as a function of ϕ_3 and ϕ_2.

The essence of this section, is that due to the spontaneously chosen non-zero value of ϕ, the $W^{\pm}$ and Z^0 bosons have acquired masses. Other particles (the fermions, e.g. the electors and quarks) also obtain their masses via interaction with the field ϕ, but in this case via the excitement of ϕ, the Higgs boson.

The ADD Model

The ADD model, invented in 1998 by Arkani-Hamed, Dvali and Dimopoulos, is an attempt to explain why the particle masses are so low compared to the mass at which gravity becomes comparable in strength to the other forces. This is done by assuming extra, curled up, dimensions in which only gravity is allowed to propagate. The other forces and all particles are restricted to live on a thin 3+1 dimensional surface, called *brane*, in the total 3 (ordinary spatial)+1 (time)+n (extra)-dimensional space.

For the gravitational field, moving freely in all dimensions, the world will,

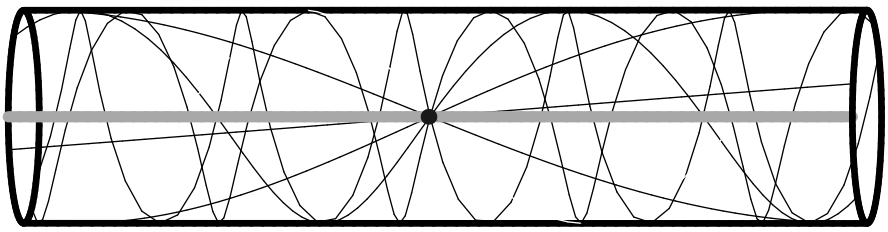

Figure 4: In the ADD scenario, our ordinary world is just a thin surface (brane) in a $3+n$ dimensional world. In this figure, the case of 1 compactified and 1 ordinary extended dimension is shown. The brane where the standard model fields, and hence we, live, is represented by the gray line. At short distances the gravitational field will behave 3+1 dimensionally, (1+1 dimensionally in the picture). At distances large compared to the compactification radius, the only effect of the extra dimensions will, however, be a weaker gravitational field, as the field lines are spread into the extra dimensions.

at distances small compared to the compactification radius R, seem to be $3+n$-dimensional, as the gravitational field has $3+n$ space dimensions to spread in. At large distances, much larger than the compactification radius, the curled up dimensions will, however, not be noticed, apart from the fact that the gravitational field is weakened by spreading into the extra dimensions, and the world will appear to only have 3 spatial dimensions. It is this weakening of the gravitational field which is thought to explain the weakness of gravity. The more extra dimensions there are, the more spread and weaker is the gravitational field.

This can actually be expressed fairly easily in formulae as well by rewriting the gravitational coupling constant G_N (the constant in eq. (9)) as $G_N = 1/M_{P(4)}^2$. Here the units are chosen such that the speed of light and the natural constant $\hbar$ both are 1. $M_{P(4)}^2$ is then (roughly) the mass at which gravity becomes as strong as the other forces, referred to as the *Planck* mass. The 4 in $M_{P(4)}$ is there just to denote that this is the Planck mass as perceived from $3+1$ dimensions. As we soon will see, there is another mass with the same role in the $3+1+n$-dimensional space. Now, in terms of $M_{P(4)}$ the gravitational law eq. (9) can (in natural units) be rewritten as

$$V(r) = -\frac{1}{M_{P(4)}^2}\frac{m_1 m_2}{r}, \qquad r \gg R. \tag{19}$$

For sufficiently short distances the gravitational law will however behave $3+n$-dimensionally and have the form

$$V(r) = -\frac{1}{M_P^{2+n}} \frac{m_1 m_2}{r^{n+1}}, \qquad r \ll R \tag{20}$$

for some *fundamental* $(3+n$-dimensional) Planck mass M_P. When gravity has expanded into the full volume of the extra dimensions this extrapolates to

$$V(r) \approx -\frac{1}{M_{P(4)}^{2+n} R^n} \frac{m_1 m_2}{r^1} \tag{21}$$

giving the relation

$$M_{P(4)}^2 \approx M_P^{2+n} R^n, \tag{22}$$

as seen by comparing eq. (21) to eq. (19). From this we conclude that, by having a large compactification radius R, we can have a large observed Planck mass $M_{P(4)}$, even though the fundamental Planck scale M_P is small, presumably comparable to the heavier fundamental particles. We also see quantitatively that the more extra dimensions we have, the smaller needs R to be, in order to obtain the same low fundamental Planck scale M_P.

If this is the explanation of the seemingly light particle masses then gravity will change behavior, and faster turn stronger with decreasing distance for distances small compared to R. This should in principle be possible to measure directly in gravitational experiments. Experiments have also been performed leading to various restrictions of the fundamental Planck scale M_P for various numbers of extra dimensions. Due to the difficulties of measuring gravity at extremely small distances there are however better ways of trying to verify/exclude the ADD scenario. In particular the Large Hadron Collider (LHC), presently under construction at CERN on the Swiss-French border close to Geneva, will supply the possibility of measuring gravitational scattering and even black holes, provided the fundamental Planck mass really is of the same order of magnitude as the heaviest particle masses.

About the black holes possibly created at LHC, it should immediately be said that these decay extremely rapidly via Hawking evaporation, in 10^{-27} seconds or so, and are no threatening, all-swallowing, vacuum cleaners. Actually, all black holes decay. It is just that it takes extremely long time, longer that the lifetime of the universe, for star-remnant black holes to decay. As the typical emitted quanta of a black hole has a wavelength of roughly the black hole radius, and the energy is inversely proportional to the wavelength, stellar-mass black holes emit only low energy quanta and are extremely cold.

Mini black holes, such as the imagined collider black holes, are instead extremely hot, and because of this, they loose energy and disappear quickly. Their extreme temperatures also make it possible for them to radiate massive particles: electrons, W:s and so on. It is this radiation, and not the black holes themselves, which possibly will be detected at LHC.

The Papers

This thesis is based on work on two fairly different topics. The first two papers concern exclusive diffractive production of the Higgs boson, more specifically, how the cross section is affected by uncertainties in the parton distribution functions. Necessary background information is presented in the following section at a level intended for a physicist with basic knowledge of field theory and QCD.

The other papers deal with various phenomenological consequences of the ADD [1] scenario. Two of the papers (IV and V) aim at a better theoretical understanding of gravitational scattering in the ADD model, whereas the other papers (III and VI) are simulations of what could be seen at colliders such as the LHC, provided the ADD model is correct. Also here the paper introductions are intended for a physicist.

Paper I and II

LHC will be a proton-proton collider, but Feynman diagrams describing production of, for example the Higgs boson, are written in terms of amplitudes involving quarks. Each proton consist, not only of three quantum-number-carrying valence quarks, but also of a sea of virtual $q\bar{q}$-pairs and gluons. These quarks and gluons also contribute to various cross sections when two protons collide.

Because of this it is necessary to introduce parton densities describing the probability to find a certain quark or gluon, *parton*, in the proton. To a first approximation the density of a particular parton depends only on its momentum fraction, x, of the total proton momentum. It does not depend on the momentum transfer scale, Q^2. In other words, to a first approximation, the proton looks the same regardless of how hard it is smashed. This is known as Bjorken scaling. To a second approximation this is no longer true, the probability of finding a certain quark or gluon depends on the momentum transfer Q^2.

While the approximate, Q^2-independent, parton distribution functions can not be found from first principles, as they depend on non-perturbative low energy QCD, the variation with Q^2 can (in some phase space regions) be predicted from QCD. This was first done in the limit of large Q^2 by Dokshitzer, Gribov, Lipatov, Altarelli and Parisi and is therefore known as the DGLAP equation [2–5]. It is based on the fact that due to the phase space available for emission, emissions ordered in transverse momenta, $k_\perp$, dominate.

This means that the emitted partons in fig. 5 have increasing $k_\perp^2$ closer to the hard interaction with momentum exchange Q^2. This makes it possible to write down an equation describing how the parton densities change with Q^2.

What is found is a weak logarithmic evolution with Q^2, in rough agreement with Bjorken scaling. As all color-charged particles are confined in hadrons, the fact that the Q^2 evolution of measured parton densities could be described by this equation, was actually an important piece of evidence for QCD.

Another phase space region, where a momentum transfer evolution equation can be written down, is the region of small momentum fraction and infinite collision energy. Here the emitted partons are instead strongly ordered in momentum fraction x. This is the domain of the BFKL equation (Balitsky, Fadin, Kuraev and Lipatov) [6].

It is possible to interpolate between the DGLAP and the BFKL-equation, and this is done by the CCFM-equation (Ciafaloni, Catani, Fiorani and Marchesini) [7, 8].

The papers I and II are however mainly based on parton densities from the Linked Dipole Chain (LDC) model [9], which is a Monte Carlo implementable reformulation and generalization of the CCFM-equation.

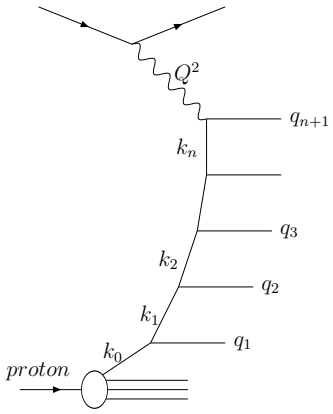

Figure 5: A diagram illustrating the parton density evolution.

For exclusive Higgs Production the situation is still more complicated. The incoming state is pp (for LHC) and the outgoing state is $p + H + p$, *only*. This is very untypical, most often when protons collide at LHC-energies ($\sim$14 TeV) they will break into hundreds of particles since the strong color force will tear them apart once one parton has interacted. In order to prevent this from happening, it must be ensured that the total parton exchange between the two protons is colorless.

The Feynman diagram under consideration is shown in fig. 6. Two gluons fuse via the heavy quark triangle sub-diagram into a Higgs boson. As we are interested in processes when, apart from the Higgs, there are only two protons in the outgoing state, another gluon must be exchanged in order to assure no net color flow. (The protons must be color singlets also after the interaction.)

In order for the protons not to break by the momentum recoil, the transverse momentum transfer must also be small, as indicated in the figure by the $k_\perp$ going around in a loop. Several types of interaction could spoil the diffractive nature of this process. Firstly, the spectator partons could undergo additional scattering reducing the probability for a diffractive event. Also, the gluons participating in the interaction can radiate, both at energies below the loop momentum $|k_\perp|$ and at energies above it. Radiation with transverse momentum below $|k_\perp|$ is, however, suppressed since such radiation would not resolve the individual exchanged gluons, but would instead only "see" a color singlet.

Radiation with transverse momentum between the momentum scale $|k_\perp|$ and the hard scale $\sqrt{Q^2} \sim M_{Higgs}$ is, on the other hand, a significant threat. This is taken into account by a non-emission probability factor, or *Sudakov* form-factor, which is the probability that no radiation is emitted between the scales $|k_\perp|$ and $\sqrt{Q}$. The probability to emit radiation above M_{Higgs} is again suppressed, since this radiation would violate the DGLAP evolution, expected to be valid here.

What is needed is therefore not the gluon distribution function $f_g(x, Q^2)$ in itself, but the *unintegrated off-diagonal* gluon distribution function $f_g(x, x', k_\perp^2, Q^2 \approx M_{Higgs}^2)$. This is said to be unintegrated since it depends on two momentum scale $k_\perp^2$ and M_{Higgs}^2. (The lower momentum scale $k_\perp^2$ is *not* integrated out.) Off-diagonal here means that the momentum fractions x and x' need not be the same.

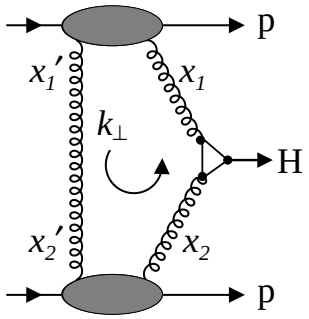

Figure 6: The basic diagram for exclusive production of the Higgs boson.

As the reader may understand, a process like this comes with large uncertainties, both from the various theoretical approximations, and from experimental lack of precision in the, four-argument, unintegrated, off-diagonal parton distribution functions. These uncertainties are the topics of paper I and II. In particular it turns out that the uncertainty in the gluon distribution associated with the typical lower momentum scale $k_\perp^2$ is large.

Paper III

As earlier mentioned black holes could be produced at the LHC if the ADD model is a correct description of our universe. For the most natural fundamental Planck masses ($M_{P(4)} \sim 1$TeV, removing the hierarchy rather than just reducing it) black holes will be copiously produced at the LHC. Their decay products, all the standard model particles, will be spread in the detectors and measured.

There is however a completely new phenomena implied by black hole production, namely the absence of standard model (in particular QCD) scattering. If two partons come inside their common Schwarzschild radius, this (is believed to) cause the partons to form a black hole. But, this also means that the partons, which otherwise would have undergone a (e.g.) QCD scattering are trapped in the black hole and do not contribute to the QCD cross section. This disappearance of QCD cross section is the topic of paper III.

Since short distance scattering corresponds to high $p_\perp$ scattering it is the high transverse momentum events which are to be turned into black hole events, and consequently the high transverse momentum events which are expected to be missing.

This would be a rather spectacular signal. No standard beyond standard model interaction is expected to "eat" cross section. (There could occasionally be negative interference, but generally the cross section is expected to increase if other interactions, such as supersymmetry, are turned on.)

The problem is that, to see this drop in cross section, one has to search in the background radiation emitted from black holes, and this turns out to be a rather overwhelming background.

Paper IV and V

If gravity can trap partons in black holes, then it should surely be strong enough to scatter them as well. In the ADD scenario, gravitational scattering events can therefore be expected at the LHC. But how will this gravitational scattering behave?

Considering the fact that semi-classical black hole decays are simulated, and that direct gravitational measurements has been a way of excluding large enough extra dimensions, I expected the gravitational scattering to resemble classical scattering in the $1/r^{n+1}$ potential from eq. (20). What I found in the papers investigating gravitational scattering was instead a contact like interaction, having a fairly even angular distributions and not appearing classically at all.

This scattering behavior is derived from the field theory obtained by linearizing the metric and deriving the Feynman rules [10, 11]. The extra dimensional metric perturbations, the Kaluza–Klein (KK) modes, can then occur as internal, as well as external, lines in the Feynman diagrams. As translational invariance is broken in these dimensions by the brane we live on, momentum in the extra dimensions is not conserved. Internal KK modes can therefore occur with all allowed momenta $m_{\bar{l}}$, and this leads to the divergent propagator integral

$$\sum_{\bar{l}} \frac{1}{-m_{\bar{l}}^2 + k^2} \sim R^n \int \frac{m^{n-1}}{-m^2 + k^2} dm \tag{23}$$

where $m = |m_{\bar{l}}|$ and the factor R comes from the density of KK modes. But, we can not have infinite amplitudes and cross sections and the authors of the original papers, where the Feynman rules where derived, imposed a cut-off for this integral without careful physical motivation.

But does momentum non-conservation really imply that we shall sum over all momenta? If the standard model fields lived on an *infinitely thin* brane, this does correspond to a flat distribution in momentum space (the Fourier

transform of a δ-function is a constant), but on the other hand, the summation of KK modes has been performed in [12] *after* Fourier transforming from k-space to r-space in our ordinary coordinates. The result of the integrals, when evaluated in this order, is the expected $1/r^{n+1}$ potential.

In paper IV, I argue that the fact that the standard model particles live on a finite brane leads to the expected $1/r^{n+1}$ potential at distances small compared to the compactification radius but large compared to the brane width.

The conclusion that the authors of the initial Feynman diagram papers have missed the importance of keeping the particles on the brane seems unavoidable to me. In fact, the terms which are important for classical scattering, "infrared terms", are referred to in [11] with the sentence: "The infrared contributions could be experimentally isolated only if the coefficients c_k turns out to be small (because of some "miraculous" cancellation of divergences in the fundamental theory)..."

This statement is simply false, and a few years later the same authors recovered classical gravitational scattering [13] (from the "infrared contributions") using the method of eikonalization. There was, however, still no remark on a finite brane size. Instead the troublesome terms (infinities) where subtracted using dimensional regularization and argued to consistently disappear in the eikonal procedure.

I do find it very surprising that it seems as if the condition that the standard model particles live on a brane, implemented via a Fourier transform, is not present in the literature, or at least, is not well spread. However, I have seen no signs of it, and I therefore include paper IV in this thesis.

While the result in [13] is sensible, and for large enough energies gives back classical scattering, the method used contains several questionable steps due to infinite amplitudes. By keeping a finite brane width throughout the calculations several unresolved questions in [13] are clarified in paper V, an the infinite integrals from [13] turns finite and calculable. The physical scattering picture obtained in the end, is actually a contact-like interaction at energies small compared to the inverse brane width. At large enough energies the classical scattering behavior is recovered.

Paper VI

In this paper the overall collider phenomenological picture emerged in paper V is investigated. This is done using event simulations, and we vary the relative sizes of the fundamental Planck scale and the inverse brane width. In particular, we argue that a finite brane thickness may prevent black holes from being formed as they may not be localized well enough in the extra dimensions. If this is the case, then the only indication of the ADD scenario at the LHC could be an increase in the number of energetic jets and the presence of missing

transverse momenta due to on shell (undetectable) KK-production. We focus on the first observable.

The consequences of the fact that gravity is colorless are also investigated. This is in contrast to QCD and also to main contributions to cross sections in most popular scenarios beyond the standard model. As QCD is a confining force, this has implications for the number of particles between the jets and could thus be used to discriminate between gravitational scattering (and other colorless scatterings) and colorful (standard model, or beyond) scattering.

Acknowledgments

I would like to express my gratitude towards Leif Lönnblad for constantly finding time form my supervision. I am also thankful to Gösta Gustafson for generous support, especially during the last stressful months of my thesis writing.

During this four years many of the most interesting discussing have however been with my boyfriend Johan Grönqvist who, despite bad health and own stress, offered much support, physicswise and otherwise.

Finally, I like the thank the most fundamental forces of nature for, in spite of their relative simplicity, giving rise to such a complex and interesting world.

References

[1] N. Arkani-Hamed, S. Dimopoulos, and G. R. Dvali *Phys. Lett.* **B429** (1998) 263–272, `hep-ph/9803315`.

[2] V.N. Gribov, L.N. Lipatov *Sov. J. Phys.* **15** (1972) 438 and 675.

[3] L.N. Lipatov *Sov. J. Phys.* **20** (1975) 94.

[4] G. Altarelli, G. Parisi *Nucl. Phys. B* **126** (1977) 298.

[5] Yu.L. Dokshitser *Sov. Phys. JETP* **46** (1977) 641.

[6] V.S. Fadin, E.A. Kuraev, L.N. Lipatov *Sov. Phys. JETP* **45** (1977) 199.

[7] M. Ciafaloni *Nucl. Phys.* **B296** (1988) 49.

[8] S. Catani, F. Fiorani, and G. Marchesini *Phys. Lett.* **B234** (1990) 339.

[9] B. Andersson, G. Gustafson, and J. Samuelsson *Nucl. Phys.* **B467** (1996) 443–478.

[10] T. Han, J. D. Lykken, and R.-J. Zhang *Phys. Rev.* **D59** (1999) 105006, `hep-ph/9811350`.

[11] G. F. Giudice, R. Rattazzi, and J. D. Wells *Nucl. Phys.* **B544** (1999) 3–38, `hep-ph/9811291`.

[12] N. Arkani-Hamed, S. Dimopoulos, and G. R. Dvali *Phys. Rev.* **D59** (1999) 086004, `hep-ph/9807344`.

[13] G. F. Giudice, R. Rattazzi, and J. D. Wells *Nucl. Phys.* **B630** (2002) 293–325, `hep-ph/0112161`.

Central Exclusive Scalar Luminosities from the Linked Dipole Chain Model Gluon Densities

Paper I

LU TP 03-47
November 2003

Central Exclusive Scalar Luminosities from the Linked Dipole Chain Model Gluon Densities

Leif Lönnblad[1]
and
Malin Sjödahl[2]
Department of Theoretical Physics, Lund University,
Sölvegatan 14A, S-223 62 Lund, Sweden

JHEP **02** 042 (2004)

Abstract
We investigate the implication of uncertainties in the unintegrated gluon distribution for the predictions for central exclusive production of scalars at hadron colliders. We use parameterizations of the $k_\perp$-unintegrated gluon density obtained from the Linked Dipole Chain model, applying different options for the treatment of non-leading terms. We find that the luminosity function for central exclusive production is very sensitive to details of the transverse momentum distribution of the gluon which, contrary to the $k_\perp$-integrated distribution, is not very well constrained experimentally.

[1]Leif.Lonnblad@thep.lu.se
[2]Malin.Sjodahl@thep.lu.se

1.1 Introduction

To detect the Higgs at hadron colliders such as the Tevatron or the LHC is far from a trivial task. Especially if it is rather light and predominantly decays into bottom quarks, the background from standard QCD processes is huge, making the expression "needle in a haystack" seem like a severe understatement. Looking for Higgs signals in the relatively clean environment of diffractive events is therefore an appealing prospect, provided the cross sections are sufficiently high. Several suggestions for what kind of diffractive processes could be used and how to calculate the corresponding cross section for the Higgs and the background have been made [1–8].

The cleanest and maybe the most promising process is usually referred to as central exclusive Higgs production, pp→p+H+p (where the + symbolizes a large rapidity gap). It was first suggested in [1,2] and has lately been developed further by Khoze, Martin and Ryskin (KhMR)[1] [5]. This process has several advantages. If the protons are scattered at small angles with small energy loss and they are detected in very forward taggers, the centrally produced system is constrained to be in a scalar state, which reduces the background from e.g. normal QCD production of b-jets. By matching the mass of the central system as measured with the central detectors, with the mass calculated from the energy loss of the scattered protons, it is possible to exclude events with extra radiation outside the reach of the detectors.

There is currently much discussion about which, if any, of the suggested diffractive Higgs processes could be detected at the LHC, and how to reliably calculate them. For a recent review we refer the reader to [10]. In this paper we will only concern ourselves with the model by KhMR and concentrate on one of its weaknesses, namely the uncertainty in their prediction due to the poorly constrained unintegrated gluon densities.

To calculate the central exclusive Higgs cross section, KhMR starts off with the standard gg→H cross section and adds the exchange of an extra gluon to ensure that no net colour is emitted by the protons. Then one must make sure that there is no additional radiation what so ever in the event, which gives rise to so-called soft and hard gap-survival probabilities. The soft survival probability ensures that the protons do not undergo any additional soft rescatterings, while the hard survival probability ensures that the there is no additional radiation from the exchanged gluons. Since the probability to emit really soft gluons diverges, it is necessary to introduce some natural cutoff, in order for the latter survival probability to remain finite. This is accomplished by letting the exchanged gluons have finite transverse momenta so that soft gluons cannot resolve the individual colour flows in the total colour singlet exchange. These

[1] We shall here refer to their calculation as KhMR to distinguish it from the KMR procedure for obtaining unintegrated gluon densities from integrated ones by Kimber, Martin and Ryskin [9].

transverse momenta must compensate each other so that the net transverse momenta of the scattered protons are zero. This means that the two gluons emitted from each proton are highly correlated and it is necessary to introduce so-called off-diagonal, or skewed, parton densities (odPDFs), which in addition must be $k_\perp$-unintegrated (oduPDFs[2]). With this formalism it is then assumed to be possible to factorize[3] the central exclusive production of any scalar resonance, R, into the standard partonic gg$\rightarrow R$ cross section multiplied by a gluon luminosity function which includes both the additional gluon exchange and the gap-survival probabilities. In this way we can turn any hadron collider with forward taggers into a kind of colour-singlet gluon collider with variable center of mass energy.

There are several uncertainties associated with this process. Both theoretical ones, such as how to calculate the soft survival probability, and experimental ones, such as how well the scattered protons can be measured. In this paper we will concentrate on another theoretical uncertainty, namely how well we know the oduPDFs which enters to the fourth power in the cross section. The quoted PDF uncertainty in [5] is a factor of two[4], which may seem large, but we will here argue that the uncertainty may be even larger.

The factor of two uncertainty was obtained by using a particular procedure to obtain the gluon oduPDF from the standard diagonal integrated gluon PDF, and then using different parameterizations for the latter. The problem with this estimate is that the diagonal integrated gluon PDF is fairly well constrained experimentally, while the diagonal unintegrated one is not, and the off-diagonal unintegrated even less so. In this paper we will use an alternative way to obtain the gluon uPDF, based on the so-called Linked Dipole Chain model [13, 14], which is a reformulation of the CCFM [15, 16] evolution for uPDFs. With the LDC model the uPDFs can in principle be better constrained since it is possible to compare with less inclusive experimental data, looking at details of the hadronic final states of events. Especially observables such as forward jet rates in DIS should be sensitive to the actual $k_\perp$-distribution of gluons in the proton. Unfortunately it turns out to be extremely difficult to reproduce such observables, even with the LDC. This is why we will here not be able to constrain the prediction for the central exclusive production, but on the contrary conclude that the uncertainties are larger than one might expect.

The outline of this paper is as follows. First we recapitulate in section 1.2 the main points of the calculation of Khoze, Martin and Ryskin. Then in

[2]Throughout this paper we shall use the following abbreviations: PDF refers to the standard diagonal integrated parton (gluon) density, uPDF is the diagonal $k_\perp$-unintegrated density, odPDF is the off-diagonal integrated and oduPDF is the off-diagonal $k_\perp$-unintegrated density.

[3]There is to our knowledge, however, no formal factorization theorem for off-diagonal, unintegrated parton densities.

[4]In later papers the quoted uncertainty is factor 2.5 up or down [11, 12]

section 1.3 we briefly describe the Linked Dipole Chain model and explain how we use it to obtain the central exclusive luminosity function. In section 1.4 we present our results and compare them with the calculation of Khoze, Martin and Ryskin, leading us to the conclusions presented in section 1.5.

1.2 Central exclusive production

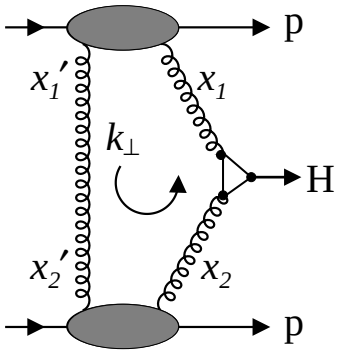

Figure 1.1: The basic diagram for exclusive production of the Higgs boson.

The general idea for central exclusive production of a scalar particle such as the Higgs boson[5] is that two gluons with no net quantum number fuse into a Higgs via the standard heavy quark triangle diagram, whereas another semi-hard gluon guarantees that there is no net colour flow between the protons. This is shown in figure 1.1, where it is also indicated that the exchanged semi-hard gluon should also compensate the transverse momentum $k_\perp$ of the gluons producing the Higgs, so that the protons are scattered with little or no transverse momenta.

Several types of radiation can destroy the diffractive character of the interaction. An additional gluon or quark which destroys the color singlet can be emitted by one of the gluons. For additional gluons of $q_\perp > k_\perp$ this will be taken care of by a *hard* survival probability given by a Sudakov form factor (see eq. (1.5) below) which guarantees that no gluon or quark with $q_\perp$ between $k_\perp$ and the hard scale given by M is emitted.

In principle there is also a probability of emitting a gluon of transverse momentum squared less then $k_\perp$ and this probability diverges for small $q_\perp$. However, the $k_\perp$ here acts as an effective cut off since a gluon with a wavelength

[5]We will in the following talk only about the Higgs, but note that the formalism is valid for the production of any scalar system of particles.

larger than $1/k_\perp$ will not be able to resolve the individual colour flow of the two gluons, but will only see a color singlet being exchanged. The assumption is that the typical $k_\perp$ will be larger than a GeV or two due to the Sudakov suppression, and rather than having a continuous suppression of softer gluons, $k_\perp$ can be used as a sharp cutoff.

Another process which reduces the number of diffractive events is additional soft rescattering of the spectator partons. This is taken care of by a soft survival probability, S^2, the value of which can be be estimated by several different models. Here we will use the same estimates as in [5] where S^2 is taken to be 0.045 for the Tevatron and 0.02 for LHC.

Finally we must make sure that the protons remain intact, which gives us a suppression depending on the momentum transfer to each the protons, $t = (p_i - p_f)^2$:

$$P = e^{b(p_i - p_f)^2},$$

which will be integrated over. Assuming that possible shrinkage effects can be neglected it simply gives a suppression factor $1/b^2$, and we will here use the same value as in [5]: $b = 4$ GeV^{-2}.

The exclusive cross section of $pp \to ppH$ is then assumesd to factorize into the form

$$\sigma = \int \hat{\sigma}_{gg\to H}(M^2) \frac{\delta^2 \mathcal{L}}{\delta y \delta \ln M^2} dy d\ln M^2$$

where $\hat{\sigma}$ denotes the basic $gg \to H$ cross section and

$$\begin{aligned} L(M,y) &= \frac{\delta^2 \mathcal{L}}{\delta y \delta \ln M^2} = S^2 [\frac{\pi}{(N_c^2-1)b} \\ &\int^{M^2/4} \frac{dk_\perp^2}{k_\perp^4} f_g(x_1, x_1', k_\perp^2, M^2/4) f_g(x_2, x_2', k_\perp^2, M^2/4)]^2 \end{aligned} \tag{1.1}$$

with $x_{1,2} = e^{\pm y} M/E_{\rm cm}$, is the luminosity function for producing two gluons attached to the central process at rapidity y and mass M of the Higgs. In principle one should be using an off-shell version of $\hat{\sigma}$ (see eg. [17]) which then would have a $k_\perp$ dependence, hence breaking the factorization, but we shall find below that the main contribution comes from rather small $k_\perp$ and at least for large masses the factorization should hold.

The equation for the luminosity contains the off-diagonal unintegrated gluon densities, $f(x, x', k_\perp^2, \mu^2)$. These should be interpreted as the amplitude related to the probability of finding two gluons in a proton carrying equal but opposite transverse momentum, $k_\perp$, and carrying energy fractions x and x' each, one of which is being probed by a hard scale μ^2. To obtain these density functions

in [5] the two step procedure presented in [18] was used. First they obtain the odPDF from the standard gluon PDF, in the here relevant limit of $x' \ll x$:

$$H(x, x', \mu^2) \approx R_g x g(x, \mu^2). \tag{1.2}$$

The R_g factor depends on the x-behavior of the PDF, so that for $xg(x, \mu^2) \propto x^{-\lambda}$ [19],

$$R_g = \frac{2^{2\lambda+3}}{\sqrt{\pi}} \frac{\Gamma(\lambda + 5/2)}{\Gamma(\lambda + 4)} \approx 1 + 0.82\lambda + 0.56\lambda^2 + \mathcal{O}(\lambda^3) \tag{1.3}$$

This factor can be taken approximately constant and we will then use the values quoted in [5]: 1.2 for the LHC and 1.4 at the Tevatron. We note, however, that it could also be taken to depend on both x and μ^2 by using[6] $\lambda = d \ln xg(x, \mu^2)/d \ln(1/x)$.

In the next step it is assumed that the oduPDF can be obtained from the odPDF in the same way as the uPDF can be obtained from the standard PDF. In the latter case one can use the KMR prescription introduced in [9], where

$$G(x, k_\perp^2, \mu^2) \approx \frac{d}{d \ln k_\perp^2} \left[xg(x, k_\perp^2) T(k_\perp^2, \mu^2) \right], \tag{1.4}$$

which then corresponds to the probability of finding a gluon in the proton with transverse momentum $k_\perp$ and energy fraction x when probed with a hard scale μ^2. T is here the survival probability of the gluon given by the Sudakov form factor,

$$-\ln T(k_\perp^2, \mu^2) = \int_{k_\perp^2}^{\mu^2} \frac{dq_\perp^2}{q_\perp^2} \frac{\alpha_S(q_\perp^2)}{2\pi} \int_0^{\frac{\mu}{\mu + k_\perp}} dz \left[z P_g(z) + n_f P_q(z) \right]. \tag{1.5}$$

To get the oduPDF one then starts from eq. (1.2) and get by analogy in the limit $x' \ll x$

$$f_g(x, x', k_\perp^2, \mu^2) \approx \frac{d}{d \ln k_\perp^2} \left[R_g x g(x, k_\perp^2) \sqrt{T(k_\perp^2, \mu^2)} \right], \tag{1.6}$$

where the square root of the Sudakov comes about because only one of the two gluons are probed by the hard scale.

In figure 1.2 we show our calculation of the luminosity function for central rapidity at the LHC using eq. (1.1). We use both a constant $R_g = 1.2$ and a varying one according to eq. (1.3) and we find that the treatment of R_g does make a difference. The latter alternative is closer to the result [5], but it is not exactly the same due to differences in the handling of the α_S in the Sudakov and

[6] Which was actually done in [5] to obtain the luminosities [20].

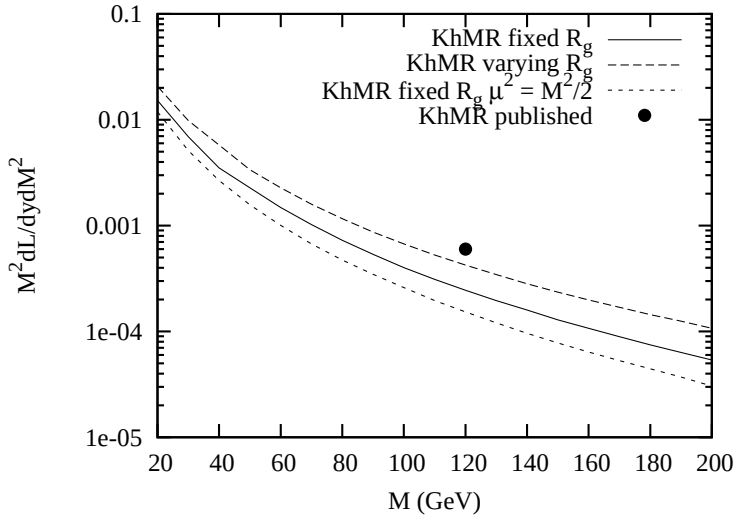

Figure 1.2: The exclusive luminosity as a function of M for fixed rapidity, $y = 0$, at the LHC, as calculated according to eqs. (1.1) and (1.6) with fixed $R_g = 1.2$ (full line) and with varying R_g according to eq. (1.3) (long-dashed line). The point is the the value quoted in [5]. Short-dashed line is the same as the full line but using the scale $\mu^2 = M^2/2$ rather than $\mu^2 = M^2/4$ in the oduPDFs.

the lower limit in the integral of eq. (1.1). We use a leading order α_S and the cutoff is taken to be the input scale of the MRST99 (central-g L300-DIS) [21] used as the starting PDF in eq. (1.2).

We note that the scale used in the oduPDFs in [5] is $\mu^2 = M^2/4$ rather than the somewhat more natural one $\mu^2 = M^2$. Although we realize that in a leading order calculation like this the scale choice is somewhat ambiguous. In figure 1.2 we show that the scale choice in fact makes a rather big difference, the luminosity function is reduced by up to 50% by increasing the scale a factor of two.

1.3 The Linked Dipole Chain Model

We will here only describe the main characteristics of the LDC model and instead refer the reader to refs. [13, 14, 22] for a more detailed description. The Linked Dipole Chain model is a reformulation and generalization of the CCFM evolution for the uPDFs. CCFM has the property that it reproduces BFKL evolution [23, 24] for asymptotically large energies (small x) and is also similar

to standard DGLAP evolution [25–28] for large virtualities and larger x. It does this by carefully considering coherence effects between gluons emitted from the evolution process, allowing only gluons ordered in angle to be emitted in the initial state, and thus contribute to the uPDFs, while non-ordered gluons are treated as final state radiation off the initial state gluons.

The LDC model is based on the observation that the dominant features of the parton chains are determined by a subset of emitted gluons, which is ordered in both light-cone components, q_+ *and* q_-, (which implies that they are also ordered in angle or rapidity y) and with $q_{\perp i}$ satisfying the constraint

$$q_{\perp i} > \min(k_{\perp i}, k_{\perp,i-1}), \qquad (1.7)$$

where q and k are the momenta of the emitted and propagating gluons respectively as indicated in figure 1.3. In LDC this subset (called "primary" gluons, or the backbone of the chain) forms the chain of initial state radiation, and all other emissions are treated as final state radiation.

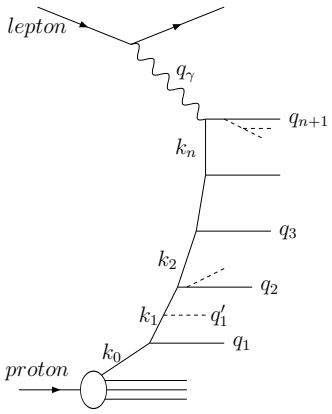

Figure 1.3: A fan diagram for a DIS event. The quasi-real partons from the initial-state radiation are denoted q_i, and the virtual propagators k_i. The dashed lines denote final-state radiation.

This redefinition of the separation between initial- and final-state implies that one single chain of initial-state emissions in the LDC model corresponds to a whole set of CCFM chains. As was shown in ref. [13], when summing over the contributions from all chains of this set, the resulting equations for the primary chains is greatly simplified. In particular the so-called non-eikonal form factors present in the CCFM splitting functions do not appear explicitly in LDC. The LDC formulation can also be easily made forward-backward symmetric, so that in DIS, the evolution can be equally well formulated from the virtual photon side or from the proton side.

In the small-x limit, keeping only the $1/z$ term of the gluon splitting function we can write the perturbative part of the gluon uPDF as the sum of all possible chains ending up with a gluon at a certain x and $k_\perp^2$

$$\mathcal{G}(x,k_\perp^2) \sim \sum_n \int \prod^n \bar{\alpha}\frac{dz_i}{z_i}\frac{d^2q_{\perp i}}{\pi q_{\perp i}^2}\theta(q_{+,i-1}-q_{+i})\theta(q_{-i}-q_{-,i-1}) \times \delta(x-\Pi z_i)\delta(\ln(k_\perp^2/k_{\perp n})^2), \qquad (1.8)$$

where $\overline{\alpha} = 3\alpha_s/\pi$. For finite x it is straight forward to add not only the $1/(1-z)$ to the gluon splitting function, as is also done in CCFM, but also to include

the full splitting function with non-singular terms. The $z = 1$ pole then needs to be regularized with a Sudakov form factor $\Delta_{\rm S}$ of the form

$$\ln \Delta_{\rm S} = -\int \frac{dq_\perp^2}{q_\perp^2} \frac{\alpha_s}{2\pi} z dz P_{\rm gg}(z) \Theta_{\rm order}, \tag{1.9}$$

where $\Theta_{\rm order}$ limits the integration to the phase space region where initial-state emissions are allowed according to LDC. It is also straight forward to add quarks in the evolution with the appropriate modification of the Sudakov form factors.

The LDC model can easily be implemented in an event generator which is then able to generate complete events in DIS with final state radiation added according to the dipole cascade model [29, 30] and hadronization according to the Lund model [31]. One advantage of having an event generator implementation is that energy and momentum can be conserved in each emission. Since the lack of momentum conservation in the BFKL formalism is the main reason for the huge next-to-leading logarithmic corrections [32], the LDC model is therefore expected to have smaller sub-leading corrections (see [33] for a more detailed discussion on this).

The perturbative form of the uPDF in eq. (1.9) needs to be convoluted with non-perturbative input PDFs, the form of which are fitted to reproduce the experimental data on F_2. This has all been implemented in the LDCMC program [34], and the resulting events can be compared directly to experimental data from eg. HERA. One of the most important observables is the rate of forward jets which is sensitive to parton evolution with unordered tranverse momenta, which is modeled by BFKL, CCFM and LDC, but is not allowed DGLAP. This observable should also be especially sensitive to the actual $k_\perp$distribution of gluons in the proton. It turns out that the forward jet rates can indeed be reproduced by LDCMC (as well as with the CCFM event generator CASCADE [35]) but only if only gluons are included in the evolution and if non-singular terms are excluded from the gluon splitting function [33]. So far there is no satisfactory explanation for this behavior.

The LDC gluon uPDF has been extracted by generating a DIS events with LDCMC and measuring the gluon density as described in [22]. The density depends on two scales, $k_\perp$and a scale, $\bar{q}$, related to the maximum angle allowed for the emitted gluons, which is related to the virtuality μ^2 of the hard subprocess. In LDC, similarly to the KMR prescription, the uPDF approximately factorizes into a single scale uPDF and a Sudakov form factor:

$$G(x, k_\perp^2, \mu^2) \approx G(x, k_\perp^2) \times \Delta_S(k_\perp^2, \mu^2). \tag{1.10}$$

This density can then be compared to other approaches and one finds that the results are quite varying as the examples in figure 1.4 shows. Even looking

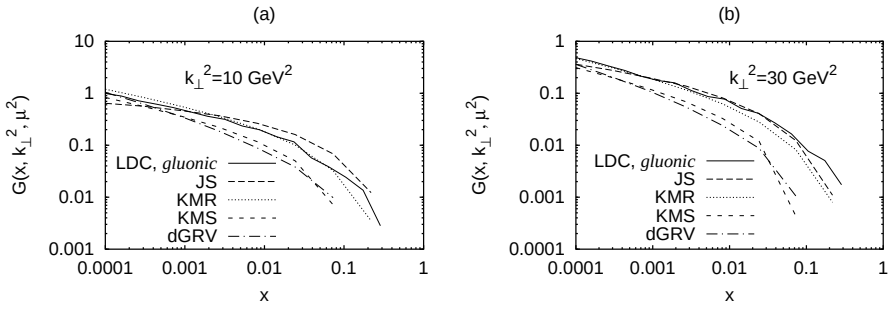

Figure 1.4: The LDC *gluonic* unintegrated gluon distribution function (full curve), compared to the corresponding results of JS [36] (long-dashed curve), KMR [9] (dotted curve), KMS [37] (short-dashed curve) and a simple derivative of the GRV [38] PDF parameterization (dash-dotted curve) as functions of x for (a) $k_\perp^2 = 10$ GeV^2 and (b) $k_\perp^2 = 30$ GeV^2. Results for the two-scaled functions, LDC, JS and KMR, with $\mu = 2k_\perp$, are shown together with the 1-scaled distribution functions of KMS and dGRV.

only at the proper two-scale uPDFs, factors of two difference are not uncommon.

Due to the $k_\perp$-unordered nature of the LDC evolution, the relationship between the uPDF and the standard gluon density is different from eq. (1.4), as the integrated gluon at a scale μ^2 also receives a contribution, although suppressed, from gluons with $k_\perp > \mu$, and in [22] the following expression was obtained:

$$\begin{aligned} xg(x,\mu^2) &= G(x,k_{\perp 0}^2)\Delta_S(k_{\perp 0}^2,\mu^2) \\ &+ \int_{k_{\perp 0}^2}^{\mu^2} \frac{dk_\perp^2}{k_\perp^2} G(x,k_\perp^2)\Delta_S(k_\perp^2,\mu^2) + \int_{\mu^2}^{\mu^2/x} \frac{dk_\perp^2}{k_\perp^2} G(x\frac{k_\perp^2}{\mu^2},k_\perp^2)\frac{\mu^2}{k_\perp^2} \end{aligned} \tag{1.11}$$

To obtain the off-diagonal densities needed for the exclusive luminosity function, we assume that a similar approximation can be made as for the KMR densities, that is, in the limit of very small x'

$$f_g^{\rm LDC}(x,x',k_\perp^2,\mu^2) \approx R_g(x,k_\perp^2)G(x,k_\perp^2)\sqrt{\Delta_S(k_\perp^2,\mu^2)}. \tag{1.12}$$

The square root of the Sudakov form factor is used, since only one of the gluons couples to the produced Higgs at the high scale. We will use both a fixed R_g factor as in section 1.2 and the one which depends explicitly on the x-dependence of the diagonal PDF taken at the relevant scale. It is currently not quite clear to us how large the uncertainties are in this procedure and we come back to it in a future publication.

The LDC uPDFs are only defined down to a cutoff, $k_{\perp 0}$, below which we will use the non-perturbative input density, g_0, and arrive at the following expression for the exclusive luminosity function:

$$\begin{aligned} L &= S^2 \left[\frac{\pi}{(N_c^2-1)b} \right. \\ &\left(\frac{1}{k_{\perp 0}^2} R_g(x_1,k_{\perp 0}^2) g_0(x_1,k_{\perp 0}^2) \Delta_S(k_{\perp 0}^2,M^2) R_g(x_2,k_{\perp 0}^2) g_0(x_2,k_{\perp 0}^2) + \right. \\ &\left. \left. \int_{k_{\perp 0}^2}^{M^2} \frac{dk_\perp^2}{k_\perp^4} R_g(x_1,k_\perp^2) G(x_1,k_\perp^2) \Delta_S(k_\perp^2,M^2) R_g(x_2,k_\perp^2) G(x_2,k_\perp^2) \right) \right]^2 . \end{aligned} \tag{1.13}$$

Comparing with eq. (1.1) we note that, besides the different form of the oduPDFs, the scale and the integration limit is taken to be M^2 rather than $M^2/4$. The exact value of the integration limit is not very important, but the scale in the Sudakov form factor is. In fact, the form of the Sudakov form factor is also different. We use

$$\ln \Delta_S(k_\perp^2,M^2) = -\int_{k_\perp^2}^{M^2} \frac{dk_\perp^2}{k_\perp^2} \frac{\alpha_s}{2\pi} \int_0^{1-k_\perp/M} dz \left[zP_g(z) + \sum_q P_q(z) \right], \tag{1.14}$$

which corresponds to the actual no-emission probability in the phase space region up to the rapidity of the produced Higgs from the incoming gluon. The different integration region in eq. (1.5) as well as the different scale used means that the Sudakov suppression in that case is weaker as shown in figure 1.5. The difference is not very large, but since the factor comes in squared in the luminosity function for $k_\perp$ of a couple of GeV the difference can easily become larger than a factor two.

One of the main differences between the LDC uPDFs and the KMR ones is that the evolution of former includes emissions with transverse momenta which may be larger than the $k_\perp$ for the probed gluon. This is, of course, kinematically allowed but should be rather suppressed. In any case, it is not clear how to handle such emissions when calculating the off-diagonal densities in eq. (1.12). To investigate the effects of such $k_\perp$-non-ordering we shall below also use as comparison an alternative LDC uPDF where the transverse momentum in the evolution has been limited to be below $k_\perp$.

1.4 Results

In the following we shall present calculations for the exclusive luminosity using three different parameterizations of the LDC uPDF. The three options differs

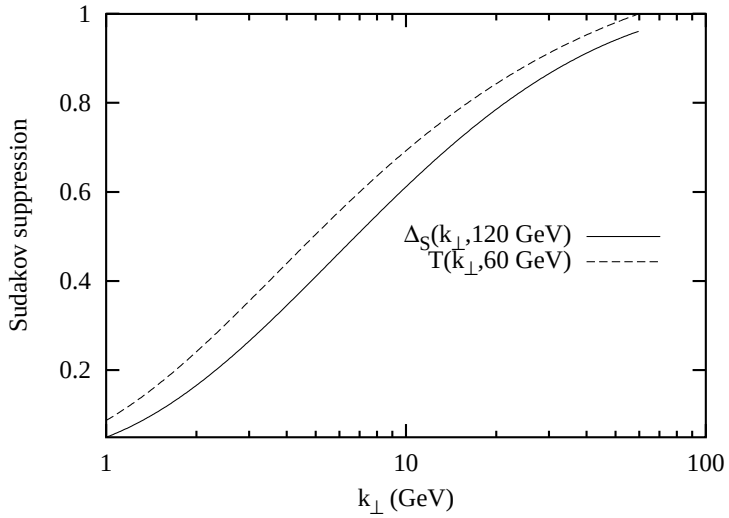

Figure 1.5: The Sudakov form factor used in the LDC calculation (full line, eq. (1.14)) compared to the one used by KhMR (dashed line, eq. (1.5)).

in the way they treat non-leading effects in the evolution and will be referred to as *standard*, *gluonic* and *leading* as described in [22]:

- *standard* is obtained with the full LDC evolution including the full splitting functions for both gluons and quarks. This option does not describe forward jets very well, but it gives an excellent description of F_2 data.
- *gluonic* is obtained by using only gluons in the LDC evolution, but with the full splitting function. This option does not describe F_2 data as well, especially not at large x, but it agrees better with standard parameterizations of the integrated gluon PDF.
- *leading* is obtained by using only gluons in the LDC evolution and only the singular terms of the gluon splitting function. Among the three it is the one which describes inclusive data the worst, on the other hand it is the only one which is able to describe the large rate of forward jets measured at HERA.

Clearly, none of these options are in perfect agreement with data, but we will use them here as a parameterization of our ignorance when it comes to unintegrated gluon densities.

In figure 1.6 and 1.7 we present our calculations of the luminosity function for the LHC and Tevatron respectively, using eq. (1.13) (with fixed $R_g = 1.2$ and 1.4 respectively). We find that the three options for the LDC evolution give very different results. At the LHC the *standard* is fairly close to the

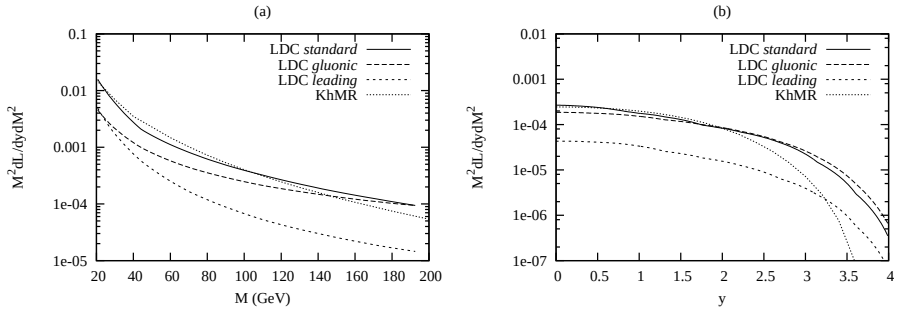

Figure 1.6: The exclusive luminosity as a function of M for fixed rapidity, $y = 0$ (a) and as a function of rapidity for fixed mass $M = 120$ GeV, at the LHC, as calculated according to eq. (1.13). Full line is *standard*, long-dashed line is *gluonic* and short dashed line is *leading*. As comparison the calculation based on KhMR is shown with a dotted line.

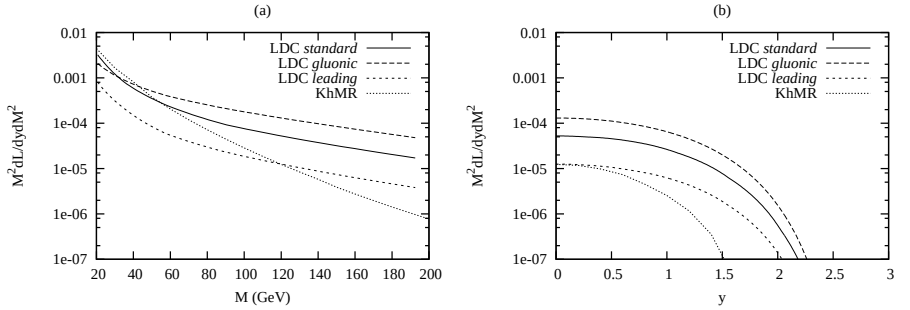

Figure 1.7: The exclusive luminosity as a function of M for fixed rapidity, $y = 0$ (a) and as a function of rapidity for fixed mass $M = 120$ GeV, at the Tevatron, as calculated according to eq. (1.13). The lines are the same as in figure 1.6.

results obtained with the KhMR calculation, while the result for *leading* is up to a factor ten below. We note that for large rapidities in figure 1.6b the differences between LDC and KhMR is larger also in shape, but this is close to the phase space limit, where one of the gluons carry a large fraction of the proton momentum and in this region the LDC parameterizations are less well constrained. The same effect is visible at the Tevatron in figure 1.7 where again the energy fractions are larger, especially for high masses.

The large difference between the three LDC options may seem surprising, especially since the standard integrated gluon PDF is generally higher for *leading* than for the other two. The explanation can be found by studying the

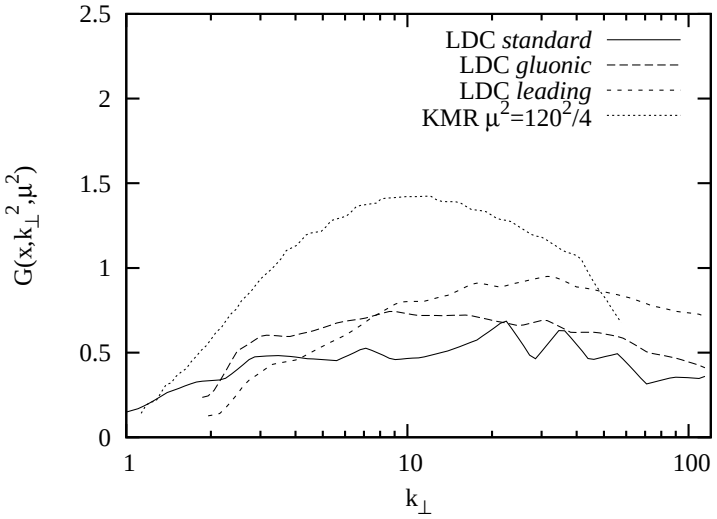

Figure 1.8: The LDC unintegrated gluon density as a function of $k_\perp$ for $\mu^2 = (120\ GeV)^2$ and $x = 120/14000$ (relevant for the luminosity function in eq. (1.13) for $M = 120$ GeV and $y = 0$). For comparison the KMR uPDF is shown for the same x but for $\mu^2 = (120/2\ GeV)^2$ (relevant for eq. (1.1)). The lines are the same as in figure 1.6.

$k_\perp$-dependence of the uPDF presented in figure 1.8. Here we see that *leading* has a harder $k_\perp$ spectrum than the the other two options and that all LDC densities have a flatter spectrum than the KMR one (which is shown at a lower scale corresponding to the one used in the luminosity function). This should be expected since the *leading* also produces more forward jets (in agreement with what is observed experimentally) and hence should give larger $k_\perp$-fluctuations. It turns out that the luminosity function is mostly sensitive to the uPDFs at $k_\perp$-values of around $2-3$ GeV, since smaller and larger values are suppressed by the Sudakov form factor and the $1/k_\perp^4$ factor respectively. Even if the differences in this region is not very large, the uPDF enters to the power four in the luminosity function, thus enhancing the differences (the difference between LDC and KMR is diminished since the square root of the Sudakov formfactor affect the LDC more than the KMR).

To investigate the uncertainties involved in going from the LDC uPDFs to the oduPDFs in eq. (1.12) we show in figure 1.9 the difference between using a fixed R_g factor and a varying one according to eq. (1.3) [7] with $\lambda =$

[7]The line is here a bit jagged due to the limited statistics in the Monte Carlo extraction of the LDC uPDF.

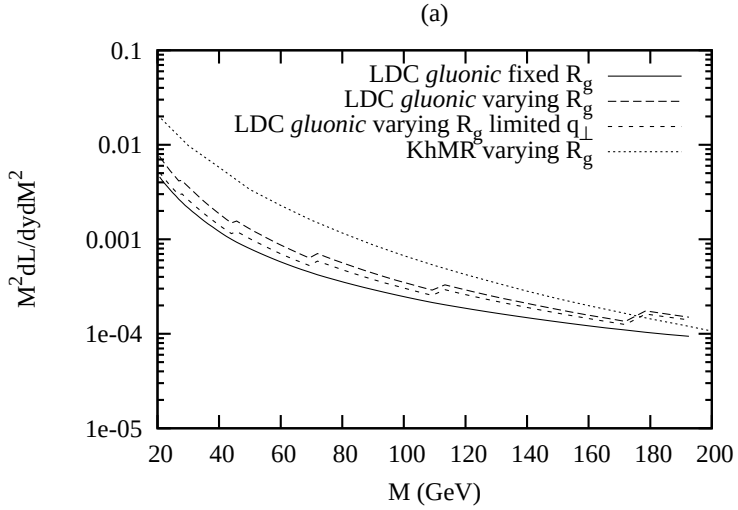

Figure 1.9: The exclusive luminosity as a function of M for fixed rapidity, $y = 0$ at the LHC, as calculated according to eq. (1.13) using the *gluonic* uPDF of LDC. Full line is with a fixed $R_g = 1.2$, long-dashed and short-dashed lines are with varying R_g but the latter uses a modified version of *gluonic* where the transverse momentum in the evolution has been limited. As comparison the calculation based on KhMR with a varying R_g is shown with a dotted line.

$d \ln G(x, k_\perp^2)/d \ln(1/x)$. Comparing with figure 1.2, we find that the differences are of the same order. We also show the effects of using an alternative version of the *gluonic* density where the transverse momentum in the evolution has been limited to be below $k_\perp$. This will not only reduce the uPDF somewhat, but it will also slow down the x-evolution, giving a smaller λ and hence a smaller R_g. As expected this effect is quite small, but still noticeable especially at small masses (small x).

1.5 Conclusions

The partonic evolution at small x is one of the least understood aspects of QCD. Although inclusive Higgs production is not a small-x process and therefore well understood in terms of collinear factorization with well constrained integrated gluon distributions, the exclusive production considered here relies on the exchange of a small-x gluon and is very sensitive to the $k_\perp$ distribution in the less constrained unintegrated gluon distributions.

In this report we have described how we calculate the exclusive luminosity

function using the unintegrated gluon distributions obtained within the LDC model, and we have found that different options give widely different results. In particular we note that the option which gives the best description of forward jet production at HERA, which should be sensitive to the actual $k_\perp$-dependence of the gluon in the proton, gives a result which is a factor ten smaller than what was reported by Khoze, Martin and Ryskin in [5]. This option is in theory a worse approximation than the other two and is similar to the double-log approximation discussed by the same authors in [39], which was also shown to give a much smaller result. Contrary to them, however, we do not dismiss the *leading* approximation, as experiments indicate that it better describes the actual $k_\perp$distrubution of the gluon.

There are several uncertainties in our calculations. The relation between the unintegrated gluon and the corresponding off-diagonal unintegrated gluon density not formally derived, but just assumed to be valid by analogy. The results are sensitive to the treatment of the R_g factor and the treatment of the $k_\perp$-unordered nature of LDC evolution. The different options used for the LDC unintegrated densities are in good agreement with different kinds of experimental observables, but none of them agrees with all important observables. It should also be noted that these densities were obtained through a fit to F_2 data only, which is mainly concentrated at small scales. At large scales which are important for reasonable values of the Higgs mass ($\gtrsim$ 120 GeV) the densities are less constrained.

The conclusion of this paper is therefore not that the previous calculations by Khoze, Martin and Ryskin is wrong in any way, but rather that they may have underestimated the uncertainties due to the unintegrated gluon density. We will not go so far as to say that the uncertainties are as large as a factor ten, but we believe that they are much larger than a factor of two. This does not mean that the prospects of using tagged forward protons to try to find the Higgs or other scalar particles at the LHC becomes less interesting, but our current understanding of the small-x sector of QCD clearly needs to be improved before we can give reliable predictions for such processes.

Acknowledgments

We would like to thank Valery Khoze and Mikhail Ryskin for important comments and discussions. In addition we have benefitted from discussions with Brian Cox, Jeff Forshaw, Gösta Gustafson and James Monk.

References

[1] A. Schafer, O. Nachtmann, and R. Schopf *Phys. Lett.* **B249** (1990) 331–335.

[2] A. Bialas and P. V. Landshoff *Phys. Lett.* **B256** (1991) 540–546.

[3] J.-R. Cudell and O. F. Hernandez *Nucl. Phys.* **B471** (1996) 471–502, hep-ph/9511252.

[4] E. Levin hep-ph/9912402.

[5] V. A. Khoze, A. D. Martin, and M. G. Ryskin *Eur. Phys. J.* **C23** (2002) 311–327, hep-ph/0111078.

[6] B. Cox, J. Forshaw, and B. Heinemann *Phys. Lett.* **B540** (2002) 263–268, hep-ph/0110173.

[7] M. Boonekamp, A. De Roeck, R. Peschanski, and C. Royon *Acta Phys. Polon.* **B33** (2002) 3485–3490, hep-ph/0205332.

[8] R. Enberg, G. Ingelman, A. Kissavos, and N. Timneanu *Phys. Rev. Lett.* **89** (2002) 081801, hep-ph/0203267.

[9] M. A. Kimber, A. D. Martin, and M. G. Ryskin *Phys. Rev.* **D63** (2001) 114027, hep-ph/0101348.

[10] A. De Roeck, V. A. Khoze, A. D. Martin, R. Orava, and M. G. Ryskin *Eur. Phys. J.* **C25** (2002) 391–403, hep-ph/0207042.

[11] A. B. Kaidalov, V. A. Khoze, A. D. Martin, and M. G. Ryskin *Eur. Phys. J.* **C31** (2003) 387–396, hep-ph/0307064.

[12] A. B. Kaidalov, V. A. Khoze, A. D. Martin, and M. G. Ryskin hep-ph/0311023.

[13] B. Andersson, G. Gustafson, and J. Samuelsson *Nucl. Phys.* **B467** (1996) 443–478.

[14] B. Andersson, G. Gustafson, and H. Kharraziha *Phys. Rev.* **D57** (1998) 5543–5554, hep-ph/9711403.

[15] M. Ciafaloni *Nucl. Phys.* **B296** (1988) 49.

[16] S. Catani, F. Fiorani, and G. Marchesini *Phys. Lett.* **B234** (1990) 339.

[17] F. Hautmann *Phys. Lett.* **B535** (2002) 159–162, hep-ph/0203140.

[18] A. D. Martin and M. G. Ryskin *Phys. Rev.* **D64** (2001) 094017, hep-ph/0107149.

[19] A. G. Shuvaev, K. J. Golec-Biernat, A. D. Martin, and M. G. Ryskin *Phys. Rev.* **D60** (1999) 014015, hep-ph/9902410.

[20] M. G. Ryskin. private communication.

[21] A. D. Martin, R. G. Roberts, W. J. Stirling, and R. S. Thorne *Eur. Phys. J.* **C14** (2000) 133–145, hep-ph/9907231.

[22] G. Gustafson, L. Lönnblad, and G. Miu *JHEP* **09** (2002) 005, hep-ph/0206195.

[23] E. A. Kuraev, L. N. Lipatov, and V. S. Fadin *Sov. Phys. JETP* **45** (1977) 199–204.

[24] I. I. Balitsky and L. N. Lipatov *Sov. J. Nucl. Phys.* **28** (1978) 822–829.

[25] V. N. Gribov and L. N. Lipatov *Yad. Fiz.* **15** (1972) 781–807.

[26] L. N. Lipatov *Sov. J. Nucl. Phys.* **20** (1975) 94–102.

[27] G. Altarelli and G. Parisi *Nucl. Phys.* **B126** (1977) 298.

[28] Y. L. Dokshitzer *Sov. Phys. JETP* **46** (1977) 641–653.

[29] G. Gustafson *Phys. Lett.* **B175** (1986) 453.

[30] G. Gustafson and U. Pettersson *Nucl. Phys.* **B306** (1988) 746.

[31] B. Andersson, G. Gustafson, G. Ingelman, and T. Sjostrand *Phys. Rept.* **97** (1983) 31.

[32] V. S. Fadin and L. N. Lipatov *Phys. Lett.* **B429** (1998) 127–134, `hep-ph/9802290`.

[33] **Small x** Collaboration, B. Andersson *et al. Eur. Phys. J.* **C25** (2002) 77–101, `hep-ph/0204115`.

[34] H. Kharraziha and L. Lönnblad *JHEP* **03** (1998) 006, `hep-ph/9709424`.

[35] H. Jung *Comput. Phys. Commun.* **143** (2002) 100–111, `hep-ph/0109102`.

[36] H. Jung and G. P. Salam *Eur. Phys. J.* **C19** (2001) 351–360, `hep-ph/0012143`.

[37] J. Kwiecinski, A. D. Martin, and A. M. Stasto *Phys. Rev.* **D56** (1997) 3991–4006, `hep-ph/9703445`.

[38] M. Glück, E. Reya, and A. Vogt *Eur. Phys. J.* **C5** (1998) 461–470, `hep-ph/9806404`.

[39] V. A. Khoze, A. D. Martin, and M. G. Ryskin *Eur. Phys. J.* **C14** (2000) 525–534, `hep-ph/0002072`.

Uncertainties on Central Exclusive Scalar Luminosities from the Unintegrated Gluon Distributions

Paper II

LU TP 04-41
December 2004

Uncertainties on Central Exclusive Scalar Luminosities from the Unintegrated Gluon Distributions

Leif Lönnblad[1]
and
Malin Sjödahl[2]
Department of Theoretical Physics, Lund University,
Sölvegatan 14A, S-223 62 Lund, Sweden

JHEP **05** 038 (2005)

Abstract
In a previous report we used the Linked Dipole Chain model unintegrated gluon densities to investigate the uncertainties in the predictions for central exclusive production of scalars at hadron colliders. Here we expand this investigation by also looking at other parameterizations of the unintegrated gluon density, and look in more detail on the behavior of these at small $k_\perp$. We confirm our conclusions that the luminosity function for central exclusive production is very sensitive to this behavior. However, we also conclude that the available densities based on the CCFM and LDC evolutions are not constrained enough to give reliable predictions even for inclusive Higgs production at the LHC.

[1]Leif.Lonnblad@thep.lu.se
[2]Malin.Sjodahl@thep.lu.se

2.1 Introduction

Detecting the Higgs boson at LHC in the "most probable" mass region around 120 GeV is far from a trivial task, such a light Higgs predominantly decays into bottom quarks making the background from standard QCD processes huge. Looking for Higgs signals in the clean environment of central diffractive events is therefore an appealing prospect, provided the cross section is sufficiently high [1–8].

In general, central exclusive events can be used for studying any scalar particle. In this paper we will only consider a Higgs boson, but our results can be trivially generalized. Central exclusive diffractive Higgs production was first suggested in [1,2] and has lately been developed further by Khoze, Martin and Ryskin (KhMR)[1] [5]. One of the main advantages compared to inclusive Higgs production is that, since the central system is constrained to be in a 0^{++} state, the normal QCD background from b-jets is heavily suppressed. By matching the mass of the central system, as measured with the central detectors, with the mass calculated from the energy loss of the scattered protons detected by very forward proton taggers, it is possible to exclude events with extra radiation outside the reach of the detectors, to ensure that the central system is indeed in a 0^{++} state.

In [10] we investigated the implications of the uncertainties in the unintegrated structure functions, uPDFs, for the KhMR calculations. Our main conclusion was that the cross section is very sensitive to the unintegrated structure functions, $G(x, k_\perp^2, m_H^2)$, in the region of $k_\perp \approx 2 - 3$ GeV. The differences in the uPDF, which enters in the final exclusive luminosity to the power of four, leeds to a variation in the result of roughly one order of magnitude. This estimate was obtained using unintegrated structure functions both from KMR [9] (used in the KhMR calculations) and different parameterizations based on the Linked Dipole Chain model, LDC [11].

In this report we have also used the CCFM-based densities described in [12], here referred to as Jung-1 and Jung-2. Both LDC and Jung have been tuned to F_2 data from HERA in the region of small $x \lesssim 0.01$ and $1.5 < Q^2 \lesssim 100$ GeV^2. Despite the similar fitting region and the similarities between CCFM and LDC evolution, it is found that the densities differ substantially in their $k_\perp$-distribution [11] even inside the fitting region. This is to be expected, since the fitting was only done to F_2, which is an integrated quantity. Below we will find that the differences at high scales, corresponding to the production of a 120 GeV Higgs, is large even for the integrated density. This can be explained by the fact that here the densities are also influenced by the large x distribution at smaller scales, well outside the region of the fit.

[1] We shall here refer to their calculations as KhMR to distinguish it from the KMR procedure for obtaining unintegrated gluon densities from integrated ones by Kimber, Martin and Ryskin [9].

In the KMR case the uPDFs are derived directly from the globally fitted integrated gluon density, MRST98 [13][2]. Hence at least the integrals of the uPDFs are well constrained. On the other hand, the $k_\perp$ dependence is uncertain since KMR assumes DGLAP evolution which works well for inclusive observables but not necessarily for $k_\perp$ sensitive ones.

The off-diagonal unintegrated parton densities (oduPDFs) which enters into the KhMR calcultaions were derived in [14] from the corresponing off-diagonal integrated one (odPDF) in the same way as the uPDFs were derived from the standard integrated PDFs in [13]. Now, while the integrated gluon PDF is fairly well constrained experimentally, the unintegrated is not, and the off-diagonal unintegrated, used in the exclusive cross section, is even less so. And any uncertainty in the uPDF will immediately be reflected in an uncertainty in the oduPDF.

There are a few weak experimental constraints on the $k_\perp$-distribution of the uPDFs. So far these constraints have not been taken into account in any fitting, but comparing models using the uPDFs with data can give us some hints about where the densities work and where they need to be improved. Since the exclusive luminosity is sensitive to the uPDF mainly in the region of a few GeV we should look for other observables sensitive to features in this region to obtain constraints. One such observable is the $k_\perp$-spectra of W and Z in hadron collisions (eg. at the Tevatron [15, 16]) for small $k_\perp$. While the main features of this can be reproduced by a calculation using KMR uPDFs [17], the small-$k_\perp$ peak is slightly too low, as can be seen in figure 2.1, indicating that KMR may be underestimating somewhat the hardness of the $k_\perp$-distribution.

Another sensitive observable is the rate of forward jets in DIS at HERA. Especially in the measured region of $k_\perp^2 \sim Q^2 \gtrsim 10$ GeV^2 and small x where standard DGLAP evolution would not contribute. Indeed, DGLAP based models severely underestimate the rate of forward jets (see eg. [18] and [19] for a discussion on this), and even though the KMR uPDFs have not been confronted with this data it is likely that they will also fail.

In general there are indications of a slightly harder $k_\perp$ distribution in the uPDFs than what is given by KMR. This is predicted by the BFKL-like CCFM evolution (and hence also LDC) on which the alternative uPDFs used in this report are based on. Such evolution includes also ladders unordered in tranverse momenta, opening up for more activity. As shown in [20] the typical evolution path, starting from the high virtuality end, is a rapid DGLAP-like evolution down to a few GeV and then a region of transverse momenta distributed as a random walk in $\log(k_\perp)$.

The layout of this paper is as follows. First we recapitulate the main points in the calculation of Khoze, Martin and Ryskin and discuss their oduPDFs in

[2]MRST98 is not the newest of PDF parameterizations, but it was used in [5], where it was also shown that the results are rather insensitive to the choice of integrated PDF.

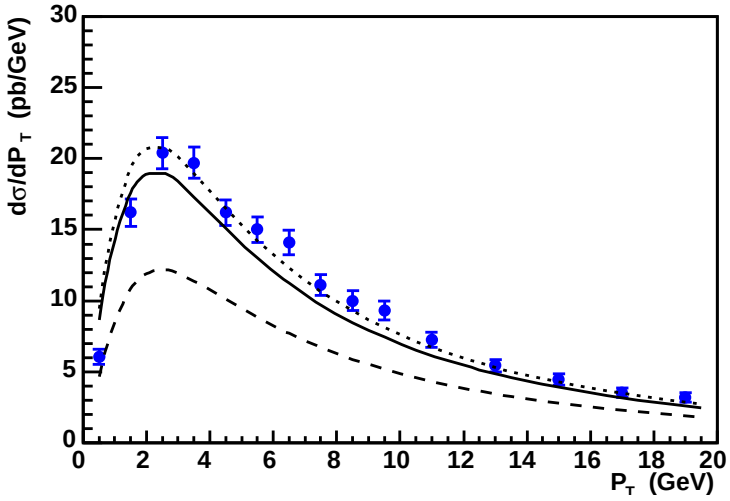

Figure 2.1: The $p_\perp$-distribution of Z^0 measured at the Tevatron [15] compared to a calculation using the KMR approach to uPDFs with different options as described in [17].

section 2.2. In section 2.3 we obtain the oduPDFs in the case of LDC and Jung respectively. Then, in section 2.4 we present and comment our results. Finally we arrive at our conclusions in section 2.5.

2.2 Central exclusive production

In a central exclusive production of a Higgs boson, two gluons with no net quantum number fuse into a Higgs via the standard heavy quark triangle diagram, whereas another semi-hard gluon exchange guarantees that there is no net colour flow between the protons. This is shown in figure 2.2, where it is also indicated that the exchanged semi-hard gluon should compensate the transverse momentum $k_\perp$ of the gluons producing the Higgs, so that the protons are scattered with little or no transverse momenta.

Several types of radiation can destroy the diffractive character of the interaction. There can be extra interactions between the spectator partons, modeled by the so called soft survival probability S^2. Also, the gluons participating in the interaction can radiate both at scales above $k_\perp$, which is modeled by the hard survival probability using a Sudakov form factor, and at scales below $k_\perp$, which is suppressed, since such gluons cannot resolve the the individual colours of the exchanged gluon pair.

This is discussed in detail in [21] and [10]. Here we just state the resulting

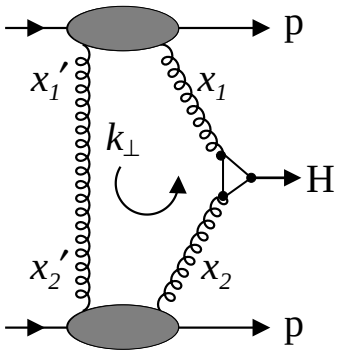

Figure 2.2: The basic diagram for exclusive production of the Higgs boson in hadron collisions.

exclusive luminosity function

$$\begin{aligned} L(M,y) &= \frac{\delta^2\mathcal{L}}{\delta y \delta \ln M^2} \qquad (2.1)\\ &= S^2\left[\frac{\pi}{(N_c^2-1)b}\int^{\mu^2}\frac{dk_\perp^2}{k_\perp^4} f_g(x_1,x_1',k_\perp^2,\mu^2) f_g(x_2,x_2',k_\perp^2,\mu^2)\right]^2 \end{aligned}$$

where $\mu^2 = M^2/4$ in the standard KhMR prescription, y denotes rapidity, b comes from the probability for the protons to remain intact, $x_{1(2)} = m_H e^{(-)y}$ and $x'_{1(2)} \sim k_\perp/\sqrt{S} \ll x_{1(2)}$. $f(x,x',k_\perp^2,\mu^2)$ is the off-diagonal unintegrated gluon density, the oduPDF, which should be interpreted as the amplitude related to the probability of finding two gluons in a proton with equal but opposite transverse momentum, $k_\perp$, and carrying energy fractions x and x' each, one of which is being probed by a hard scale μ^2.

The cross section is then obtained by

$$\sigma = \int \hat{\sigma}_{gg\to H}(M^2)\frac{\delta^2\mathcal{L}}{\delta y \delta \ln M^2} dy d\ln M^2$$

where M is the invariant mass of the central system, in this case the Higgs mass. In principle one should use a off-shell version of $\hat{\sigma}$ (see eg. [22]) which then would have a $k_\perp$ dependence, and hence break the factorization. However, for the exclusive cross section the main contribution comes from rather small $k_\perp$ and, at least for large masses, the factorization should hold. Since the cross

section, in the exclusive case, is a convolution of the luminosity and the matrix element it suffices to study the difference in luminosity to investigate the effects of different oduPDFs.

Besides the oduPDFs, the only other main uncertainty in eq. (2.1) is the soft survival probability S^2. We have made a separate study using the multiple interaction model in PYTHIA [23, 24] in the same way as was done for the WW→H process in [25]. Taking the probability of having no additional scatterings in Higgs production[3] using theparameters of the so-called Tune-A by Rick Field [26], we estimate the survival probability to be 0.040 for the Tevatron and 0.026 for the LHC. This is remarkably close to the values used in [5] obtained in the so-called two-channel eikonal approach [27].

In the KhMR case the oduPDF [5] are obtained in a two step procedure presented in [14]. In the first step the off-diagonal parton distribution functions, odPDF, are extracted from the standard gluon PDF, in the relevant limit of $x' \ll x$:

$$H(x, x', \mu^2) \approx R_g x g(x, \mu^2). \tag{2.2}$$

Although we will use a constant R_g factor of 1.2, we note that it in general depends on both x and μ^2. The consequences for the luminosity function of a non-constant R_g are moderate and briefly discussed in [10].

In the second step it is assumed that the oduPDF can be obtained from the odPDF in the same way as the uPDF can be obtained from the standard PDF. In the latter case one can use the KMR prescription introduced in [9], where

$$G(x, k_\perp^2, \mu^2) \approx \frac{d}{d \ln k_\perp^2} \left[x g(x, k_\perp^2) T(k_\perp^2, \mu^2) \right], \tag{2.3}$$

which then corresponds to the probability of finding a gluon in the proton with transverse momentum $k_\perp$ and energy fraction x when probed with a hard scale μ^2. T is the survival probability of the gluon given by the Sudakov form factor,

$$\ln T(k_\perp^2, \mu^2) = - \int_{k_\perp^2}^{\mu^2} \frac{dq_\perp^2}{q_\perp^2} \frac{\alpha_S(q_\perp^2)}{2\pi} \int_0^{\frac{\mu}{\mu + q_\perp}} dz \left[z P_g(z) + n_f P_q(z) \right]. \tag{2.4}$$

To get the oduPDF one then starts from eq. (2.2) and get by analogy in the limit $x' \ll x$

$$f_g(x, x', k_\perp^2, \mu^2) \approx \frac{d}{d \ln k_\perp^2} \left[R_g x g(x, k_\perp^2) \sqrt{T(k_\perp^2, \mu^2)} \right], \tag{2.5}$$

where the square root of the Sudakov comes about because only one of the two gluons are probed by the hard scale.

[3] We here used inclusive Higgs production, but the result should be the same for the exclusive case.

The hard scale μ in the oduPDF and in the Sudakov form factor is in the KhMR approach argued to be $m_H/2$. In fact the number is $0.62 \cdot m_H$ and comes from a tuning to reproduce full one-loop vertex corrections [28]. For LDC, below, we will be less ambitious and simply use m_H as scale.

2.3 Unintegrated parton densities

A general comment concerning the unintegrated gluon densities used in the KhMR calculations is that the KMR prescription essentially corresponds to taking one step backward in a DGLAP-based initial-state parton shower, to *unintegrate* the integrated PDF. As mentioned in the introduction, there are indications that such a prescription underestimates the hardness of the $k_\perp$-distribution of the uPDF.

In the following we will investigate uPDFs based on CCFM and LDC evolution, where emissions unordered in $k_\perp$ are explicitly included, and could increase the hardness of the $k_\perp$-distribution. We will also inversigate a more crude model. If the unordered emissions corresponds to a random walk in $\log(k_\perp)$ as suggested in [20], this could be modelled by an additional *intrinsic* transverse momenta, similar to what is expected from the non-perturbative fermi-motion included in most parton shower generators, but with an average transverse momentum well in the perturbative region of a couple of GeV. We will consider such intrinsic transverse momenta in section 2.4.2.

2.3.1 The Linked Dipole Chain uPDF

The Linked Dipole Chain model [29, 30] is a reformulation and generalization of the CCFM [31–34] evolution for the unintegrated gluon. CCFM has the property that it reproduces BFKL evolution [35, 36] for asymptotically large energies (small x) and is also similar to standard DGLAP evolution [37–40] for larger virtualities and larger x. It does this by carefully considering coherence effects between gluons emitted from the evolution process, allowing only gluons ordered in angle to be emitted in the initial state, and thus contribute to the uPDFs, while non-ordered gluons are treated as final state radiation off the initial state gluons. LDC differs from CCFM by the fact that it is ordered both in positive and negative light cone momenta, q_+ and q_-, of the emitted gluons, a treatment which categorizes more emissions as final state emission as compared to CCFM. This symmetric ordering in both q_+ and q_-, which also implies ordering in rapidity y or angle, together with the additional requirement that the transverse momentum of an emitted gluon must be larger than the $k_\perp$ of the propagator gluon before or after the emission, greatly simplifies the evolution equations and has as a consequence that the uPDF approximately

factorizes into a one-scale density multiplied by the Sudakov form factor:

$$G(x,k_\perp^2,\mu^2) \approx G(x,k_\perp^2) \times \Delta_S(k_\perp^2,\mu^2), \tag{2.6}$$

where

$$\ln \Delta_S(k_\perp^2,M^2) = -\int_{k_\perp^2}^{M^2} \frac{dq_\perp^2}{q_\perp^2}\frac{\alpha_s}{2\pi}\int_0^{1-q_\perp/M} dz \left[zP_g(z)+\sum_q P_q(z)\right]. \tag{2.7}$$

The LDC model has been implemented in an event generator which is then able to generate complete events in DIS with final state radiation added according to the dipole cascade model [41,42] and hadronization according to the Lund model [43]. One advantage of having an event generator implementation is that energy and momentum can be conserved in each emission. Since the lack of momentum conservation in the BFKL formalism is the main reason for the huge next-to-leading logarithmic corrections [44], the LDC model is therefore expected to have smaller sub-leading corrections (see [18] for a more detailed discussion on this).

The perturbative form of the uPDF needs to be convoluted with non-perturbative input PDFs, the form of which are fitted to reproduce the experimental data on F_2. This has all been implemented in the LDCMC program [45,46], and the resulting events can be compared directly to experimental data from eg. HERA. The LDC gluon uPDF can then be extracted by generating DIS events with LDCMC and measuring the gluon density as described in [11]. Due to the $k_\perp$-unordered nature of the LDC evolution, the relationship between the uPDF and the standard gluon density is different from eq. (2.3), as the integrated gluon at a scale μ^2 also receives a contribution, although suppressed, from gluons with $k_\perp > \mu$, and in [11] the following expression was obtained:

$$\begin{aligned} xg(x,\mu^2) &= G_0(x)\Delta_S(k_{\perp 0}^2,\mu^2) \\ &+ \int_{k_{\perp 0}^2}^{\mu^2}\frac{dk_\perp^2}{k_\perp^2}G(x,k_\perp^2)\Delta_S(k_\perp^2,\mu^2) + \int_{\mu^2}^{\mu^2/x}\frac{dk_\perp^2}{k_\perp^2}G(x\frac{k_\perp^2}{\mu^2},k_\perp^2)\frac{\mu^2}{k_\perp^2}, \end{aligned} \tag{2.8}$$

where $G_0(x)$ is the non-perturbative input parameterization at the cutoff scale $k_{\perp 0}$.

Note that a sharp cutoff $k_{\perp 0}$ is assumed, which could cause problems in calculations sensitive to the small-$k_\perp$ behavior. To avoid this we redefine the uPDF as

$$G(x,k_\perp^2,\mu^2) = \begin{cases} a\left(\frac{k_\perp^2}{k_{\perp 0}^2}\right)^a G_0(x)\Delta_S(k_{\perp 0}^2,\mu^2) & k_\perp < k_{\perp 0} \\ G(x,k_\perp^2)\Delta_S(k_\perp^2,\mu^2) & k_{\perp 0} < k_\perp < \mu \\ G(x\frac{k_\perp^2}{\mu^2},k_\perp^2)\frac{\mu^2}{k_\perp^2} & \mu < k_\perp < \mu/\sqrt{x} \end{cases}, \tag{2.9}$$

where a can either be set to 1, as was effectively done in [10], or to $G(x, k^2_{\perp 0})/G_0(x)$ which makes the distribution continuous across $k_{\perp 0}$. In this way we get the standard form

$$xg(x, \mu^2) = \int_0^\infty \frac{dk^2_\perp}{k^2_\perp} G(x, k^2_\perp, \mu^2), \tag{2.10}$$

and we find that our results are not very sensitive to the choice of a.

To obtain the off-diagonal densities needed for the exclusive luminosity function, we assume that a similar approximation can be made as for the KMR densities, that is, in the limit of very small x'

$$f_g^{\mathrm{LDC}}(x, x', k^2_\perp, \mu^2) \approx R_g G(x, k^2_\perp) \sqrt{\Delta_S(k^2_\perp, \mu^2)}. \tag{2.11}$$

The square root of the Sudakov form factor is used, since only one of the gluons couples to the produced Higgs at the high scale, and we could equivalently have written

$$f_g^{\mathrm{LDC}}(x, x', k^2_\perp, \mu^2) \approx R_g \sqrt{G(x, k^2_\perp, \mu^2) G(x, k^2_\perp, k^2_\perp)}. \tag{2.12}$$

Clearly this is not completely equivalent to eq. (2.5), but it is a prescription which can be used for any uPDF, not only the KMR one. Using eq. (2.12) for the KMR uPDFs (ie. using eq. (2.3)) we find that the exclusive luminosity function is underestimated by $\approx 50\%$ for a Higgs mass of 120 GeV as compared to using the more correct eq. (2.5). Hence we expect that the exclusive luminosities obtained for the LDC and also for the Jung uPFDs below, will be underestimated by approximately the same factor.

2.3.2 The Jung 2003 uPDF parameterizations

The Jung 2003 [12] unintegrated parton distribution functions are based on standard CCFM evolution and was obtained using a Monte Carlo implementing forward evolution[4]. The main difference w.r.t. LDC is, as mentioned above, that CCFM allows more emissions in the initial state, which makes it more infrared sensitive and which prevents the simple factorization into a one-scale density and a Sudakov form factor as in eq. (2.6). Another difference is that CCFM only describes gluon evolution, while in the LDC it is also possible to include quarks.

Just as for LDC, the perturbative CCFM evolution needs to be convoluted with non-perturbative input parton density, the parameters of which are determined by a fit to F_2 at small x determined at HERA.

To produce full events the Jung uPDFs may be convoluted with an appropriate off-shell matrix element (eg. $\gamma^* g^* \to \mathrm{q}\overline{\mathrm{q}}$) and the final state partons

[4]Based on the SMALLX program [47, 48].

can then be generated in a backward evolution algorithm implemented in the CASCADE program [49].

To obtain the off-diagonal densities, we use the same procedure as in LDC given by eq. (2.12),

$$f_g^{\text{Jung}}(x, x', k_\perp^2, \mu^2) \approx R_g \sqrt{G(x, k_\perp^2, \mu^2) G(x, k_\perp^2, k_\perp^2)}, \tag{2.13}$$

but note that the equivalence with eq. (2.11) does not hold since the factorization in eq. (2.6) is absent in the Jung uPDFs.

2.3.3 Summary of uPDFs

Within the three different procedures for obtaining uPDFs there are a number of optional behaviors to choose from which are summarized in table 2.1. For KMR we can choose different integrated densities to start from, but that has already been shown to only give rise to moderate differences [5]. Since the integrated PDFs have been fitted to a wide range of inclusive data, the description of such observables are trivially also reproduced by the KMR uPDFs. For less inclusive observables the situation is less clear, and as argued in the introduction there are indications that the KMR procedure will underestimate slightly the hardness of the $k_\perp$-distribution especially at small $k_\perp$. And although it has been showed to be able to reproduce inclusive jet cross sections in deeply inelastic scattering at HERA [50], it is not likely that it will be able to explain the forward jet rates with $k^2_{\perp jet} \sim Q^2$.

In [10] we used the three different options for the LDC densities introduced in [11], which differ in the splitting functions included in the evolution. The *standard* option includes all splitting functions and hence includes also the evolution of quarks. The *gluonic* and *leading* options only includes gluons and differs in that the latter only includes the leading $1/z$ and $1/(1-z)$ terms in the gluon splitting function. All give reasonable fits to HERA F_2 measurements in the region $x < 0.01$ and 1 GeV$^2 \lesssim Q^2 \lesssim 100$ GeV^2. The *standard* option also describes F_2 at higher x values where the contribution of valence quarks is more important. Clearly the *standard* option is theoretically more appealing. However, of the three options only the *leading* is able to satisfactorily describe forward jets indicating that the other two probably underestimates somewhat the hardness of the $k_\perp$-distribution of the gluon.

The Jung 2003 distributions also come with different options. Here we will use Jung-1 and Jung-2 which are similar to the LDC *leading* and *gluonic* options respectively in that the former only uses the leading terms in the gluon splitting functions, while the latter uses the full splitting function. Also these give a good description of F_2 in the fitted region of $x < 0.01$ and 1 GeV$^2 \lesssim Q^2 \lesssim 100$ GeV^2. When used in the CASCADE generator, only the Jung-1 is able to give a good

uPDF	evolution	splittings	inclusive observables	forward jets
KMR	DGLAP	full	globally good fit	probably not
standard	LDC	full	HERA F_2	no
gluonic	LDC	full gluon	HERA F_2 at small x	no
leading	LDC	singular gluon	HERA F_2 at small x	yes
Jung-1	CCFM	singular gluon	HERA F_2 at small x	yes
Jung-2	CCFM	full gluon	HERA F_2 at small x	no

Table 2.1: Summary of the different uPDFs used in this report, indicating the differences in evolution and the ability to reproduce experimental observables.

description of forward jets. Also for other observables the Jung uPDFs give results which are consistent with the ones obtained with LDC.

2.4 Results

Armed with these six uPDFs and their corresponding off-diagonal densities, we now want to see how they influence the exclusive luminosity function at LHC energies. But before we do this we want to compare the uPDFs in general to see if they at all make sense at the scales involved when considering Higgs production at LHC.

2.4.1 Inclusive Higgs production

First we look in figure 2.3 at the uPDFs relevant for producing a central exclusive 120 GeV Higgs at the LHC, i.e. $x = x_H = m_H/\sqrt{S}$ and $\mu = m_H = 120$ GeV. What is shown is the logarithmic density in $k_\perp$ and clearly there are large differences between the uPDFs both in shape and normalization. For the shape the LDC densities stick out as they do not tend to zero for $k_\perp \to \mu$. This is as expected for LDC evolution with unordered $k_\perp$-evolution. CCFM will also allow $k_\perp > \mu$, but it seems that this is more suppressed for high scales. For the shapes we can also imagine a rough agreement between *standard*, *gluonic* and Jung-2, while *leading* and Jung-1 are clearly harder. This is also expected as the absence of nonsingular terms in *leading* and Jung-1 enhances the radiation from gluons.

The difference in normalization also shows up in the predictions for inclusive Higgs production. This is shown in figure 2.4. In figure 2.4a we show the square of the integrated gluon densities, which would enter in a calculation using collinear factorization. In figure 2.4b we use the $k_\perp$-dependence of the

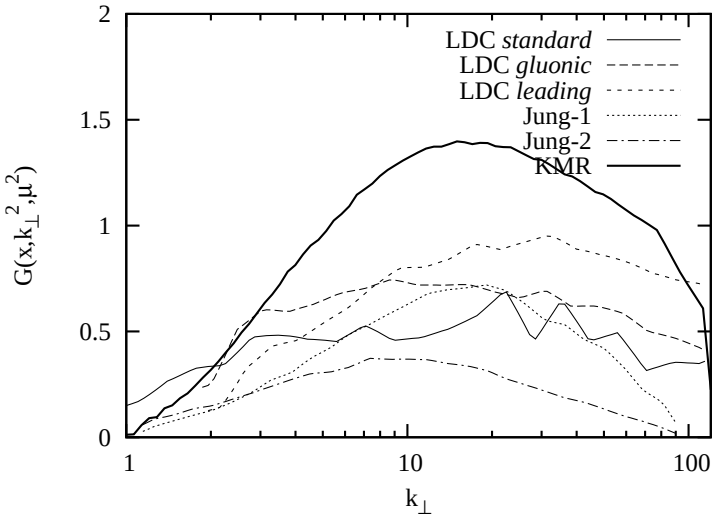

Figure 2.3: The unintegrated gluon densities as a function of $k_\perp$ for $\mu = m_H = 120$ GeV and $x = x_H = m_H/\sqrt{S} \approx 0.086$. The full line is LDC *standard*, long-dashed is LDC *gluonic*, short-dashed LDC *leading*, dotted is Jung-1, dash-dotted is Jung-2 and the thick full line is KMR. The wiggly shape of the LDC curves is due to low statistics when extracting them in [11].

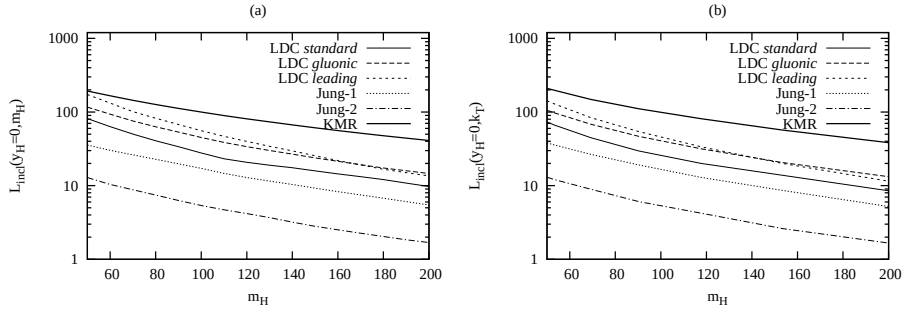

Figure 2.4: The inclusive gluon luminosity for central Higgs production as a function of m_H. (a) is simply the square of the integrated gluon density, while (b) is properly integrated over $k_\perp$ and includes the $k_\perp$-dependence of the off-shell matrix element. The lines are the same as in figure 2.3.

off-shell matrix element given in [22]:

$$\hat{\sigma}^*(m_H, \vec{k}_{\perp 1}, \vec{k}_{\perp 2}) = \hat{\sigma}_0 \cdot 2 \left(\frac{m_{\perp H}^2 \cos(\phi)}{m_H^2 + k_{\perp 1}^2 + k_{\perp 2}^2} \right)^2, \tag{2.14}$$

where $\vec{k}_{\perp 1}$ and $\vec{k}_{\perp 2}$ are the incoming transverse momenta, ϕ the angle between them, $m_{\perp H}$ the resulting transverse mass of the Higgs, and $\hat{\sigma}_0$ is the standard on-shell matrix element. This gives us the inclusive luminosity function,

$$L(m_H, y) = \int \frac{dk_{\perp 1}^2}{k_{\perp 1}^2} \frac{dk_{\perp 2}^2}{k_{\perp 2}^2} d\phi \frac{\hat{\sigma}^*}{\hat{\sigma}_0} G(x_1, k_{\perp 1}^2, \mu^2) G(x_2, k_{\perp 2}^2, \mu^2), \tag{2.15}$$

where $x_{1,2} = m_{\perp H} e^{\pm y}$ and $\mu = m_{\perp H}$. We use this scale also for KMR, since this is what was used in the case of W and Z production [17]. As seen in figure 2.4 there are small, but not insignificant differences between the collinear and off-shell versions. In fact the off-shell version takes into account some of the beyond leading order effects which are absent in our LO collinear approximation.

Clearly the differences in the inclusive luminosity are too large to be taken as genuine uncertainties in the prediction for the Higgs cross section. For such integrated quantities we expect the standard DGLAP approach implemented in KMR to give a reasonably predictive answer, and we conclude that the CCFM and LDC based densities parameterizations simply are not well enough constrained to give reasonable predictions for Higgs production at the LHC. The problem is that the Jung and LDC densities have only been fitted to F_2 at HERA which means mainly small x and Q^2, while for Higgs production we have much larger scales and through evolution we are also sensitive to the large-x behavior at lower scales, which is not well constrained.

If the LDC and Jung densities are not constrained enough to predict inclusive Higgs production at the LHC, it is unlikely that they are able to say anything predictive about exclusive Higgs production. However, although the normalization is uncertain, it may still be possible that these densities have some predictive power on the $k_\perp$-dependence of the uPDF. In figure 2.5 we show the normalized $k_\perp$-distribution of a centrally produced Higgs at the LHC as predicted by the different uPDFs, and we see that the differences are large, but not unreasonable. We find that the spectra are harder for *leading* and Jung-1 than for *standard*, *gluonic* and Jung-2, which is expected since the former only have singular terms in the gluon splitting function which allows the gluon to radiate more.

2.4.2 Exclusive Higgs production

Although we do not believe that the LDC/Jung uPDFs can be used to give any prediction for neither the inclusive or exclusive luminosity, it is not unlikely

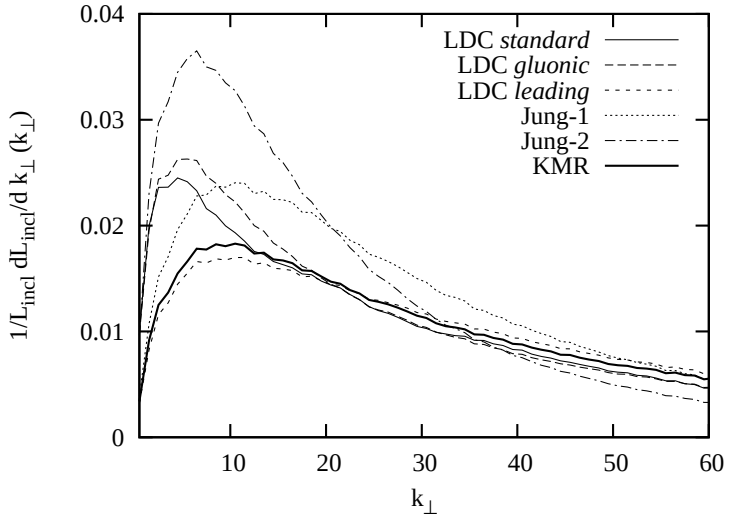

Figure 2.5: The normalized $k_\perp$-distribution of a central Higgs produced at LHC as predicted by using different uPDFs. The lines are the same as in figure 2.3.

that they actually have some predictive power on the ratio of the two. We saw above that the normalized $k_\perp$-distribution of the Higgs looks reasonable. In addition, although the uPDFs enters to the power 4 in the exclusive luminosity function, according to eqs. (2.12) and (2.13), the high scale uPDF only enters with power 2 while the other two powers depend on lower scales where the uPDFs may be better constrained. Hence, the uncertainty from the evolution to high scales may cancel in the ratio.

In figure 2.6 we show the ratio between the exclusive and the inclusive luminosity functions for fixed central rapidity as a function of m_H according to eqs. (2.1) and (2.15). There are clearly large differences, probably too large to be attributed to anything else than that the LDC and Jung densities simply are not constrained enough to give any reasonable predictions.

We know that the inclusive luminosity in eq. (2.1) is mostly sensitive to $k_\perp$-values around a couple of GeV, and we can see that the Jung-1 is much lower than Jung-2 which can be attributed to the fact that Jung-1 has a harder $k_\perp$-distribution than Jung-2 reducing the density in this region relative to higher $k_\perp$. Similarly *leading* is much lower than *standard* and *gluonic* and again the former has a harder $k_\perp$-distribution than the two latter. But since there are large differences in general between LDC and Jung we cannot say that the differences simply does not come from the fact that all these uPDFs are too unconstrained.

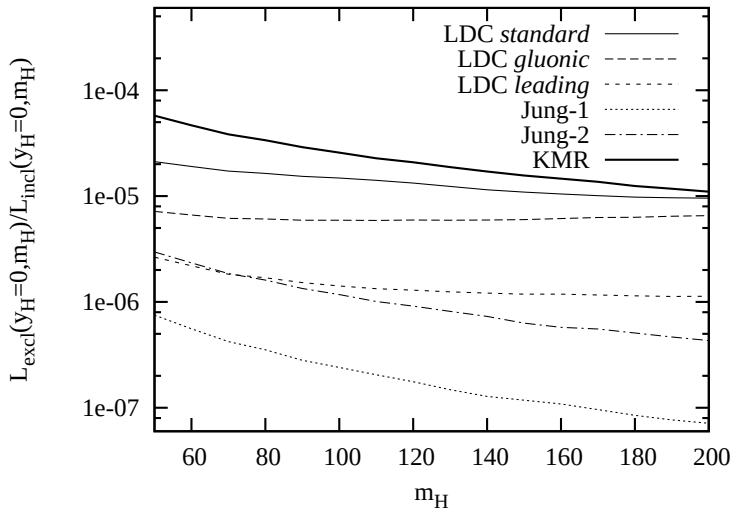

Figure 2.6: The ratio of the exclusive to inclusive luminosity function at fixed central rapidity as a function of m_H. The lines are the same as in figure 2.3.

To focus on the uncertainties in the $k_\perp$ distribution of the uPDFs, we instead concentrate only on the KMR densities, where we know that the overall normalization is well constrained, and study what happens if we simply shift the $k_\perp$ distribution slightly, while keeping the integrated PDF fixed. We know that the $k_\perp$-spectrum of the Z and W at the Tevatron can be well described by standard DGLAP based parton showers if a Gaussian intrinsic $k_\perp$ with a width of a couple of GeV is added to the incoming quarks [51]. Judging from figure 2.1 it does not seem unlikely that the shape would be better reproduced if the KMR uPDF was modified in the same way.

In figure 2.7a we see the effect of such an intrinsic $k_\perp$ on the $k_\perp$-distribution of a 120 GeV Higgs at fixed central rapidity at LHC. The effect is small, especially compared to the effects in figure 2.5. However, the effect on the exclusive luminosity is large, as can be seen in figure 2.7b. Adding a Gaussian intrinsic $k_\perp$ with a width of $\sqrt{2}$ GeV reduces the luminosity by approximately a factor 2. And we conclude that the exclusive production of Higgs at the LHC is very sensitive to the small-$k_\perp$ distribution of the unintegrated gluon.

Using such high intrinsic $k_\perp$ may seem unreasonable. However, as we explained in the beginning of section 2.3 we do not believe that this intrinsic $k_\perp$ is of purely non-perturbative origin, but comes from the unordered evolution not included in the KMR uPDF (and oduPDF). For Z production at the Tevatron in figure 2.1, an intrinsic $k_\perp$ of one or two GeV may be sufficient to get

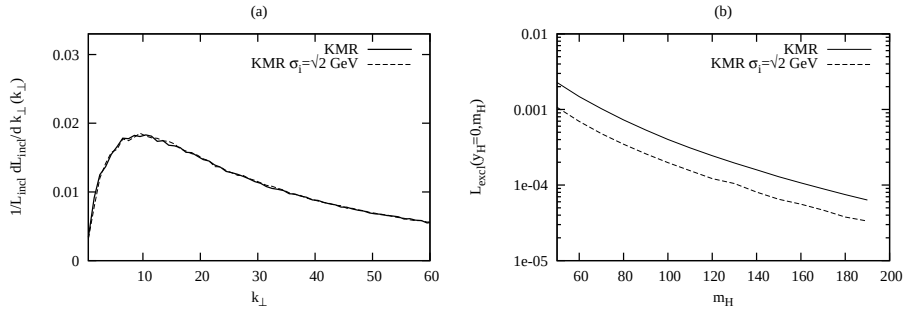

Figure 2.7: (a) The normalized $k_\perp$-distribution of a central Higgs produced at LHC as predicted by using KMR uPDFs with different Gaussian intrinsic $k_\perp$ added. (b) The exclusive luminosity function (eq. (2.1)) at fixed central rapidity as a function of m_H calculatedusing KMR uPDFs with different Gaussian intrinsic $k_\perp$ added. In both cases the full line corresponds to no intrinsic $k_\perp$ and dashed line corresponds to a Gaussian intrinsic $k_\perp$ with a width of $\sqrt{2}$ GeV.

a good fit. However, here we are dealing with incoming gluons which readiate more than quarks, and we also have smaller x, which increases the phase space for unordered evolution. To model this, it is not unreasonable to use an even higher intrinsic $k_\perp$.

2.5 Conclusions

The main conclusion of this article is a negative one. The predictive powers of the unintegrated gluon density functions as fitted only to small-x HERA data is very poor when applied to exclusive Higgs production at LHC. In fact, not even inclusive Higgs production at the LHC is well constrained with these uPDFs. However, looking at the qualitative differences between these uPDFs we can learn something about where the uncertainties come from. Here we have argued that there are problems not only with the overall normalization of the uPDFs at the high scales under consideration, but also the actual $k_\perp$-distribution at small $k_\perp$ is important. The reason is clearly visible in the $k_\perp$-integration in the exclusive luminosity function, where the main contribution comes from transverse momenta in the region of a couple of GeV.

The situation is quite different when it comes to the uPDF derived from the integrated gluon density using the KMR prescription. Here we believe the overall normalization to be well determined by the global PDF fits, and the predictions for inclusive Higgs production should be trustworthy. However, the prediction for the distribution of small $k_\perp$values is less certain and there is

evidence that eg. the $k_\perp$distribution for W and Z production at the Tevatron obtained from the KMR prescription is a bit to high for small $k_\perp$. This is consistent with the behavior of DGLAP-based parton shower approaches, which are closely related to the KMR approach, which typically need an additional gaussian intrinsic $k_\perp$ of one or two GeV to reproduce W and Z transverse momentum spectra. We have found that introducing an intrinsic $k_\perp$ in the KMR uPDF in the calculation of the exclusive luminosity function will give a clear reduction.

We will not try to use our findings to make an estimate of the uncertainties involved in the KhMR predictions for the exclusive Higgs production at the LHC and elsewhere. Clearly there is a need to find better experimental observables to constrain the (off-diagonal) unintegrated gluon density before we can make precise predictions. We do feel that the published KhMR predictions may be too high, but clearly they should give the right order of magnitude, and the prospect of using the exclusive process to study the Higgs at the LHC is still a very interesting one.

Acknowledgments

We would like to thank Hannes Jung, Valery Khoze and Misha Ryskin for valuable discussions.

References

[1] A. Schafer, O. Nachtmann, and R. Schopf *Phys. Lett.* **B249** (1990) 331–335.
[2] A. Bialas and P. V. Landshoff *Phys. Lett.* **B256** (1991) 540–546.
[3] J.-R. Cudell and O. F. Hernandez *Nucl. Phys.* **B471** (1996) 471–502, `hep-ph/9511252`.
[4] E. Levin `hep-ph/9912402`.
[5] V. A. Khoze, A. D. Martin, and M. G. Ryskin *Eur. Phys. J.* **C23** (2002) 311–327, `hep-ph/0111078`.
[6] B. Cox, J. Forshaw, and B. Heinemann *Phys. Lett.* **B540** (2002) 263–268, `hep-ph/0110173`.
[7] M. Boonekamp, A. De Roeck, R. Peschanski, and C. Royon *Acta Phys. Polon.* **B33** (2002) 3485–3490, `hep-ph/0205332`.
[8] R. Enberg, G. Ingelman, A. Kissavos, and N. Timneanu *Phys. Rev. Lett.* **89** (2002) 081801, `hep-ph/0203267`.
[9] M. A. Kimber, A. D. Martin, and M. G. Ryskin *Phys. Rev.* **D63** (2001) 114027, `hep-ph/0101348`.
[10] L. Lönnblad and M. Sjödahl *JHEP* **02** (2004) 042, `hep-ph/0311252`.

[11] G. Gustafson, L. Lönnblad, and G. Miu *JHEP* **09** (2002) 005, hep-ph/0206195.
[12] M. Hansson and H. Jung hep-ph/0309009.
[13] A. D. Martin, R. G. Roberts, W. J. Stirling, and R. S. Thorne *Eur. Phys. J.* **C4** (1998) 463–496, hep-ph/9803445.
[14] A. D. Martin and M. G. Ryskin *Phys. Rev.* **D64** (2001) 094017, hep-ph/0107149.
[15] **D0** Collaboration, B. Abbott *et al. Phys. Rev.* **D61** (2000) 032004, hep-ex/9907009.
[16] **CDF** Collaboration, T. Affolder *et al. Phys. Rev. Lett.* **84** (2000) 845–850, hep-ex/0001021.
[17] G. Watt, A. D. Martin, and M. G. Ryskin *Phys. Rev.* **D70** (2004) 014012, hep-ph/0309096.
[18] **Small x** Collaboration, B. Andersson *et al. Eur. Phys. J.* **C25** (2002) 77–101, hep-ph/0204115.
[19] **Small x** Collaboration, J. R. Andersen *et al. Eur. Phys. J.* **C35** (2004) 67–98, hep-ph/0312333.
[20] G. Gustafson and G. Miu *Eur. Phys. J.* **C23** (2002) 267–274, hep-ph/0110143.
[21] V. A. Khoze, A. D. Martin, and M. G. Ryskin *Eur. Phys. J.* **C26** (2002) 229–236, hep-ph/0207313.
[22] F. Hautmann *Phys. Lett.* **B535** (2002) 159–162, hep-ph/0203140.
[23] T. Sjostrand and M. van Zijl *Phys. Rev.* **D36** (1987) 2019.
[24] T. Sjöstrand, and others *Comput. Phys. Commun.* **135** (2001) 238–259, arXiv:hep-ph/0010017.
[25] Y. L. Dokshitzer, V. A. Khoze, and T. Sjostrand *Phys. Lett.* **B274** (1992) 116–121.
[26] R. Field, "Min-Bias and the Underlying Event at the Tevatron and the LHC." http://www.phys.ufl.edu/∼rfield/cdf/FNAL_Workshop_10-4-02.pdf. Talk presented at the Fermilab ME/MC Tuning Workshop, October 4, 2002.
[27] A. B. Kaidalov, V. A. Khoze, A. D. Martin, and M. G. Ryskin *Eur. Phys. J.* **C21** (2001) 521–529, hep-ph/0105145.
[28] A. B. Kaidalov, V. A. Khoze, A. D. Martin, and M. G. Ryskin *Eur. Phys. J.* **C31** (2003) 387–396, hep-ph/0307064.
[29] B. Andersson, G. Gustafson, and J. Samuelsson *Nucl. Phys.* **B467** (1996) 443–478.
[30] B. Andersson, G. Gustafson, and H. Kharraziha *Phys. Rev.* **D57** (1998) 5543–5554, hep-ph/9711403.
[31] M. Ciafaloni *Nucl. Phys.* **B296** (1988) 49.
[32] S. Catani, F. Fiorani, and G. Marchesini *Phys. Lett.* **B234** (1990) 339.

[33] S. Catani, F. Fiorani, and G. Marchesini *Nucl. Phys.* **B336** (1990) 18.
[34] G. Marchesini *Nucl. Phys.* **B445** (1995) 49–80, hep-ph/9412327.
[35] E. A. Kuraev, L. N. Lipatov, and V. S. Fadin *Sov. Phys. JETP* **45** (1977) 199–204.
[36] I. I. Balitsky and L. N. Lipatov *Sov. J. Nucl. Phys.* **28** (1978) 822–829.
[37] V. N. Gribov and L. N. Lipatov *Yad. Fiz.* **15** (1972) 781–807.
[38] L. N. Lipatov *Sov. J. Nucl. Phys.* **20** (1975) 94–102.
[39] G. Altarelli and G. Parisi *Nucl. Phys.* **B126** (1977) 298.
[40] Y. L. Dokshitzer *Sov. Phys. JETP* **46** (1977) 641–653.
[41] G. Gustafson *Phys. Lett.* **B175** (1986) 453.
[42] G. Gustafson and U. Pettersson *Nucl. Phys.* **B306** (1988) 746.
[43] B. Andersson, G. Gustafson, G. Ingelman, and T. Sjostrand *Phys. Rept.* **97** (1983) 31.
[44] V. S. Fadin and L. N. Lipatov *Phys. Lett.* **B429** (1998) 127–134, hep-ph/9802290.
[45] H. Kharraziha and L. Lönnblad *JHEP* **03** (1998) 006, hep-ph/9709424.
[46] H. Kharraziha and L. Lönnblad *Comput. Phys. Commun.* **123** (1999) 153.
[47] G. Marchesini and B. R. Webber *Nucl. Phys.* **B349** (1991) 617–634.
[48] G. Marchesini and B. R. Webber *Nucl. Phys.* **B386** (1992) 215–235.
[49] H. Jung *Comput. Phys. Commun.* **143** (2002) 100–111, hep-ph/0109102.
[50] G. Watt, A. D. Martin, and M. G. Ryskin *Eur. Phys. J.* **C31** (2003) 73–89, hep-ph/0306169.
[51] E. Thome hep-ph/0401121.

QCD-Supression by Black Hole Production at the LHC

Paper III

LU TP 05-25
June 2005

QCD-Supression by Black Hole Production at the LHC

Leif Lönnblad[1]
and
Malin Sjödahl[2]
Department of Theoretical Physics, Lund University,
Sölvegatan 14A, S-223 62 Lund, Sweden
and
Torsten Åkesson [3]
Department of Physics, Lund University,
Box 118, S-221 00 Lund, Sweden

JHEP **09** 019 (2005)

Abstract
Possible consequences of the production of small black holes at the LHC for different scenarios with large extra dimensions are investigated. The effects from black hole production on some standard jet observables are examined, concentrating on the reduction of the QCD cross section. It is found that black hole production of partons interacting on a short enough distance indeed seem to generate a drastic drop in the QCD cross section. However from an experimental point of view this will in most cases be camouflaged by energetic radiation from the black holes.

[1]Leif.Lonnblad@thep.lu.se
[2]Malin.Sjodahl@thep.lu.se
[3]Torsten.Akesson@hep.lu.se

3.1 Introduction

Since the theory of Large Extra Dimensions by Arkani-Hamed Dvali and Dimopoulos (ADD) first saw light in 1998 [1] there has been much discussion in the literature about the prospect for observing these large extra dimensions in colliders (see e.g. [2–6]). In particular the signal of small black holes which can be produced if the Planck scale, M_{P}, is of order TeV has been discussed. However, there is another characteristic of black hole events; the signal of no signal [7]. If we e.g. consider the dijet cross section as a function of invariant mass, $\sqrt{\hat{s}}$, then for some large invariant mass, the partons which otherwise would have undergone a QCD scattering may instead be trapped in a black hole which would lead to a falling dijet cross section as a function of invariant mass.

This argument is clearly oversimplified. Requiring a large $\hat{s}$ ensures a small extension of the interaction in beam direction. However, to form a black hole the energy has to be well confined also in transverse direction. The absolute range of a QCD interaction is set by the virtuality of the propagator, Q^2. This sets the timescale of the fluctuation and we therefore expect that interactions with a large enough virtuality takes place over a small enough space such that it is really possible to form a black hole, at least if the mass is high enough to avoid uncertainties due to quantum gravity. Hence, the dijet cross section would only fall off for high enough $E_\perp$ of the jets. Of course, some of the produced black holes may themselves decay into hard partons, filling up the jet spectrum at high masses and $E_\perp$, but we expect that spectra to look quite different from standard QCD.

For energies much larger than the Planck scale, corresponding to a Compton wavelength much smaller than the Schwarzschild radius of a black hole with that energy, we expect classical gravity to give the correct result, and a produced black hole would evaporate by emitting particles with the thermal spectra from Hawking radiation. The problem is that in colliders we would first probe the Planck scale region where quantum gravitational effects should come into play.

Approaching the Planck scale from below, where gravity starts to become important, but still is not strong enough to trap partons in black holes, we would expect gravitational scattering, to leading order simply $2 \to 2$ partonic scatterings [8–10]. As the energy increases, the gravitational scattering would transform into small black hole events. On the other hand approaching from above using the approximation of Hawking radiation we would expect the black holes to decay to *a few* particles.

In this transition region we are sensitive to unknown quantum gravity effects, but from general continuity arguments we would expect the black holes to decay into a small number of particles, preferably two. Then as the energy increases we expect the black holes to emit more and more particles looking

more and classical and, in the end for $M \gg M_{\rm P}$, we would expect the thermal spectra from Hawking radiation.

Hence, in searching for a drop in the cross section, a more complicated jet spectra will appear with increasing E_T scales. First there will be an increase of the cross section due to gravitational interactions. Then, as black holes begin to form, they are expected to decay to relatively few particles which will sometimes be identified as jets, resulting in an increase of the cross section. At high enough jet scales, however, we expect the jet cross section to completely die out, since the QCD component of the hard scattering will disappear and the black hole decay products will be softer as the black hole masses increase.

From the point of view of searching for large extra dimensions it is, of course, the increased cross section which will be easiest to see, already at scales much below where black holes are formed. But an increase in the jet cross section could be attributed to many different kinds of *new physics*, while the disappearance of Standard Model cross sections is not normally expected from new physics processes.

So, while the above mentioned effects (gravitational scattering and black hole decay products) are well worth looking for, we will devote this paper to the black hole 'eating' of the QCD cross section, and we will do this by using phenomenological event generator models. We intend to get back to the other issues in future publications.

I this paper we start with a brief review of the ADD and the, somewhat different, Randall–Sundrum (RS) [11] extra-dimension scenarios in section 3.2. The model for generating and decaying black holes is described in section 3.3, while the many theoretical uncertainties are discussed in section 3.4. In section 3.5 we present and comment on our results and in section 3.6 we make the concluding remarks and suggest further studies.

3.2 Models of large extra dimensions

3.2.1 Basics of ADD

The aim of the Arkani-Hamed Dvali and Dimopoulos (ADD) model [1] is to solve the hierarchy problem of the differences in scale between the electro-weak scale, 100 – 1000 GeV, and the scale where gravitation becomes important, 10^{19} GeV. This is done by introducing large extra dimensions with some compactification radius, R. Although the compactification radius is typically taken to be the same in all extra dimensions it could in principle vary. For distances much smaller than the size of the extra dimensions (here assumed to be the same) we will then have a Newton's law of the form [1]

$$V(r) \sim \frac{M}{M_{\rm P}^{n+2}} \frac{1}{r^{n+1}}, \tag{3.1}$$

where n is the number of extra dimensions and M_{P} the fundamental $n+4$ dimensional Planck mass. On the hand, for $r \gg R$ gravity has expanded to the full volume of the extra dimensions and we get [1]

$$V(r) \sim \frac{M}{M_{\mathrm{P}}^{n+2}} \frac{1}{R^n} \frac{1}{r}. \tag{3.2}$$

But this must equal to Newton's law in 3+1 dimensions so we conclude that the observed four dimensional Planck mass M_{P4} is (up to small volume factors)

$$M_{\mathrm{P4}}^2 \sim M_{\mathrm{P}}^{n+2} R^n. \tag{3.3}$$

This explains how we could have a fundamental Planck scale almost at the electroweak scale but an observed Planck scale at 10^{19} GeV. Requiring that the fundamental Planck scale is the same as the electroweak scale, $\sim$ TeV, gives a compactification radius of the solar system for one extra dimension. This is trivially excluded from observations. Two extra dimensions gives $R \sim$ mm, which is indirectly excluded from various cosmological and astrophysical constraints. The same holds for $R \sim$ nm, corresponding to three extra dimensions. However for four or more extra dimensions it is still possible to have a fundamental Planck scale at the order of a TeV (A more complete listing is given in e.g. [6]).

Since the black holes considered here are well within the range $r \ll R$, the Schwarzschild radius can be calculated analogous to the 3+1 dimensional case. The result is [12]

$$r_{\mathrm{Sch}} = \frac{1}{\sqrt{\pi} M_{\mathrm{P}}} \left[\frac{M_{\mathrm{BH}}}{M_{\mathrm{P}}} \frac{8\Gamma(\frac{n+3}{2})}{n+2} \right]^{\frac{1}{n+1}} \tag{3.4}$$

where Γ is the Euler gamma function.

The temperature is given by [12]

$$T = \frac{n+1}{4\pi r_{\mathrm{Sch}}}. \tag{3.5}$$

This means that more massive holes are colder. The mass dependence is however much weaker than in 4 dimensions since the radius changes less with mass. The dependence on the number of extra dimensions is dominated by the factor $n+1$ in the numerator. Hence black holes in many dimensions are hotter.

3.2.2 Basics of RS

A somewhat different model was introduced one year after the ADD-model by Randall and Sundrum [11]. In the Randall–Sundrum model, RS, which has only

one extra dimension, the metric doesn't factorize. Instead the 4 dimensional metric is multiplied by a "warp" factor which depends on the coordinate, $y \in [-\pi, \pi]$, in the fifth dimension

$$ds^2 = e^{-2|y|/l}\eta_{ij}dx^i dx^j + dy^2. \tag{3.6}$$

In the above expression η_{ij} is our normal (flat) four dimensional metric with indices running from 0 to 3 and l is the radius in the anti-de Sitter space. By taking the warp factor to be an exponent, and by assuming the gauge fields (and hence us) to live in the most shrinked slice, $y = \pi$, of the five dimensional world, a large hierarchy can be accomplished by letting gravity propagate in the full space.

We note that it has been suggested (see eg. [13]) that black holes in the RS model can only be formed on the Planck brane, which effectively means that there would be no black holes produced in a collider. However, it was also suggested [14] that the naked singularity obtained instead, could be covered on the Standard-Model brane. Such a singularity could then be produced in a collider and would evaporate as gravitational radiation into the bulk (where it is naked) at the Planck time scale. As this radiation is not detected it would appear as missing energy.

On the other hand, if a black hole is formed, but is stable on collider time scales as argued in [15], the hole could (if gauge charged) be detected. It is, however, unlikely that this would affect the signals studied here, and we have chosen to ignore this effect.

If a RS black hole is sufficiently small, such that it is not affected by the bulk curvature, the radius is still given by eq. (3.4) [16]. Hence, in either of the above mentioned cases for black holes/naked singularities in the Randall–Sundrum scenario, there will be no Hawking radiation which populates the spectra, but there will be a drop in total cross section for standard model interactions. Furthermore the cross section would be the same as in the ADD scenario with one extra dimension for small enough black holes [16].

For the purpose of this paper, we ignore all the uncertainties of whether or not black holes are possible in the RS model. In fact, we do not use any details of the RS model, but use it only as an example of a model which could produce black holes/naked singularities at large cross sections at a collider, but where the decay products of the hole would not be detectable. For our investigations this is then a best-case scenario.

3.3 Black hole production and decay

To study the effect on QCD-jets on LHC we have used PYTHIA [17] to generate the QCD events. To lowest order we here have two partons with energy

fractions, x_1 and x_2, and an invariant mass, $\hat{s} = x_1 x_2 s$, which scatter and give rise to two outgoing partons with transverse momenta, $p_\perp \approx \sqrt{Q^2}$. For this process to be trapped in a black hole, we require the whole process to be located within the Schwarzschild radius, $r_{\rm Sch}(\hat{s})$. Looking at the momenta of the incoming partons in their combined rest frame we must require that their wavelength, $\lambda_l \propto 2/\sqrt{\hat{s}}$, is less than $r_{\rm Sch}$. The corresponding requirement in the transverse direction gives the requirement: $\lambda_\perp \propto 1/p_\perp < r_{\rm Sch}$.

Of course, it is questionable if these requirements are enough, maybe the wavelengths should be *much* smaller than $r_{\rm Sch}$. In any case it is reasonable to introduce a parameter, and we will require $\lambda < r_{\rm Sch}/P$, where we use $P = 1$ as a standard value. From the longitudinal requirement we then get a minimum mass of a black hole from

$$M_{\rm min} = 2P/r_{\rm Sch}(M_{\rm min}). \tag{3.7}$$

We then get a cutoff in the standard QCD cross section, given by the following step-functions (which in general could be replaced by more smooth suppression functions):

$$\begin{aligned}\frac{d\sigma_{\rm QCD}(Q^2)}{dQ^2 d\hat{s}} = \int dx_1 dx_2 \sum_{i,j} f_i(x_1,Q^2) f_j(x_2,Q^2) \frac{\hat{\sigma}_{ij}^{\rm QCD}(\hat{s},Q^2)}{dQ^2} \times \\ \delta(\hat{s} - x_1 x_2 s) \left[1 - \Theta(\hat{s} - M_{\rm min}^2)\Theta(Q^2 - \frac{P^2}{r_{\rm Sch}^2(\hat{s})})\right]\end{aligned} \tag{3.8}$$

where the sum runs over all parton types.

Instead of the QCD process we will get black holes with the cross section

$$\begin{aligned}\frac{\sigma^{\rm BH}(\hat{s})}{d\hat{s}} = \int dx_1 dx_2 \sum_{i,j} f_i(x_1,Q^2) f_j(x_2,Q^2) \hat{\sigma}^{\rm BH}(\hat{s}) \times \\ \delta(\hat{s} - x_1 x_2 s)\Theta(\hat{s} - M_{\rm min}^2),\end{aligned} \tag{3.9}$$

where $Q = P/r_{\rm Sch}(\hat{s})$. The partonic cross section is simply given by $\hat{\sigma} = \pi r_{\rm Sch}^2$, but also here one could imagine a smooth transition and a factor in front (see section 3.4.2 below).

3.3.1 CHARYBDIS

We here describe the most important properties of the black hole event generator CHARYBDIS, which we have used to generate black holes and their decays. The complete references are [18, 19].

In CHARYBDIS two partons create a black hole according to (3.9)[1], which then decays by Hawking radiation. The procedure of the decay is such that

[1] By default the scale Q^2 is taken to be $\hat{s}$ in CHARYBDIS, but we have used the option with $Q^2 = 1/r_{\rm Sch}^2$ [5], since this gives a more continuous transition from eq. (3.8).

momentum, charge, color and baryon numbers are conserved. The decay products are chosen democratically among the standard model particles according to their degrees of freedom (color and spin). The energy of an emitted particle is taken from a Planck spectra modified with the gray-body factor of the particle. The temperature is given by eq. (3.5) where the black hole mass by default is taken to be the remaining mass of the hole, but this may be modified such that the initial temperature is kept throughout the evaporation. The motivation for keeping the initial temperature could be that it is anyhow dubious to treat the black hole as a thermalized object considering the speed of the decay [4].

One problem is that even if a black hole would be created well above the Planck scale, i.e. well within the classical regime, it would evaporate and eventually reach the Planck scale. And, although we do not know what physics looks like at the Planck scale, there must be a way of terminating the decay.

The CHARYBDIS method for this is to have a free parameter, set by the user, which gives the number of particles the hole decays to in the end, where the end can be defined either as when the black hole reaches the Planck mass, or - if it happens before - when one of the emitted particles happens to get a momentum so large that energy and momentum conservation would be violated for a two body decay.

3.4 Uncertainties

First of all it should be pointed out that the major lack in our description is the absence of a theory for quantum gravity. As we do not know what physics we will encounter at the Planck scale it is impossible to make an error estimate in the traditional sense. However we may still discuss which uncertainties will effect our results. Roughly these can be classified in three groups. The first concerns non black hole gravitational events, the second the production of black holes, and the third deals with the decay of the black holes.

Apart from the uncertainties associated with quantum gravity there is of course also an uncertainty in the QCD jet cross section. A recent evaluation of the effect from the uncertainties in the parton distribution functions, and in the NLO QCD theory, is published in [20]. In this paper a comparison is made between the calculated cross section and the Tevatron Run 1b data, and the uncertainty in the jet cross section for the LHC is estimated to be up to a factor 2.5 at a jet-ET of 5 TeV. This effect is important for many QCD and other Standard Model studies, however, it is an effect that can be neglected for the main conclusions in this paper as can be seen in e.g. figure 3.

3.4.1 Non black hole gravitational events

As mentioned in the introduction it is highly unlikely that black holes is the major gravitational effect. In the ADD scenario the amplitude for perturbative scattering is calculated in [8] and the dijet cross section is spelled out (using the Planck scale as cut of for the Kaluza Klein modes) in e.g. [9]. While the effect on jet production from gravitational scattering is large, it has the disadvantage of depending on a free parameter for the cutoff. Furthermore, as it is a perturbative expansion it cannot be applied close in the Planck region. This means that when searching for the signal of a disappearing QCD cross section, we have to do that in a spectra which is already modified by gravitational scattering in a basically unknown way. In this paper we will not further investigate this issue, and these processes are not included in the simulation. Although they should have a large effect on the cross section close to the Planck scale, we will here mostly be concerned with the behavior well beyond this scale.

3.4.2 The formation of a black hole

There are several unresolved issues concerning the formation of mini black holes. Firstly there is an uncertainty already at the classical level. The naive formula is $\sigma(M_{\mathrm{BH}}) = \pi r_{\mathrm{Sch}}^2$. Classical numerical simulations indicates that this value should be multiplied by a factor $\sim 0.7 - 3$, increasing with the number of extra dimensions [21, 22]. (For a discussion about the effects of quantum fluctuations based on wave packages, see [23, 24].) During the formation some energy may be lost as gravitational energy reducing the remaining mass for Hawking radiation [22, 25].

Secondly the factorization of the parton level cross section can be questioned since the process is inherently non-perturbative [26].

Another fundamental issue concerns the onset of black hole production. One may argue that no black holes should be formed below *roughly* the Planck scale since this is (approximately) the mass scale where the Compton wave length equals the black hole radius. This is the view point taken in eq. (3.7). Combining eq. (3.7) and eq. (3.4) we get the following relation for M_{min}

$$M_{\mathrm{min}} = M_{\mathrm{P}} \pi^{\frac{n+1}{2(n+2)}} \left[\frac{n+2}{8\Gamma(\frac{n+3}{2})} \right]^{\frac{1}{n+2}} (2P)^{(n+1)/(n+2)}. \tag{3.10}$$

We have used $P = 1$ as a standard value in this paper. Numerically the value of M_{min} is then approximately twice the Planck mass.

As for Q^2, used in the parton distribution functions when generating the black holes, we like to use the same constant in the inverse relation between length and mass as in eq. (3.7) and this is what gave us $Q = P/r_{\mathrm{Sch}}$. While, in

principle, the scale in the parton distribution functions and the minimal mass could be varied independently we have chosen not to.

One could also think of more sophisticated ways, where the nature of the force is taken into account, of relating the 'interaction distance' to momentum but that is beyond the scope of this article.

3.4.3 The decay of a black hole

It is common to divide the decay of a mini black hole into 3 different phases. In the first the asymmetry of the black hole, due to energy momentum and gauge charge distribution, is lost. This is therefore referred to as the "balding phase", and it cannot be incorporated into CHARYBDIS as the spectra of this phase is not known. Furthermore, gravitational radiation can be emitted on the brane. As this radiation is not detected it will appear as a missing energy. This radiation has also not been included in CHARYBDIS, where black holes decay only into standard model particles.

The second phase is the Hawking evaporation phase. This is the phase most accurately described by CHARYBDIS. However there are still a few discrepancies. One is that CHARYBDIS uses the spectra of a non-rotating Schwarzschild black hole, while the differential cross section would favor a Kerr hole with large angular momentum, see e.g. [5]. A rotating black hole may emit a significant part of the total radiation into the bulk [27–30]. There is not yet a consensus in the literature about how much is emitted into the bulk, but it is not inconceivable that it is as much as 50%. As large impact parameters are favored this may significantly diminish the observed radiation. Also, it may be possible for the black hole to recoil off the brane, emitting further Hawking radiation in the bulk [31, 32].

In principle the gauge charges of the black holes should also be taken into account. In the case of no extra dimensions and large black holes ($M_{\mathrm{BH}} \gg M_{\mathrm{P}}$) the suppression of charged particles due to the electrostatic potential is argued to be a small effect of a few per cent [33]. But since QCD is a significantly stronger force, and since the black holes considered here are small, the effect of QCD may be sizable. Again this is not properly included in CHARYBDIS. There is, however, effectively a bias for events with few charges since charge is conserved, implying that more events with large charge emission are thrown away.

It can also be questioned if it is correct to treat these mini black holes as thermalized considering their rapid decay [4][2]. From the point of view of this study a varying temperature is however the most conservative choice since a hotter (thermalized) hole gives fewer decay products and hence is more difficult to distinguish from the QCD dijet background. We hence chose a time varying

[2] On the other hand the decay may be slowed down as argued in [15].

temperature. An example of the difference between a varying and a non varying temperature can be found in [26].

Furthermore, it has been argued that the rapid decay may lead to the black hole becoming surrounded by a *chromosphere* of soft partons which could suppress emission of hard partons [34]. Such effects are not included in CHARYBDIS and, again, our results will be on the conservative side w.r.t. the disappearance of hard jets.

In the final phase the black hole will disappear. Even if a black hole is produced well above the Planck scale it will evaporate and eventually enter the Planck region. As previously mentioned, the CHARYBDIS treatment of this problem is to let the user chose the number of particles to which the black hole should decay in the end. For this study we have consistently used 2, partly because this gives the most continuous transition from a non black hole gravitational event, and partly since it is the most conservative assumption as it gives the largest number of very energetic particles. For the same reasons we have chosen to define the "end" of the evaporation as whatever happens first of the black hole reaching the Planck mass, or a decay product having a forbidden momentum as explained in section 3.3.1.

In total, the "mistreatment" by effectively using (Schwarzschild black hole) Hawking radiation for all phases, terminated by a two-particle decay, will lead to a maximum radiation of standard model particles and to a harder spectrum than if additional effects are taken into account. The simulation is therefore based on conservative assumptions w.r.t. searching for the disappearance of standard QCD jet production.

3.5 Results

To investigate possible effects of black-hole production on standard QCD observables, we have used the PYTHIA event generator (version 6.227) [17] for the standard QCD processes together with the CHARYBDIS program [18] for the production of black holes and their decays. We have studied predictions for the $E_\perp$ spectrum of jets and the dijet invariant mass spectrum at the LHC using a cone algorithm with a cone radius of 0.7 and a minimum $E_\perp$ of 250 GeV assuming a calorimeter with 0.1×0.1 resolution in the pseudo rapidity interval $|\eta| < 2.5$.

PYTHIA was set to generate standard QCD events using CTEQ5L parton distributions [35], but for the extra dimensions scenarios, the differential cross section was cut off according to eq. (3.8).

Black holes were produced according to eq. (3.9) and decayed with the CHARYBDIS program, while additional parton showering was handled by

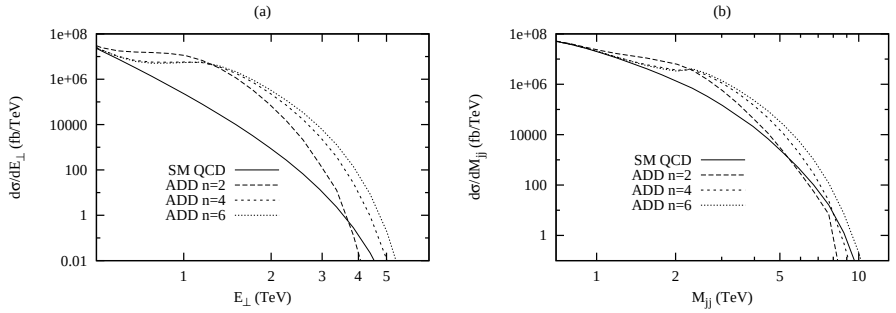

Figure 3.1: Differential jet cross sections for the ADD scenario with $M_{\mathrm{P}} = 1$ TeV and $P = 1$ for two (long-dashed line), four (short-dashed) and six (dotted) extra dimensions, compared with the Standard Model prediction (full line). (a) shows the cross section as a function of the transverse energy of the hardest jet and (b) the cross section as a function of the invariant mass of the two hardest jets in an event.

PYTHIA.[3] Apart from the the scale in the parton distribution functions, the varying Planck mass, minimal mass, number of extra dimensions and the decision of when to terminate the decay, the default settings of CHARYBDIS were used.

In figure 3.1 the differential jet cross section is shown as a function of the transverse energy of the hardest jet, and the dijet cross section as a function of dijet invariant mass for the two hardest jets, for two, four and six extra dimensions (ADD), $M_{\mathrm{P}} = 1$ TeV and $P = 1$ (corresponding to $M_{\mathrm{min}} = 2.24$ TeV). Studying the case of two extra dimensions we find that, although the main effect is an increase in cross section due to the production of black holes in the regions just above the Planck mass, the spectra do indeed fall below the standard model spectra for very large $E_\perp$ and invariant masses. The effect should be clearly visible at the LHC where we would e.g. expect over a hundred events with M_{jj} above 8.5 TeV with an integrated luminosity of 100 fb^{-1} (corresponding to one year of running at 10^{34} $cm^{-2}s^{-1}$) for standard QCD, while with black hole production there would be basically none. In the $E_\perp$ spectrum the effect would be harder to see, and only a couple events expected above 4 TeV from standard QCD would disappear in a $n = 2$ ADD scenario.

However, two extra dimensions is excluded from observations, and if we increase the number of extra dimensions the temperature rises according to eq. (3.5). As seen in figure 3.1 this results in a drastic increase in the number of hard jets, making it seem rather unlikely that we will observe the QCD drop

[3]Hadronization was not included in the simulations presented here, but we have checked that our results do not change if hadronization is added.

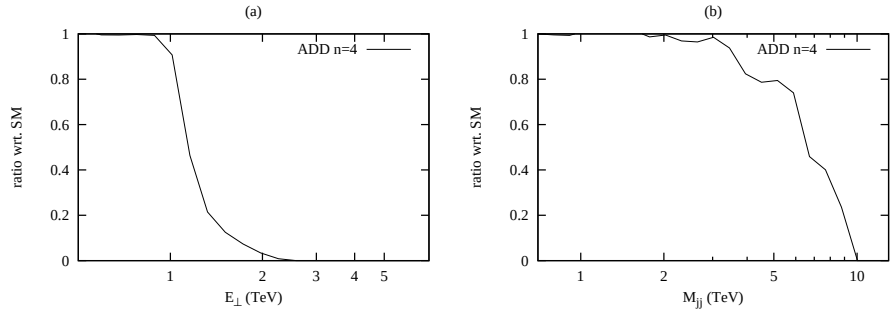

Figure 3.2: The number of pure QCD events for 4 extra dimensions, $M_{\mathrm{P}} = 1$ and $P = 1$ divided by the number of QCD events in a Standard Model world as a function of (a) the transverse energy of the hardest jet and (b) the invariant mass of the two hardest jets in an event.

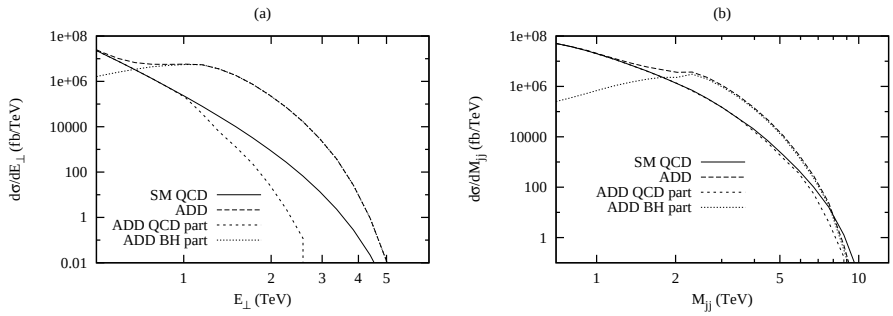

Figure 3.3: Differential jet cross sections for the ADD scenario with $M_{\mathrm{P}} = 1$ TeV and $P = 1$ for four extra dimensions (long-dashed line), compared with the Standard Model prediction (full line). Also shown are the contributions from events with (dotted line) and without (short-dashed line) black holes. (a) shows the cross section as a function of the transverse energy of the hardest jet and (b) the cross section as a function of the invariant mass of the two hardest jets in an event.

at LHC without further efforts to distinguish QCD and black hole jets. But in principle it is an enormous effect. This can be illustrated by plotting the ratio of QCD events in an ADD world, with e.g. 4 extra dimensions, and QCD events in a four dimensional standard model world. This is shown in figure 3.2.

The QCD drop can also be clarified by decomposing the contribution to the cross section of standard events and black hole decay products as in figure 3.3. As expected the 'shoulder' in the spectra is completely dominated by the black

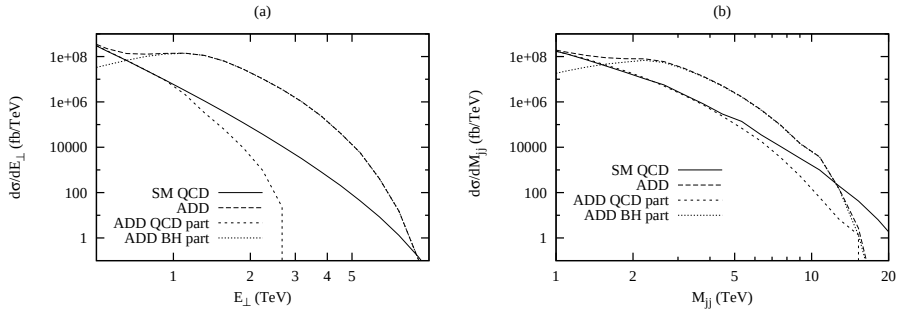

Figure 3.4: Differential jet cross sections at a 40 TeV pp-collider for the ADD scenario with $M_{\mathrm{P}} = 1$ TeV and $P = 1$ for four extra dimensions (long-dashed line), compared with the Standard Model prediction (full line). Also shown are the contributions from events with (dotted line) and without (short-dashed line) black holes. (a) shows the cross section as a function of the transverse energy of the hardest jet and (b) the cross section as a function of the invariant mass of the two hardest jets in an event.

hole decay products. The drop in the QCD cross section is also seen, however, from an experimental point of view it is completely hidden behind the black hole decay products.

Eventually, for high enough energies the QCD drop must appear, since light black holes cannot decay to particles with energy greater than half the black hole mass, and heavier black holes typically will produce less energetic decay products as the temperature is lower.

However, as seen in figure 3.4 for a imagined 40 TeV *pp*-collider it turns out that the (large) probability for producing a heavy black hole, which then emits an unlikely heavy (Boltzmann suppressed) particle, dominates over the QCD cross section for rather large transverse energies and invariant dijet masses.

The effect of varying P, and hence also the minimal mass M_{min}, is shown in figure 3.5 where $P = 1$ for $M_{\mathrm{P}} = 1$ TeV (giving $M_{\mathrm{min}} = 2.24$ TeV) is compared to $P = 1/2$ for $M_{\mathrm{P}} = 2$ TeV ($M_{\mathrm{min}} = 2.51$ TeV) and $P = 1$ for $M_{\mathrm{P}} = 2$ TeV ($M_{\mathrm{min}} = 4.48$ TeV). Comparing the lines which have the same M_{P} but differ in P and M_{min} we see that the extra black holes which are produced if M_{min} is lowered, contribute to the low energy end of the spectrum despite the fact that they are hotter. This is because the emitted quantum must have an energy less than half the black hole energy. On the other hand, the high energy end of the spectra, where the total cross section eventually would fall below the standard model QCD cross section, is left more or less unaffected. This means that the choice of M_{min} is not particularly important for determining the point where the cross section drop would be observed. Unfortunately this does not imply

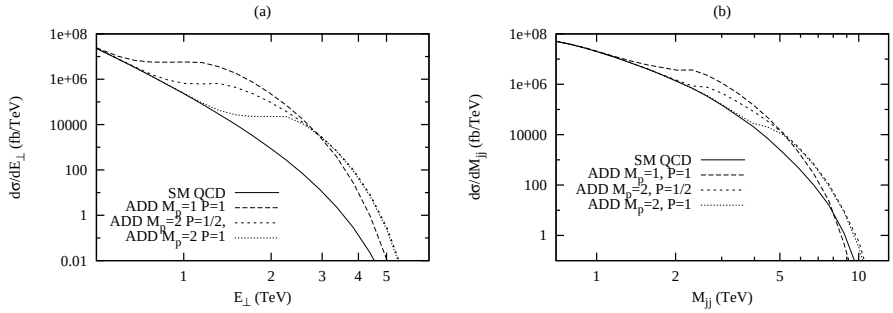

Figure 3.5: Differential jet cross sections for the ADD scenario for four extra dimensions with $M_{\rm P} = 1$ TeV and $P = 1$ (long-dashed line), $M_{\rm P} = 2$ TeV and $P = 1$ (short-dashed) and $M_{\rm P} = 2$ TeV and $P = 1/2$ (dotted line) compared with the Standard Model prediction (full line). (a) shows the cross section as a function of the transverse energy of the hardest jet and (b) the cross section as a function of the invariant mass of the two hardest jets in an event.

that it is insensitive to Planck scale physics as recoil effects on the black hole emitting the energetic quanta cannot be neglected.

An increased Planck mass results in a later onset of black hole production and therfore less particles in the low energy end of the black hole decay spectrum. On the other hand there are more particles in the high energy end as the temperature is increased according to eq. (3.5). For a higher Planck mass it would therfore, as expected, be more difficult to observe the QCD drop.

One could try to eliminate the extremely energetic black hole events with a thrust cut to regain the QCD drop, but it does not work particularly well since the rest of the black hole which emitted the energetic quanta will have a large momentum in opposite direction. The event will thus (from a clustering point of view) look like a dijet event. Another option is to try a smaller cone radius. This has a significant effect in the case of 2 extra dimensions, making the drop clearly visible also in the $E_\perp$-spectrum, but turns out to be less effective in the higher dimensional cases since the black holes there are hotter.

The overall impression for the ADD scenario is thus that it will be hard to observe the QCD drop without further efforts to discriminate between the QCD and black hole radiation. On the other hand we have made the case worse than it may be in several ways. We have ignored that some energy will be carried away by invisible gravitational radiation, thus reducing the observed background from black hole decay products, and we have maximized the number of energetic particles by choosing a varying temperature and a 2-body decay in the end of the evaporation.

If the black holes do not decay on collider timescales, or if a naked singu-

larity which decays in the bulk is formed, as may be the case in the Randall–Sundrum scenario, there is no radiation to camouflage the QCD cross section disappearance. Its disappearance may then be a key signal, as shown in figure 3.6.

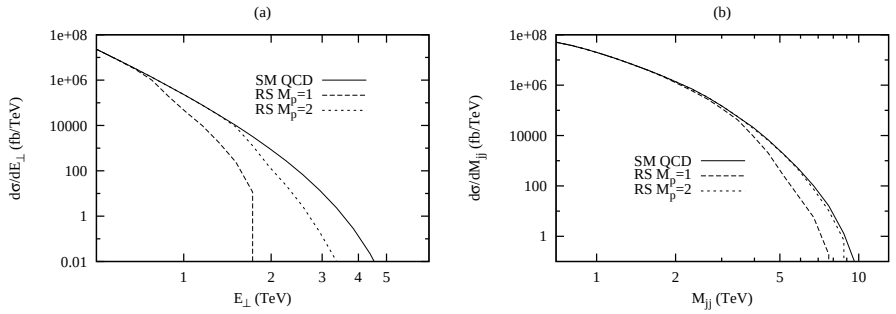

Figure 3.6: Differential jet cross sections for the RS scenario with $P = 1$ and $M_{\mathrm{P}} = 1$ TeV (long-dashed line) and $M_{\mathrm{P}} = 2$ TeV (short-dashed line), compared with the Standard Model prediction (full line). (a) shows the cross section as a function of the transverse energy of the hardest jet and (b) the cross section as a function of the invariant mass of the two hardest jets in an event.

3.6 Conclusion and outlook

We have seen that black hole production of partons interacting on a short enough distance indeed seem to generate a drastic drop in the QCD cross section at LHC. However if the created black holes decay on collider timescales as expected in the ADD scenario, this drop will (naively) be completely hidden by the black hole decay products even for rather large transverse energy/invariant dijet mass. On the other hand, if the black holes are stable on collider time scales there is no Hawking radiation to camouflage the QCD drop and the absence of QCD events may be a key signal.

The point where the extra-dimensional black hole plus standard model cross section falls below the four dimensional standard model cross section is sensitive to the number of extremely energetic quanta emitted by small black holes and this depends on physics in the Planck region. While we cannot exclude (due to the large theoretical uncertainties) that a drop below the standard model QCD-cross section will be observed at the LHC, it is unlikely (at least in this simple form) to be important for the identification of the ADD model. Inventing mores sophisticated methods for distinguishing the black hole jets from other jets may on the other hand be well worth the effort.

Finally we point out that it is, in a sense, unphysical to consider standard model and black hole events without taking gravitational, non black hole, events into account. Surely the gravitational events will play a major role close to the Planck mass. For scatterings with momentum transfer far above the plank mass we expect black hole events to dominate. We intend to further investigate the effect of gravitational interaction in future publications.

References

[1] N. Arkani-Hamed, S. Dimopoulos, and G. R. Dvali *Phys. Lett.* **B429** (1998) 263–272, `hep-ph/9803315`.

[2] I. Antoniadis, N. Arkani-Hamed, S. Dimopoulos, and G. R. Dvali *Phys. Lett.* **B436** (1998) 257–263, `hep-ph/9804398`.

[3] R. Emparan, G. T. Horowitz, and R. C. Myers *Phys. Rev. Lett.* **85** (2000) 499–502, `hep-th/0003118`.

[4] S. Dimopoulos and G. Landsberg *Phys. Rev. Lett.* **87** (2001) 161602, `hep-ph/0106295`.

[5] S. B. Giddings and S. Thomas *Phys. Rev.* **D65** (2002) 056010, `hep-ph/0106219`.

[6] P. Kanti *Int. J. Mod. Phys.* **A19** (2004) 4899–4951, `hep-ph/0402168`.

[7] T. Banks and W. Fischler `hep-th/9906038`.

[8] T. Han, J. D. Lykken, and R.-J. Zhang *Phys. Rev.* **D59** (1999) 105006, `hep-ph/9811350`.

[9] D. Atwood, S. Bar-Shalom, and A. Soni *Phys. Rev.* **D62** (2000) 056008, `hep-ph/9911231`.

[10] M. A. Doncheski *eConf* **C010630** (2001) P314, `hep-ph/0111149`.

[11] L. Randall and R. Sundrum *Phys. Rev. Lett.* **83** (1999) 3370–3373, `hep-ph/9905221`.

[12] R. C. Myers and M. J. Perry *Ann. Phys.* **172** (1986) 304.

[13] D. Karasik, C. Sahabandu, P. Suranyi, and L. C. R. Wijewardhana *Phys. Rev.* **D69** (2004) 064022, `gr-qc/0309076`.

[14] D. Karasik, C. Sahabandu, P. Suranyi, and L. C. R. Wijewardhana *Phys. Rev.* **D70** (2004) 064007, `gr-qc/0404015`.

[15] R. Casadio and B. Harms *Int. J. Mod. Phys.* **A17** (2002) 4635–4646, `hep-th/0110255`.

[16] L. A. Anchordoqui, H. Goldberg, and A. D. Shapere *Phys. Rev.* **D66** (2002) 024033, `hep-ph/0204228`.

[17] T. Sjöstrand, and others *Comput. Phys. Commun.* **135** (2001) 238–259, arXiv:hep-ph/0010017.

[18] C. M. Harris, P. Richardson, and B. R. Webber *JHEP* **08** (2003) 033, hep-ph/0307305.

[19] C. M. Harris and P. Kanti *JHEP* **10** (2003) 014, hep-ph/0309054.

[20] D. Stump *et al. JHEP* **10** (2003) 046, hep-ph/0303013.

[21] H. Yoshino and Y. Nambu *Phys. Rev.* **D67** (2003) 024009, gr-qc/0209003.

[22] H. Yoshino and V. S. Rychkov hep-th/0503171.

[23] S. B. Giddings and V. S. Rychkov *Phys. Rev.* **D70** (2004) 104026, hep-th/0409131.

[24] V. S. Rychkov hep-th/0410041.

[25] V. Cardoso, E. Berti, and M. Cavaglia hep-ph/0505125.

[26] C. M. Harris *et al.* hep-ph/0411022.

[27] D. N. Page *Phys. Rev.* **D14** (1976) 3260–3273.

[28] V. P. Frolov and D. Stojkovic *Phys. Rev.* **D67** (2003) 084004, gr-qc/0211055.

[29] V. P. Frolov and D. Stojkovic *Phys. Rev.* **D68** (2003) 064011, gr-qc/0301016.

[30] D. Stojkovic *Phys. Rev. Lett.* **94** (2005) 011603, hep-ph/0409124.

[31] V. P. Frolov and D. Stojkovic *Phys. Rev.* **D66** (2002) 084002, hep-th/0206046.

[32] V. P. Frolov and D. Stojkovic *Phys. Rev. Lett* **89** (2002) 151302, hep-th/0208102.

[33] D. N. Page *Phys. Rev.* **D16** (1977) 2402–2411.

[34] L. Anchordoqui and H. Goldberg *Phys. Rev.* **D67** (2003) 064010, hep-ph/0209337.

[35] **CTEQ** Collaboration, H. L. Lai *et al. Eur. Phys. J.* **C12** (2000) 375–392, hep-ph/9903282.

Gravitational Scattering in the ADD Model Revisited

Paper IV

LU TP 06-10
August 2006

Gravitational Scattering in the ADD Model Revisited

Malin Sjödahl[1]
Department of Theoretical Physics, Lund University,
Sölvegatan 14A, S-223 62 Lund, Sweden

Submitted to EPJC

Abstract
It is argued that the assumption that the standard model particles live on a finite brane in the ADD model does in itself imply a finite propagator for virtual Kaluza–Klein mode exchange. The part of the propagator relevant for large distance scattering is cut-off-independent for scattering at distances large compared to the brane width. The matrix element corresponding to this part can also, at least for an odd number of extra dimensions, be Fourier transformed to position space, giving back the extra-dimensional version of Newton's law. For an even number of extra dimensions a corresponding result is found by requiring that Newton's law should be recovered.

[1]Malin.Sjodahl@thep.lu.se

4.1 Introduction

The ADD model [1–3] aims at explaining the hierarchy between the weak scale and the Planck scale. This is done by introducing extra, compactified, dimensions in which only gravity is allowed to propagate. At distances small compared to the compactification radius, but large compared to the Planck length and the thickness of the brane, the gravitational force will be enhanced and behave essentially as in a $4+n$ dimensional world, where n is the number of extra dimensions. If the extra dimensions are large enough, the enhanced gravitational force opens up for the possibility of gravitational scattering and black hole production at present, or soon upcoming, collider experiments.

To quantify the amount of gravitational interaction, the theory was put on a perturbative field-theoretical basis in [4, 5]. The perturbations of the extra dimensional part of the metric enter as massive Kaluza–Klein (KK) modes in the Lagrangian. When these modes are internal states they have to be summed over which lead the authors of [4, 5] to the following divergent propagator integral

$$\sum_{\bar{l}} \frac{1}{-m_{\bar{l}}^2 + k^2} \sim R^n \int \frac{m^{n-1}}{-m^2 + k^2} dm. \tag{4.1}$$

Here $\bar{l}$ enumerates the allowed momenta, $m_{\bar{l}}$, in the extra dimensions, m is the absolute value of $m_{\bar{l}}$, R is the compactification radius[1] and k^2 is the momentum squared of the $3+1$-dimensional part of the propagator. (This object, without Lorentz structure, will somewhat sloppily be referred to as a propagator.) For the above approximation to be valid, the compactification radius of the extra dimensions clearly have to be large compared to other relevant length scales. As it stands, the integral eq. (4.1) is explicitly divergent for $n \geq 2$. However, when arriving at eq. (4.1), the physical condition that the standard model fields are confined to the brane was not taken into account.

Instead the problem of the divergent integral was approached in [4, 5] by introducing a cut-off M_s, argued to be of the same order of magnitude as the fundamental Planck scale, M_p. (A physical motivation for a cut-off was later considered in [6, 7] by the introduction of a brane tension, and various mathematical shapes of cut-offs have been discussed in [8]). For $n > 2$, and exchanged momentum small compared to M_s, the Kaluza–Klein summation of t-channel (or s-channel) amplitudes then gave a propagator behaving as

$$\frac{1}{n-2} R^n M_s^{n-2} \sim \frac{1}{G_{N(4)}} \frac{1}{n-2} \frac{M_s^{n-2}}{M_p^{n+2}} \tag{4.2}$$

[1] R is here used to denote the compactification radius, rather than the compactification circumference.

where $G_{N(4)}$ is the ordinary 3+1-dimensional Newton's constant related to R and M_p via $G_{N(4)}^{-1} \approx R^n M_p^{n+2}$. (In [4] M_p and M_s are taken to be the same in the calculation of the propagator.) In the Born approximation the cross section would then be given by [9]

$$\frac{d\sigma}{dz} \sim \frac{s^3}{(n-2)^2} \left(\frac{M_s^{n-2}}{M_p^{n+2}} \right)^2 F(\text{spin}, z), \tag{4.3}$$

where z is the cosine of the scattering angle in the center of mass system, s the squared sum of the incoming particles momenta and F a function taking spin dependence into account.

A different approach to calculating the influence of the Kaluza–Klein modes, was presented in [2] when deriving Newton's law. In this case the summation of Kaluza–Klein modes was performed in the classical limit, *after* Fourier transforming our normal momentum space to coordinate space [2], giving rise to the expected $3+n$ dimensional version of Newton's law,

$$\frac{V(r)}{m_1 m_2} \sim \int_{-\infty}^{\infty} d\overline{m} \int_{-\infty}^{\infty} d\overline{k} \frac{1}{\overline{m}^2 + \overline{k}^2} e^{i\overline{k}\cdot\overline{r}} \sim \int_0^{\infty} dm m^{n-1} \frac{e^{-mr}}{r} \sim \frac{1}{r^{n+1}} \tag{4.4}$$

where $r = |\overline{r}|$. Eq. (4.2) and eq. (4.4) may seem to contradict each other. Especially, eq. (4.2) gives the same form of the gravitational scattering potential regardless of the number of extra dimensions, namely a δ-function at $\overline{r} = 0$. Equation (4.4), on the other hand, gives different scattering behavior for different number of extra dimensions. We will see in the next section that k-dependent correction terms to eq. (4.2) are important for the classical limit as the $1/r^{n+1}$-potential can not be recovered by Fourier transforming the non-relativistic matrix element corresponding to eq. (4.2) to ordinary position space.

We will later implement the physical condition that standard model fields live on a brane via a Fourier transform. To be consistent with this we should really add a factor $i\overline{y} \cdot \overline{m}$, where $\overline{y}$ is the coordinate in the extra dimensions, in the exponent and then integrate over a narrow distribution in $\overline{y}$. However, as the $\overline{m}$ integral is explicitly convergent when evaluated after the $\overline{k}$ integral as in eq. (4.4), the addition of $i\overline{y} \cdot \overline{m}$ in the exponent would not change the result in the classical limit when the distance is much larger than the brane thickness. In essence, what will be done in this paper is nothing but calculating eq. (4.4) in the reversed order, starting with the m-integral.

The Fourier transform to position space w.r.t. the extra dimensions is performed (for an odd number of extra dimensions) in section 4.2. In section 4.3 we show that the parts of the propagator relevant for the large distance limit can be further Fourier transformed to position space w.r.t. our normal dimensions giving back the extra-dimensional version of Newton's law. We also

find a corresponding "KK-summed propagator" for an even number of extra dimensions by requiring that Newton's law should be recovered. Finally we summarize and conclude in section 4.4.

4.2 Fourier transformation to position space in the extra dimensions

As the standard model fields are assumed to live on the brane, any measurement of gravitational scattering will be in position space w.r.t. the extra dimensional coordinates and in momentum space w.r.t. our ordinary coordinates. We therefore search for the corresponding propagator. To find it we introduce a coordinate $\overline{y}$, with absolute value y, in the extra dimensions. Later we will be interested in a narrow distribution around $\overline{y} = \bar{0}$ corresponding to a small extension of the standard model fields into the bulk. Searching for a propagator which is in position space w.r.t. the extra dimensions also corresponds to imposing the condition of locality. As the standard model fields live on a brane they will only be sensitive to KK modes which overlap with the brane.

Fourier transforming eq. (4.1) to position space with respect to the extra dimensions now gives for $n \geq 3$

$$\begin{aligned} D(k,y) &= \sum_{\overline{l}} \frac{1}{-m_{\overline{l}}^2 + k^2} e^{i\overline{l}\cdot\overline{y}/R} \qquad (4.5) \\ &\approx R^n S_{n-1} \int_0^\pi \sin(\theta)^{n-2} d\theta \int_0^\infty dm \frac{m^{n-1}}{-m^2+k^2} e^{imy\cos(\theta)} \\ &= R^n S_{n-1} \int_{-1}^1 d\cos(\theta)(1-\cos^2(\theta))^{(n-3)/2} \int_0^\infty dm \frac{m^{n-1} e^{imy\cos(\theta)}}{-m^2+k^2} \end{aligned}$$

where S_{n-1} is the surface of a unit sphere in $n-1$ dimensions (from integration over the angles on which the integrand does not depend) and the factor R^n comes from the density of Kaluza–Klein modes. For an odd number of extra dimensions this can, with $x = \cos(\theta)$, be rewritten as

$$\begin{aligned} D(k,y) &= R^n S_{n-1} \int_{-1}^1 dx (1-x^2)^{(n-3)/2} \\ &\quad \int_0^\infty dm \left(- \sum_{j=0}^{(n-3)/2} m^{n-3-2j} k^{2j} + \frac{k^{n-1}}{-m^2+k^2} \right) e^{imyx}. \qquad (4.6) \end{aligned}$$

From this form we see that the terms in the sum are either k-independent, and therefore correspond to δ-functions at $\overline{r} = \bar{0}$ in ordinary position space,

or are even powers of k and correspond to derivatives of the δ-function. (This is easily seen by Fourier transforming from k-space to r-space component by component.) These terms are therfore localized to distance zero in ordinary space and can not be important in the classical region, where wave packages are well separated and do not overlap.

If we imagine the brane to have a finite narrow distribution (such as a Gaussian) around $\overline{y} = \bar{0}$ in the extra dimensions, the $1/r^{n+1}$-law will be modified at distances similar to the brane thickness. The terms in the sum will then give (possibly) large but finite contributions. These terms, which depend on the extension of the brane, are important when the wave functions overlap and will then give an interaction similar to that from eq. (4.3) (until the unitarity condition sets in) but they will not be further investigated here. Instead we concentrate on the term relevant for large distance and large energy scattering (the classical limit) coming from the last term in parentheses in eq. (4.6). The contribution to the integral from this term, called $\hat{D}(k)$, is easily evaluated in the limit of small y (corresponding to a narrow distribution) and is given by

$$\hat{D}(k) \approx R^n \frac{\pi S_n}{2} \left(\sqrt{-k^2}\right)^{n-2} i^{n+1}. \tag{4.7}$$

It is easy to show that this result holds also for one extra dimension, and therefore for any odd number of extra dimensions.

For an even number of extra dimensions the propagator in eq. (4.5) is also turned finite by (for example) a Gaussian distribution in y-space corresponding to a Gaussian distribution in m-space. In this case there is however no finite term which directly corresponds to the classical potential.

The expression eq. (4.7), which is in momentum space with respect to our normal dimensions, and in position space with respect to the extra dimensions, has the following properties:

i It gives back Newton's law, eq. (4.4). This will be demonstrated in section 4.3.

ii It depends on the number of extra dimensions in a non-trivial way, such that, as the gravitational force increases faster with smaller distance in position space for many extra dimensions, this is reflected in a faster increase with larger k in momentum space.

iii It does not depend on an arbitrary cut-off as long as the cut-off ($\approx 1/$(brane thickness)) is much larger than k. This implies that it is not dominated by metric perturbations of the scale $1/M_p$ for scatterings corresponding to much larger distances. This is the case for eq. (4.1) integrated to $M_s \approx M_p$.

iiii It is the part of the propagator which is argued to contribute to the all order exponentiated eikonalized amplitude in [10] (apart from what appears to be a sign misprint).

4.3 Fourier transformation to position space in our ordinary dimensions

To obtain the 3+1+n dimensional version of Newton's law we take the classical limit such that the energy is given by the mass, multiply with the coupling constant $4\pi G_{N(4)}$ and Fourier transform eq. (4.7) to position space. Using $\kappa = |\overline{k}|$ we have

$$\begin{aligned}\frac{V(r)}{m_1 m_2} &= 4\pi G_{N(4)} R^n \frac{\pi S_n}{2} i^{n+1} \frac{S_3}{2} \frac{1}{(2\pi)^3} \int_{-1}^{1} d\cos(\theta) \int_0^\infty d\kappa \kappa^2 \kappa^{n-2} e^{i\kappa r \cos(\theta)} \\ &= 4\pi G_{N(4)} R^n \frac{\pi S_n S_3}{4(2\pi)^3} i^{n+1} \frac{1}{ir} \int_0^\infty d\kappa \kappa^{n-1} (e^{i\kappa r} - e^{-i\kappa r}). \end{aligned} \tag{4.8}$$

This can be evaluated by introduction of a small convergence factor

$$\begin{aligned}\frac{V(r)}{m_1 m_2} &= 4\pi G_{N(4)} R^n \frac{\pi S_n S_3}{4(2\pi)^3} i^{n+1} \frac{1}{ir} \times \\ &\quad \lim_{\epsilon \to 0} \left(\frac{d}{dr}\right)^{n-1} \int_0^\infty d\kappa \left[\frac{e^{i\kappa r - \epsilon\kappa}}{i^{n-1}} - \frac{e^{-i\kappa r - \epsilon\kappa}}{(-i)^{n-1}}\right] \\ &= G_{N(4)} R^n \frac{\pi S_n (4\pi)^2}{4(2\pi)^3} i^{n+1} \frac{1}{ir} \frac{1}{i^{n-1}} \times \\ &\quad \lim_{\epsilon \to 0} \left(\frac{d}{dr}\right)^{n-1} (-1) \left[\frac{-i}{r + i\epsilon} - \frac{i(-1)^{n-1}}{r - i\epsilon}\right] \\ &= -G_{N(4)} R^n S_n \frac{\Gamma(n)}{r^{n+1}}, \end{aligned} \tag{4.9}$$

where the last step only is valid for an odd number of extra dimensions. This is the same result as in [2] (apart from a minus sign which is neglected in [2], the gravitational potential must be attractive), i.e. gravitational scattering enhanced by the large density of Kaluza–Klein modes, corresponding to a large coupling constant.

The strategy so far has been to start from the propagator and argue that we can get back Newton's law. Clearly this argument could be turned upside down. Using the result in eq. (4.4) [2], we could alternatively search for the "propagator" giving the expected potential when Fourier transformed to position space. Again this would give us a term of the form k^{n-2} for an odd number of extra dimensions. For an even number of extra dimensions we settle with this argument, showing that the term

$$\hat{D}(k) \approx R^n \frac{S_n}{2} (-1)^{\frac{n-2}{2}} \left(\sqrt{-k^2}\right)^{n-2} \ln(-k^2) \tag{4.10}$$

gives the desired form. The logarithm of a dimension-full quantity may seem disturbing. Replacing it by $\ln(-k^2/k_0^2)$ for some k_0 we note that the $k^{n-2}\ln(k_0^2)$-term would only contribute at $\overline{r}=0$ when Fourier transformed to position space. This means that, just as in the case of an odd number of extra dimensions, we have a local interaction which depends on properties of the brane. We also note that, just as for odd n, requiring the standard model particles to live on a thin bane by introducing a (narrow) distribution in y-space we would have a (wide) distribution in m-space giving a (large) finite value for the propagator.

Fourier transforming the non-relativistic version of eq. (4.10) to position space we find the potential

$$\begin{aligned}\frac{V(r)}{m_1m_2} &= 4\pi G_{N(4)}R^n\frac{S_n}{2}(-1)^{\frac{n-2}{2}}\frac{S_3}{2}\frac{1}{(2\pi)^3}\times \\ &\int_{-1}^{1}d\cos(\theta)\int_0^\infty d\kappa\kappa^2\kappa^{n-2}\ln(\kappa^2)e^{i\kappa r\cos(\theta)} \\ &= G_{N(4)}R^n\frac{S_n(4\pi)^2}{4(2\pi)^3}\frac{(-1)^{\frac{n-2}{2}}}{ir}\int_0^\infty d\kappa\kappa^{n-1}\ln(\kappa^2)2i\sin(\kappa r).\end{aligned} \tag{4.11}$$

For n even we get after evaluating the integral [11]

$$\frac{V(r)}{m_1m_2} = -G_{N(4)}R^nS_n\frac{\Gamma(n)}{r^{n+1}}. \tag{4.12}$$

This is the multidimensional version of Newton's law. We also note that eq. (4.10) is the part of the propagator argued to contribute to the all order eikonalized amplitude in [10].

4.4 Conclusion and outlook

We have shown that requiring the standard model particles to live on a finite brane, leads to a convergent result for the KK propagator. The part of the propagator which is seen to be relevant for large energy and large distance scattering can also (at least for an odd number of extra dimensions) be Fourier transformed to position space w.r.t. our ordinary coordinates, giving back Newton's law. For an even number of extra dimensions we have found a similar expression by requiring that we should get back Newton's law in the classical limit, when all coordinates are Fourier transformed to position space.

It should be pointed out that, although the part of the tree-level amplitude relevant for large distance scattering, is calculated to a finite value, we can not use eq. (4.7) and eq. (4.10) for calculating cross sections with the Born

approximation. This is so because, at low energies the thickness of the brane is important, and at high energies an all order eikonal summation has to be performed [10]. This calculation is however more reliably performed by keeping a finite brane width throughout the calculations and will be considered separately.

Acknowledgments

I am thankful to Leif Lönnblad, Johan Grönqvist, Gösta Gustafson, Pavel Kurasov and Johan Bijnens for useful discussions and comments on the manuscript and to Gian Giudice for making me aware of some of the cited articles.

References

[1] N. Arkani-Hamed, S. Dimopoulos, and G. R. Dvali *Phys. Lett.* **B429** (1998) 263–272, `hep-ph/9803315`.

[2] N. Arkani-Hamed, S. Dimopoulos, and G. R. Dvali *Phys. Rev.* **D59** (1999) 086004, `hep-ph/9807344`.

[3] I. Antoniadis, N. Arkani-Hamed, S. Dimopoulos, and G. R. Dvali *Phys. Lett.* **B436** (1998) 257–263, `hep-ph/9804398`.

[4] T. Han, J. D. Lykken, and R.-J. Zhang *Phys. Rev.* **D59** (1999) 105006, `hep-ph/9811350`.

[5] G. F. Giudice, R. Rattazzi, and J. D. Wells *Nucl. Phys.* **B544** (1999) 3–38, `hep-ph/9811291`.

[6] M. Bando, T. Kugo, T. Noguchi, and K. Yoshioka *Phys. Rev. Lett.* **83** (1999) 3601–3604, `hep-ph/9906549`.

[7] T. Kugo and K. Yoshioka *Nucl. Phys.* **B594** (2001) 301–328, `hep-ph/9912496`.

[8] G. F. Giudice and A. Strumia *Nucl. Phys.* **B663** (2003) 377–393, `hep-ph/0301232`.

[9] D. Atwood, S. Bar-Shalom, and A. Soni *Phys. Rev.* **D62** (2000) 056008, `hep-ph/9911231`.

[10] G. F. Giudice, R. Rattazzi, and J. D. Wells *Nucl. Phys.* **B630** (2002) 293–325, `hep-ph/0112161`.

[11] I. M. Gradshteyn and I. Ryshik, *Table of Integrals Series, and Products.* Academic Press, USA, 1994.

Gravitational Scattering in the ADD Model at High and Low Energies

Paper V

LU TP 06-26
August 2006

Gravitational Scattering in the ADD Model at High and Low Energies

Gösta Gustafson[1]
and
Malin Sjödahl[2]
Department of Theoretical Physics, Lund University,
Sölvegatan 14A, S-223 62 Lund, Sweden

Submitted to JHEP

Abstract
Gravitational scattering in the ADD model is considered at both sub- and transplanckian energies using a common formalism. By keeping a physical cut-off in the KK tower associated with virtual KK exchange, such as the cut-off implied from a finite brane width, troublesome divergences are removed from the calculations in both energy ranges. The scattering behavior depends on three different energy scales: the fundamental Planck mass, the collision energy and the inverse brane width. The result for energies low compared to the effective cut-off (inverse brane width) is a contact-like interaction. At high energies the gravitational scattering associated with the extra dimensional version of Newton's law is recovered.

[1]Gosta.Gustafson@thep.lu.se
[2]Malin.Sjodahl@thep.lu.se

5.1 Introduction

The ADD model [1–3] is an attempt to solve the hierarchy problem, by introducing extra dimensions in which only gravity is allowed to propagate. For distances smaller than the assumed compactification radius, R [1], the gravitational potential will then be altered and has the form

$$\frac{V(r)}{m_1 m_2} = -G_{N(4)} R^n S_n \frac{\Gamma(n)}{r^{n+1}} \tag{5.1}$$

where n is the number of extra dimensions, $G_{N(4)}$ denotes the ordinary 3+1-dimensional Newton's constant, $S_n = 2\pi^{n/2}/\Gamma(n/2)$ is the surface of a unit sphere in n dimensions and $\Gamma(n)$ is the Euler Gamma function. This implies that the strength of gravity increases much faster with smaller distance as compared with the normal $1/r$ behavior, and the fundamental Planck scale (related to the mass scale where the corresponding de Broglie wave length equals the black hole radius) is reduced and given by

$$M_D = \frac{1}{(8\pi R^n G_{N(4)})^{\frac{1}{n+2}}}. \tag{5.2}$$

The presence of strong gravity at distances smaller than the compactification radius opens up for the possibility of observing gravitational scattering and black hole production at collider experiments and in cosmic rays. To eliminate the hierarchy problem, and not only reduce it, the new Planck scale should be of the order TeV, and LHC will be a quantum gravity probing machine.

In order to quantify the amount of gravitational interaction, the theory was formulated as a field theory in [5,6]. As the extra dimensions are compactified, the allowed wave numbers (and hence momenta) in these dimensions are quantized Kaluza–Klein (KK) modes. The KK modes can of course enter both as external and internal particles in the Feynman diagrams derived from the theory. When the KK modes are internal (as for elastic gravitational scattering) they have to be summed over. The problem is that the sum over KK modes diverges for 2 or more extra dimensions,

$$\sum_{\overline{l}} \frac{1}{-m_{\overline{l}}^2 + k^2} \approx S_n R^n \int \frac{m^{n-1}}{-m^2 + k^2} dm. \tag{5.3}$$

Here $\overline{l}$ enumerates the allowed KK modes with momenta $m_{\overline{l}}$ in the extra dimensions, $m = |m_{\overline{l}}|$, and k is the exchanged 4-momentum in our normal space. (We will for simplicity call this object a propagator, despite the fact that the Lorentz structure is not included.)

[1] Here we use the notations of [4], such that R is the radius and not the circumference.

In the original papers [5, 6] this divergence problem was dealt with by introducing a sharp cut-off, M_s, argued to be of the same order of magnitude as the Planck mass, as new physics anyhow is expected to occur at the Planck scale. Various mathematical forms of cut-offs have also been discussed in [7]. For $n \geq 3$ and momentum transfers small compared to M_s, the sum was then estimated to give

$$\sim \frac{1}{n-2} R^n M_s^{n-2} \approx \frac{1}{G_{N(4)}(n-2)} \frac{M_s^{n-2}}{M_D^{n+2}}. \tag{5.4}$$

In the Born approximation this would lead to a cross section of the form [8]

$$\frac{d\sigma}{dz} \sim \frac{s^3}{(n-2)^2} \left(\frac{M_s^{n-2}}{M_D^{n+2}} \right)^2 F(\text{spin}, z) \tag{5.5}$$

where z is cosine of the scattering angle in the center of mass system, $\sqrt{s}$ the total cms energy, and F a function taking spin dependence into account.

Ordinary gravitational scattering in $3+n$ dimensions would correspond to a potential $\propto 1/r^{(n+1)}$, but the scattering given by eq. (5.5) has a completely different angular behavior. In particular the expected forward peak is totally absent. Fourier transforming the amplitude in eq. (5.4) to position gives a δ-function potential, $\propto \delta(\bar{r})$, and the corresponding Born approximation cross section in eq. (5.5) is therefore isotropic. Thus it is obvious that the approximation in eq. (5.4) does not contain the full story of gravitational scattering in the ADD model.

An attempt to solve this problem has been presented by Giudice, Rattazzi, and Wells [4]. These authors point out two important facts:

i) For an interaction with a large Born amplitude but a short range, the cross section is not determined by the Born term alone. Higher order loop corrections reduce the cross section and guarantee that the unitarity constraint is obeyed.

ii) The constant term in eq. (5.4), which represents a dominant part of the amplitude in eq. (5.3), corresponds to a contribution to the cross section from zero impact parameter, and should therefore give a negligible contribution to the cross section, at least when the incoming wave packages do not overlap. Consequently the important part of the amplitude in eq. (5.3) must in this case be the smaller k-dependent terms, which have been neglected in eq. (5.4).

In case the interaction is dominated by small angle scattering the cross section can be calculated in the eikonal approximation, in which the all-loop summation exponentiates [9–11]. The cross section is then given by

$$\sigma_{\text{el}} \quad = \quad \int d^2\bar{b}_\perp \, |(1 - e^{i\chi(\bar{b}_\perp)})|^2$$

$$\sigma_{\rm tot} = \int d^2\bar{b}_\perp \, 2Re(1 - e^{i\chi(\bar{b}_\perp)}) \tag{5.6}$$

$$\text{with } \chi(\bar{b}_\perp) = \frac{1}{2s}\int \frac{d^2\bar{q}_\perp}{(2\pi)^2} e^{i\bar{q}_\perp\cdot\bar{b}_\perp} A_{\rm Born}(\bar{q}_\perp^2). \tag{5.7}$$

Thus, if the absolute value of the eikonal, χ, is small compared to 1, we in general expect small corrections from the higher order loop contributions, while for large χ-values the cross section saturates, and the effective integrand in eq. (5.6) is close to 1. We also note that when χ is real, the scattering is purely elastic. In this paper we will focus on elastic collisions mediated via (multiple) exchange in the t-channel.

It is also pointed out in [4] that in the eikonal limit the Born amplitude does not depend on the spin of the colliding particles, and is therefore universal. Expressed in the fundamental Planck mass M_D in eq. (5.2) it is given by [4]

$$A_{\rm Born}(k^2) = \frac{s^2}{M_D^{n+2}} \int \frac{d^n\bar{m}}{k^2 - \bar{m}^2}. \tag{5.8}$$

In [4] a divergent part is subtracted from the integral in eq. (5.3) or (5.8) using dimensional regularization. This subtracted part corresponds to a narrow potential localized at $\bar{r} = 0$. Although the remainder is singular for n equal to an even integer, its Fourier transform (the eikonal χ in eq. (5.7)) is finite everywhere. Assuming the eikonal approximation to be applicable in the transplanckian region $s \gg M_D^2$, the authors of [4] thus obtains a reasonable result, where the gravitational scattering cross section grows with energy $\propto (s/M_D^{n+2})^{2/n}$. However, we ought to be worried by the fact that the part of the amplitude, remaining after the subtraction, grows for larger momentum transfers, and is largest for backward scattering. This implies that the conditions for the eikonal approximation are not satisfied. The formal problems with divergent integrals also indicate that this result could be regarded as based more on physical intuition than on a solid theoretical foundation. These uncertainties also make it difficult to estimate the limit beyond which the result should be applicable, and how the gravitational scattering behaves for lower energies.

In this paper we want to study in more detail the result of various physical effects, which can tame the divergences. These effects give effective cut-offs for high-mass KK modes at some scale (here referred to as M_s), which does not have to be the same as the Planck scale M_D. Our result does indeed confirm the relevance of the eikonal approximation and the result in [4] at very high energies. For lower energies the behavior is different, wide angle scattering is dominant and the amplitude does not exponentiate. Instead the all-loop summation gives a geometric series. This implies that there will be a change in the energy dependence, and for lower energies the cross section varies more rapidly, proportional to $\propto s^2 M_s^{2n-2}/M_D^{2n+4}$.

We want to emphasize that in this paper we do not discuss phenomena like black hole formation or other nonlinear gravitational effects, which are expected to modify the final states for very high energies and central collisions. For a discussion of such effects we refer to ref. [3, 4, 12–17]. We also neglect possible interference with strong and electro-weak effects and we study reactions for non-identical particles such that KK modes appears only in the t-channel. Some remarks on s- and u-channels are however made in secs. 5.6.3-5.6.5.

The approach in [4] will be discussed in more detail in sec. 5.2. In sec. 5.3, we will introduce a finite width of the brane, on which the standard model particles are assumed to live, and see how this leads to a finite amplitude. A similar effect is obtained by assuming that the position of the brane is not fixed in the extra dimensions [18, 19]. Fluctuations in the brane then result in a kind of surface tension or "brane tension". The Born term is discussed in sec. 5.4 and higher order loop corrections in sec. 5.5. Here we also study in which kinematical regions the Born term dominates, where the eikonal approximation is valid, and the behavior of the cross section in regions where the scattering is approximately isotropic. The results for scattering cross sections in those different kinematical regions are then presented in sec. 5.6. Finally we will summarize and conclude in sec. 5.7.

5.2 Problems and divergences

The integral in eq. (5.3) or (5.8) is divergent for $n \geq 2$ and $n \leq 0$, but converges for n-values in the intermediate range $0 < n < 2$. To give a physical meaning to the integral for $n \geq 2$, a finite result can be obtained by analytic continuation from smaller n-values, corresponding to a dimensional regularization. The resulting amplitude, presented in [4], is given by the expression[2]

$$A_{\rm Born}(k^2) = -\pi^{\frac{n}{2}}\Gamma\left(1-\frac{n}{2}\right)\left(\frac{-k^2}{M_D^2}\right)^{\frac{n}{2}-1}\left(\frac{s}{M_D^2}\right)^2. \tag{5.9}$$

We see that this expression is finite for odd integers n, but singular for even n, where the Γ-function has poles.

The result in eq. (5.9) is equivalent to a subtraction of terms, which are proportional to δ-functions or derivatives of δ-functions at $\bar{r} = 0$, and therefore may be expected to give negligible contributions to the cross section. Inserting eq. (5.9) into the two-dimensional Fourier transform in eq. (5.7), we see that this integral is also divergent. It can be given a finite result by introduction of a convergence factor:

$$\chi = -\left(\frac{b_c}{b}\right)^n, \text{ with } b_c = \left[\frac{s(4\pi)^{\frac{n}{2}-1}\Gamma(n/2)}{2M_D^{n+2}}\right]^{1/n}. \tag{5.10}$$

[2] We have here inserted a minus sign not present in [4].

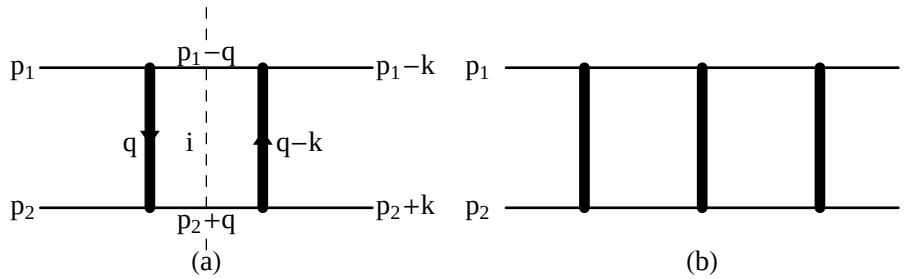

Figure 5.1: (a) The one-loop contribution corresponding to exchange of two KK modes. The KK modes are drawn as thick lines and standard model particles as thin lines. (b) The two-loop contribution.

We note that although the amplitude $A_{\rm Born}$ in eq. (5.9) is singular for even n, χ is finite. Thus $\chi(b)$ (like the potential $V(r)$, to be discussed below) can be analytically continued to finite values for all n-values. (A finite amplitude, which corresponds to a potential proportional to $1/r^{n+1}$ for n even, is $\propto (-k^2)^{n/2-1} \ln(-k^2)$.)

The result in eq. (5.10) is a single power $\propto 1/b^n$, and the scale factor (or characteristic impact parameter) b_c is defined so that $|\chi| = 1$ when $b = b_c$. If this expression is inserted into eq. (5.6), we see that the term quadratic in χ, which is the Born term, dominates the integrand for $b > b_c$, where $\chi < 1$, but higher order corrections are important in constraining the scattering probability for $b < b_c$.

In ref. [4] it is assumed that eqs. (5.6) and (5.10) should give a realistic approximation to gravitational scattering in the transplanckian region $s \gg M_D^2$ (apart from special effects like black hole formation, which are treated separately). The net result is then that the total scattering cross section grows with energy proportional to b_c^2, or equivalently $\propto (s/M_D^{n+2})^{2/n}$, (cf. eq. (5.43) below).

The exponentiation in the eikonal approximation in eq. (5.6) follows when the scattering is dominated by small angles [9–11]. The one-loop contribution is then dominated by its imaginary part, and the all-loop summation gives an exponential.

The one-loop diagram in fig. 5.1a is given by the following expression:

$$A_{1-\rm loop}(k^2) = \frac{-i}{2} \int \frac{d^4q}{(2\pi)^4} A_{\rm Born}(q^2) A_{\rm Born}((k-q)^2) \frac{1}{(p_1-q)^2} \frac{1}{(p_2+q)^2}. \tag{5.11}$$

Here p_1 and p_2 denote the momenta of the incoming particles, the total momentum exchange is k and the loop momentum q.

The imaginary part of the integral in eq. (5.11) is coming from on-shell intermediate states (denoted i in fig. 5.1), and can be calculated using the Cutcosky cutting rules. This implies that the two propagators in eq. (5.11) are replaced by δ-functions, which (with the approximation $q^2 \approx \bar{q}_\perp^2$) gives the result

$$A_{1-\mathrm{loop}}(k^2) = \frac{i}{4s}\int \frac{d^2\bar{q}_\perp}{(2\pi)^2} A_{\mathrm{Born}}(-\bar{q}_\perp^2) A_{\mathrm{Born}}(-(\bar{k}_\perp - \bar{q}_\perp)^2). \tag{5.12}$$

If A_{Born} falls off for large $k_\perp$, the Fourier transform to impact parameter space of the one-loop contribution is proportional to $\chi^2(\bar{b}_\perp)$. The sum over multi-loop ladder diagrams with different number of KK exchanges exponentiates to $(i\chi - \chi^2/2 + ...) = e^{i\chi} - 1$, and the all order eikonal amplitude is given by

$$A_{\mathrm{eik}}(k^2) = -2is\int d^2\bar{b}_\perp e^{i\bar{k}_\perp\cdot\bar{b}_\perp}(e^{i\chi} - 1). \tag{5.13}$$

With the Born amplitude in eq. (5.9) we have, however, some problems. First the real part of the integral in eq. (5.11) is not small and negligible compared to the imaginary part. It is strongly divergent for $n \geq 2$, as A_{Born} increases proportional to q^{n-2} or $q^{n-2}\ln(-q^2)$ for large q. Secondly the integral in eq. (5.12) should only go over physical intermediate states, which means $q_\perp < \sqrt{s}/2$. The Fourier transform of the convolution in eq. (5.12) gives χ^2 only if the integrand in eq. (5.12) falls off so rapidly, that the integral effectively can be extended to all $q_\perp$. This is not the case with the amplitude in eq. (5.9).

We conclude that, although the result in eq. (5.10) and (5.6) is an intuitively reasonable result for scattering in a rapidly falling potential, it should be worrying that it is derived from an amplitude, which grows for large momentum transfers and large scattering angles, while the eikonal approximation is proven to be valid only when scattering at small angles is dominating.

At the root of this problem lies the fact that the subtraction, which gives the amplitude in eq. (5.9) and is a result of the analytic continuation in the number of extra dimensions, does *not* automatically remove all parts corresponding to δ-functions at $\bar{r} = 0$. The definition of the potential as the Fourier transform of eq. (5.9) is problematic. To illustrate this we study the most simple example represented by the case $n = 3$. In the rest frame we have $k_0 = 0$ and $k^2 = -\bar{k}^2$. The integral in eq. (5.8) is then proportional to

$$\begin{aligned}\int \frac{m^2\, dm}{\bar{k}^2 + m^2} &= \int \frac{(m^2 + \bar{k}^2 - \bar{k}^2)dm}{\bar{k}^2 + m^2} = \int dm - \bar{k}^2 \int \frac{dm}{\bar{k}^2 + m^2} \\ &= \int dm - |\bar{k}| \int \frac{dx}{1 + x^2} = \int dm - |\bar{k}|\frac{\pi}{2}.\end{aligned} \tag{5.14}$$

The first term, the integral, represents an infinite subtraction. Its three-dimensional Fourier transform gives a δ-function at $\bar{r} = 0$ with an infinite

weight. The second term corresponds to the result in eq. (5.9). We may try to define its Fourier transform $\hat{V}(\bar{r})$ as a distribution in the standard way, multiplying with a test function and interchanging the order of integration. For test functions of the form $\exp(-a\,r^2)$ we then get (with $k \equiv |\bar{k}|$ and the constant C appearing in eq. (5.25))

$$\begin{aligned}\int d^3r e^{-a\,r^2}\hat{V}(\bar{r}) &\equiv C(-\frac{\pi}{2})\int d^3k\,k\int d^3r e^{-a\,r^2}e^{i\bar{r}\bar{k}} \\ &= -C\frac{\pi}{2}\int d^3k\,k e^{-k^2/4a}(\frac{\pi}{a})^{\frac{3}{2}} \\ &= -C16\pi^{\frac{7}{2}}\sqrt{a}. \end{aligned} \tag{5.15}$$

We note that this result is finite, and goes towards 0 when the test function approaches a constant, i.e. when $a \to 0$. For $r \neq 0$ we find $\hat{V}(r) = C4\pi^2/r^4$ by Fourier transforming from $\bar{k}$ to $\bar{r}$ using a convergence factor. Integrating this contribution with the test function above, we get the divergent result

$$C16\pi^3\int_0^\infty e^{-a\,r^2}\frac{dr}{r^2}. \tag{5.16}$$

Thus this definition, $\hat{V}(r) = C4\pi^2/r^4$ for $r > 0$, is incomplete since the result in eq. (5.15) is finite while the integral in eq. (5.16) is infinite. It looks as if a δ-function, $\delta(\bar{r})$, with infinite weight is missing.

We conclude that the separation in eq. (5.14) does not in itself remove all terms related to δ-functions at $\bar{r} = 0$. Instead we argue in the next section that dynamical effects will remove the divergencies and give finite results.

In the next section we will consider possible mechanisms, which can suppress high KK masses and give an effective cut-off to the integral in eq. (5.8). These mechanisms have real dynamical motivations, and we will see that such finite cut-offs do remove all divergences and give well-defined results. For high energies the Born amplitude indeed falls off for large momentum transfers, and the eikonal approximation is applicable. For lower energies this is not the case, and we will in secs. 5.4 - 5.6 discuss the resulting amplitudes and cross sections for different relations between the energy, the Planck mass, and the cut-off scale.

5.3 Possible solutions

In the ADD model the standard model particles are assumed to live on a thin brane. The mechanism behind this assumption could possibly be taken from string theory [3], but is not a part of the ADD model itself. The problems discussed in the previous section are related to contributions from KK modes

with very high masses. In a relativistic quantized theory there are also formal problems with an infinitely thin and infinitely rigid brane. If the brane is not infinitely thin, but has a finite width, this will effectively suppress the coupling to high-mass KK modes, with wavelengths shorter than the brane width. If the brane really is infinitely thin, then it must be impossible to determine its position with infinite accuracy. In [18,19] it is demonstrated that the fluctuations in the position of the brane suppresses high-mass KK modes, in a way similar to the effect of a finite brane width. The emission or absorption of a KK mode gives a recoil to the brane, and the fluctuations in the location of the brane can then be regarded as a result of an effective "surface tension" in the brane.

Let us for definiteness study the effect of the assumption that the standard model fields penetrate a finite distance into the extra dimensions, which gives an effective finite width to the brane [20]. (The possibility of fluctuating branes, studied in [18,19], give similar results, albeit with a different physical interpretation.) To be specific we assume a Gaussian extension, but this assumption is not essential for our conclusions. Thus we assume the standard model fields to have a wave function with the extension

$$\psi(\overline{y}) = \left(\frac{M_s}{\sqrt{2\pi}}\right)^{\frac{n}{2}} e^{-\overline{y}^2 M_s^2/4} \tag{5.17}$$

into the extra dimensions, with $\overline{y}$ denoting the coordinate in the extra dimensions. The overlap between two standard model fields and a KK mode of mass m (what we have in a vertex) is then proportional to

$$\int d\overline{y}\, e^{i\overline{m}\cdot\overline{y}} \left(\frac{M_s}{\sqrt{2\pi}}\right)^{2\frac{n}{2}} e^{-\overline{y}^2 M_s^2/2} = e^{-m^2/(2M_s^2)} \tag{5.18}$$

or, in other words, the squared absolute value of the wave function in $\overline{y}$-space Fourier transformed to m-space. The exchange of a KK mode will have this suppression factor occurring twice, once at every vertex. In total the exchange of a KK mode with mass m will therefore contribute to the sum in eq. (5.8) with a suppression factor

$$e^{-m^2/M_s^2}. \tag{5.19}$$

Implementing the physical requirement that the standard model particles live on a narrow brane does therefore in itself imply a finite "effective" propagator,

$$R^n S_n \int \frac{dm\, m^{n-1}}{k^2 - m^2} e^{-m^2/M_s^2} \tag{5.20}$$

for the exchange of 4-momentum k. (The factor R^n comes from the density of KK modes and $S_n = 2\pi^{n/2}/\Gamma(n/2)$ is the unit surface of a sphere in n

dimensions.) We note in particular that this expression (in contrast to the expression in eq. (5.9)) falls off like $1/k^2$ for large momentum transfers, such that $-k^2 \gg M_s^2$. This implies that for high energies, $s \gg M_s^2$, t-channel interaction is dominated by small values of $-k^2/s$, i.e. by small angles.

In the following sections we will show that the Fourier transform of the propagator in eq. (5.20) gives a potential, which falls off $\propto 1/r^{n+1}$ for distances larger than the brane width, given by $1/M_s$, and smaller than the compactification radius. Outside this range, both for $r < 1/M_s$ and for $r > 2\pi R$ (where the massless graviton dominates), it varies $\propto 1/r$. We will also study the resulting scattering cross sections under different kinematic conditions.

5.4 The Born term

5.4.1 Amplitude

As described in section 5.3, several physical mechanisms result in effective cut-offs for high masses in the KK propagator. After multiplying eq. (5.20) by the coupling $4\pi G_{N(4)}$, contracting Lorentz indices (not explicitly included here), and using the relation $G_{N(4)}^{-1} = 8\pi R^n M_D^{2+n}$ we get the following result for the Born amplitude for ultra-relativistic small angle scattering:

$$A_{\rm Born}(t) = \frac{s^2}{M_D^{n+2}}\, S_n \int_0^\infty \frac{dm\, m^{n-1}}{k^2 - m^2}\, e^{-m^2/M_s^2}. \tag{5.21}$$

For large angels there are less important corrections from spin polarization which we neglect here and in the following. This integral is convergent and finite for all negative values of $k^2 = t$ (including 0 when $n \geq 3$). It is easy to find the result in the limits of large and small (negative) t-values.

- *Large momentum transfers; $-t \gg M_s^2$*

  When $-t$ is large compared to M_s^2, the term m^2 in the denominator in eq. (5.21) can be neglected, which gives the result:

$$A_{\rm Born}(t) \approx \frac{s^2}{M_D^{n+2}}\, S_n \int_0^\infty \frac{dm\, m^{n-1}}{t} e^{-m^2/M_s^2} = \pi^{n/2} \left(\frac{M_s}{M_D}\right)^n \frac{s^2}{M_D^2 \cdot t}. \tag{5.22}$$

  Thus for large momentum transfers (larger than the cut-off) the Born amplitude falls off proportional to $1/t$.

- *Small momentum transfers; $-t \ll M_s^2$*

  For smaller t, and $n > 2$, the integral is dominated by m-values of the order of M_s, and therefore t can now be neglected in the denominator. We then get the approximately constant result:

$$A_{\rm Born}(t) \approx \frac{-s^2}{M_D^{n+2}} S_n \int_0^\infty dm\, m^{n-3}\, e^{-m^2/M_s^2}$$
$$= -\frac{2\pi^{n/2}}{(n-2)} \left(\frac{M_s}{M_D}\right)^n \frac{s^2}{M_D^2 M_s^2}. \qquad (5.23)$$

Thus for momentum transfers, which are small compared to the cut-off, the Born amplitude is approximately constant for $n > 2$. For $n = 2$ the result for small t has instead a slowly varying logarithmic dependence, proportional to $\ln(-M_s^2/t)$.

5.4.2 Potential

To get the classical non-relativistic potential we start directly from the effective propagator in eq. (5.20) multiplied with the coupling constant $4\pi G_{N(4)}$. Going to the rest frame, where $k_0 = 0$ and $t = -\bar{k}^2$ we find the corresponding potential as the three-dimensional Fourier transform:

$$\frac{V(r)}{m_1 m_2} = \frac{1}{2s^2} \int \frac{d^3\overline{k}}{(2\pi)^3}\, e^{i\bar{k}\bar{r}} A_{\rm Born}(-\bar{k}^2)$$
$$= \frac{-1}{2M_D^{n+2}} \frac{S_n}{(2\pi)^3} \int_0^\infty dm\, m^{n-1}\, e^{-m^2/M_s^2} \int \frac{d^3k e^{i\bar{k}\bar{r}}}{m^2 + \bar{k}^2} =$$
$$= \frac{-1}{2M_D^{n+2}} \frac{S_n}{(2\pi)^3} 2\pi^2 \int_0^\infty dm\, m^{n-1} e^{-m^2/M_s^2} \cdot \frac{e^{-mr}}{r}. \qquad (5.24)$$

This represents a weighted sum of Yukawa potentials. The integral can be expressed in terms of error functions, but we are here primarily interested in the behavior for large and small values of r.

- *Large distances; $r > 1/M_s$*

  For distances larger than the brane thickness the integral is effectively cut off by the factor e^{-mr}, and the result becomes insensitive to the Gaussian cut-off e^{-m^2/M_s^2}. It is then approximated by

$$\frac{V(r)}{m_1 m_2} \approx \frac{-1}{2M_D^{n+2}} \frac{S_n}{4\pi} \int_0^\infty dm m^{n-1} \cdot \frac{e^{-mr}}{r} = \frac{-S_n\, \Gamma(n)}{8\pi M_D^{n+2}} \cdot \frac{1}{r^{n+1}}. \qquad (5.25)$$

  We see that for distances large compared to the brane thickness (but small compared to the compactification radius) we recover the result from eq. (5.1), a potential falling off proportional to $1/r^{n+1}$, corresponding to the expected

$(3+n)$-dimensional version of Newton's law. When r is increased, smaller m-values $\sim 1/r$ are important in the integral in eq. (5.24) or (5.25). The phase space factor m^{n-1} then gives this power-like fall off for distances large compared to M_s.

- *Short distances; $r < 1/M_s$*

  For smaller r-values we find instead that the factor e^{-mr} is irrelevant, and the result is

$$\frac{V(r)}{m_1 m_2} = \frac{-1}{2M_D^{n+2}} \frac{S_n}{4\pi} \frac{1}{r} \int_0^\infty dm\, m^{n-1}\, e^{-m^2/M_s^2} = \frac{-\pi^{n/2}}{8\pi} \frac{M_s^n}{M_D^{n+2}} \cdot \frac{1}{r}. \quad (5.26)$$

  Due to the cut-off, the integral in eq. (5.24) is dominated by m-values close to M_s for all r-values smaller than $1/M_s$. Thus, when the distance is smaller than the brane width, the result is a potential proportional to $1/r$, corresponding to a standard 3-dimensional Coulomb potential, although with a coupling constant $\sim M_s^n/M_D^{n+2} \sim (M_s R)^n G_{N(4)}$ instead of $G_{N(4)}$. Thus the coupling is enhanced by a factor $\sim (M_s R)^n = (\frac{\text{compactification radius}}{\text{brane width}})^n$.

5.4.3 Eikonal

In a similar way we can calculate the eikonal $\chi(b)$ by a two-dimensional Fourier transform in the transverse coordinates:

$$\begin{aligned}
\chi(b) &= \frac{1}{2s} \int \frac{d^2\bar{k}_\perp}{(2\pi)^2}\, e^{i\bar{k}_\perp \bar{b}_\perp} A_{\text{Born}}(-\bar{k}_\perp^2) = \\
&= \frac{-s}{2M_D^{n+2}} \frac{S_n}{(2\pi)^2} \int_0^\infty dm\, m^{n-1}\, e^{-m^2/M_s^2} \int d^2\bar{k}_\perp e^{i\bar{k}_\perp \bar{b}_\perp} \frac{1}{m^2 + \bar{k}_\perp^2} = \\
&= \frac{-s}{2M_D^{n+2}} \frac{S_n}{(2\pi)^2} 2\pi \int_0^\infty dm\, m^{n-1} e^{-m^2/M_s^2} \int_0^\infty \frac{k_\perp dk_\perp}{m^2 + k_\perp^2}\, J_0(k_\perp b) = \\
&= \frac{-s}{2M_D^{n+2}} \frac{S_n}{2\pi} \int_0^\infty dm\, m^{n-1} e^{-m^2/M_s^2} K_0(mb). \quad (5.27)
\end{aligned}$$

This integral can be expressed in terms of confluent hypergeometric functions of the second kind:

$$\chi(b) = -\frac{s M_s^n}{M_D^{n+2}} \Gamma(\frac{n}{2}) \frac{\pi^{n/2-1}}{8} U(\frac{n}{2}, 1, \frac{M_s^2 b^2}{4}). \quad (5.28)$$

This expression can easily be used in numerical calculations. For an intuitive picture, the result for large and small b-values can be estimated in the same way as the approximations in eqs. (5.25, 5.26).

- *Large impact parameters; $b \gg 1/M_s$*

  For large arguments the asymptotic behavior of the Bessel function $K_0(mb)$ is proportional to $\exp(-mb)/\sqrt{mb}$. This implies that for large b the Gaussian cut-off is unessential, and we find the eikonal

$$\begin{aligned}\chi(b) &\approx \frac{-s}{2M_D^{n+2}}\frac{S_n}{2\pi}\int dm\, m^{n-1}\, K_0(mb) = \frac{-s}{M_D^{n+2}}\frac{S_n}{\pi}2^{n-4}\,\Gamma^2(n/2)\cdot\frac{1}{b^n} \\ &= \frac{-s}{2M_D^{n+2}}(4\pi)^{\frac{n}{2}-1}\Gamma\left(\frac{n}{2}\right)\cdot\frac{1}{b^n}. \qquad (5.29)\end{aligned}$$

- *Small impact parameters; $b \ll 1/M_s$*

  For small arguments we have $K_0(mb) \approx \ln(1/(mb))$, which implies

$$\begin{aligned}\chi(b) &\approx \frac{-s}{2M_D^{n+2}}\frac{S_n}{2\pi}\int dm\, m^{n-1}\, e^{-m^2/M_s^2}\ln\left(\frac{1}{mb}\right) \\ &= \frac{\pi^{\frac{n}{2}-1}}{4}\frac{s}{M_D^2}\left(\frac{M_s}{M_D}\right)^n\left(\ln(M_s b)+\frac{1}{2}\psi(\frac{n}{2})\right) \qquad (5.30)\end{aligned}$$

  where $\psi(\frac{n}{2})$ is the psi or digamma function.

Thus we see that the eikonal falls off $\propto 1/b^n$ for large b, and grows logarithmically when $b \to 0$. Using the quantity b_c from eq. (5.10) and keeping only the dominant term $\ln(M_s b)$ in eq. (5.30), we can write the results in the form

$$\chi(b) \approx -\left(\frac{b_c}{b}\right)^n;\ \ b > b_d \qquad (5.31)$$

$$\chi(b) \approx \frac{-(b_c\, M_s)^n}{2^{n-1}\Gamma(n/2)}\ln\left(\frac{1}{M_s b}\right);\ \ b < b_d \qquad (5.32)$$

$$\text{with } b_d \equiv \frac{1}{M_s} \qquad (5.33)$$

$$\text{and } b_c \equiv \left[\frac{s(4\pi)^{\frac{n}{2}-1}\Gamma(n/2)}{2M_D^{n+2}}\right]^{1/n}. \qquad (5.34)$$

The separation line $b_d = 1/M_s$ is an estimate of the b-value where $\chi(b)$ changes behavior. As an example fig. 5.2 shows these approximations for χ together with the exact result for $n = 3$ and $\sqrt{s} = M_D = 1$ in units such that $M_s = 1$. As χ is proportional to s/M_D^{n+2}, a change in s and/or M_D just corresponds to a shift of all curves the same distance up or down.

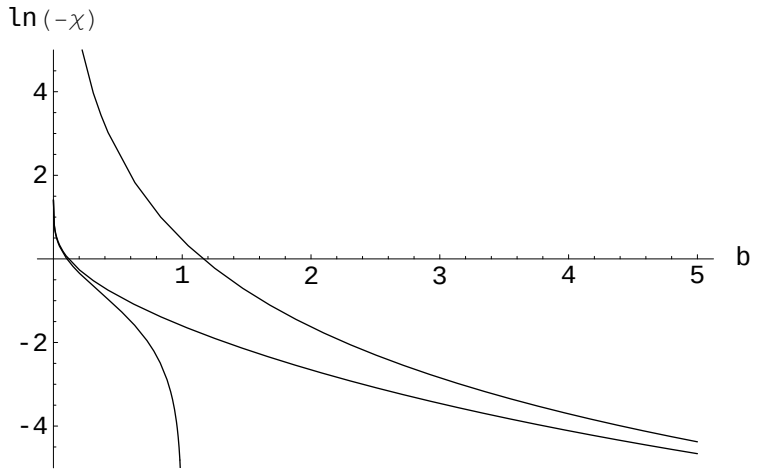

Figure 5.2: The logarithm of $|\chi|$ as a function of impact parameter for $n = 3$. The curves show the example where $\sqrt{s}$, M_D, and M_s have the same magnitude, and the units are chosen such that $\sqrt{s} = M_D = M_s = 1$. This also implies that $b_d = 1$. The uppermost line is the large b limit of χ taken from eq. (5.31) and the lowermost line is the small b limit of χ taken from eq. (5.32). The interpolating line is the exact expression eq. (5.28). Note that a change in s and/or M_D, keeping M_s constant, just corresponds to shifting all curves up or down.

5.5 Higher order loop corrections

We note that three different energy scales enter the expressions for the Born amplitude in eqs. (5.21, 5.28): $\sqrt{s}$, M_D, and M_s. Here $\sqrt{s}$ is the total energy in the scattering, M_D is the fundamental Planck scale determined by the compactification radius R, and M_s is related to the width of the brane (or the brane tension). The result depends on the relative magnitude of these quantities, and in the following we will successively discuss five different kinematical regions, which are illustrated in fig. 5.3.

5.5.1 Eikonal regions, $s \gg M_s^2$

We study the scattering process in the overall cm system, where the momentum exchange has no 0-component, $k = (0; \bar{k})$ and $t = -\bar{k}^2$. From eq. (5.22) we see that $A_{\rm Born}$ falls off $\propto 1/\bar{k}^2$ for $\bar{k}^2 > M_s^2$. Thus for high energies, such that $s \gg M_s^2$, corresponding to region 1 and 2 in fig. 5.3, the Born term is dominated by small values of $\bar{k}^2/s$, i.e. small angles. This implies that the eikonal approximation is applicable. We note in particular that it is M_s rather

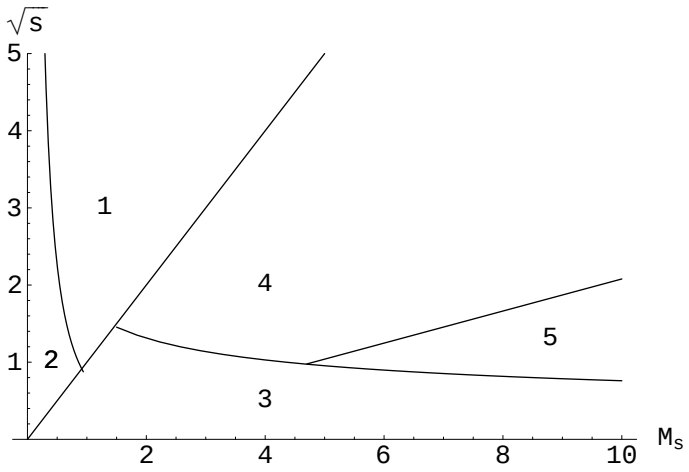

Figure 5.3: The $(\sqrt{s}, M_s)$-plane for $n = 3$ and $M_D = 1$. The straight line separating region 1 and 4 is $\sqrt{s} = M_s$ while straight line separating region 4 and 5 is the line where the real and imaginary parts in eq. (5.38) have equal magnitude. The power-like curve separating region 1 and 2 is $\sqrt{s_{cd}}$ from eq. (5.36) as a function of M_s and the line separating the regions 4 and 5 from region 3 is the line where $|A_{\rm Born}X| = 1$, see eq. (5.38). In the regions 1 and 2 $\sqrt{s}$ is larger than M_s, and, at least for $\sqrt{s} \gg M_s$, the eikonal approximation is correct. In region 1 the eikonal is, depending on b, either large compared to 1 or given by eq. (5.31). In region 2 on the other hand the b-range where χ is small includes a region where it is described by eq. (5.32). In region 3 the correction corresponding to higher order loops is small, but in region 4 it is important to assure unitarity.

than M_D, that sets the scale for when the eikonal approximation is relevant. The one-loop contribution is here dominated by its imaginary part, obtained when the particles in the intermediate state i in fig. 5.1a are on shell. The contributions from multi-loop ladder diagrams (fig. 5.1b) exponentiate, and the scattering amplitude is given by eq. (5.13):

$$A_{\rm eik}(k^2) = 2is \int d^2\bar{b}_\perp e^{i\bar{k}_\perp \cdot \bar{b}_\perp}(1 - e^{i\chi}). \tag{5.35}$$

From eq. (5.35) we see that the higher order corrections are important when χ is of order 1 or larger. Correspondingly the Born term dominates when $|\chi| < 1$. We see from eqs. (5.32, 5.33) that χ varies only logarithmically when b is decreased below the point $b = b_d$. The importance of the higher order corrections for the integrated cross section therefore depends on whether or

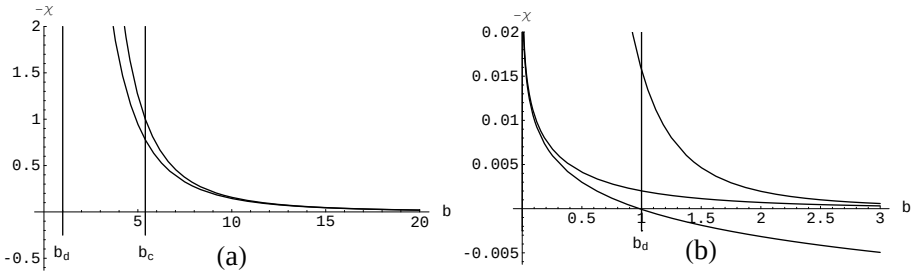

Figure 5.4: $-\chi$ as a function of impact parameter for two examples with $n = 3$. (a) High energies corresponding to region 1 in fig. 5.3, with $\sqrt{s} = 10$ TeV, $M_s = 1$ TeV and $M_D = 1$ TeV. The upper curve is the approximate expression in eq. (5.29), and the lower curve the exact expression eq. (5.38). (b) Kinematics corresponding to region 2 in fig. 5.3, $\sqrt{s} = 0.1$ TeV $M_s = 1$ TeV and $M_D = 1$ TeV. The upper curve is the approximate high b expression in eq. (5.31), the lower curve the approximate low b expression in eq. (5.32) and the interpolating line is the exact expression in eq. (5.28).

not $|\chi(b_d)| > 1$. This relation is satisfied whenever $b_c > b_d$, or equivalently when $s > s_{cd}$, with s_{cd} given by

$$s_{cd} = \frac{2}{(4\pi)^{\frac{n}{2}-1}\Gamma(\frac{n}{2})}\frac{M_D^{n+2}}{M_s^n}. \tag{5.36}$$

This defines the boundary between region 1 and region 2 in fig. 5.3. In region 1 higher order terms are important for $b < b_c$, and the exponentiation in eq. (5.35) is essential to keep the amplitude within the unitarity constraints.

The difference between regions 1 and 2 is illustrated in fig. 5.4. Fig. 5.4a corresponds to region 1, where the energy is high, and $b_c > b_d$. The absolute value of the eikonal χ is smaller than 1 for $b > b_c$, and in this range the approximation in eq. (5.31) is relevant. For $b < b_c$, $|\chi|$ is large and rapidly varying, which causes the exponent in eq. (5.35) to oscillate rapidly.

Fig. 5.4b corresponds to region 2. Here $|\chi| < 1$ except in a very small region

$$b < \frac{1}{M_s}\exp\left(-\frac{4M_D^{n+2}\pi^{1-\frac{n}{2}}}{sM_s^n}\right) \tag{5.37}$$

around the origin. Therefore the Born term dominates the cross section, and higher order terms give only small corrections.

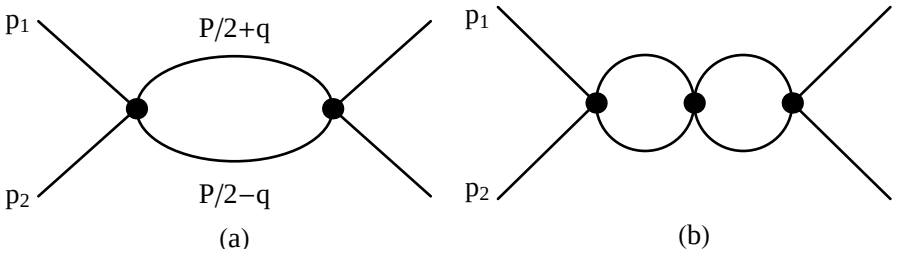

Figure 5.5: When the exchanged momentum is small compared to M_s, the KK propagators are effectively replaced by vertex factors. The diagrams in fig. 5.1 can then be drawn as above with only standard model particle lines.

5.5.2 Non-eikonal regions, $s < M_s^2$

The Born amplitude in eq. (5.23) is almost independent of the momentum exchange $\bar{k}$ when $k \ll M_s$. When $\sqrt{s} \ll M_s$ (regions 3, 4, and 5 in fig. 5.3) this includes all kinematically allowed $\bar{k}$-values, which implies that the scattering is almost isotropic. Thus the exchange of the KK modes corresponds effectively to a contact interaction. (For wide-angle scattering we also expect corrections from spin polarization. This effect is neglected in the following.) The one-loop contribution in fig. 5.1a is then represented by the diagram in fig. 5.5a, which is easily calculated. We denote the momenta in the intermediate state $P/2 \pm q$, with $P = p_1 + p_2$, as indicated in fig. 5.5a, and in the cms we have $P = (W, \bar{0})$. The vertices are then given by the Born term in eq. (5.23), with an effective cut-off when $q = M_s$. The result is therefore

$$\begin{aligned} A_{1-\mathrm{loop}}(k^2) &= \frac{-i}{2}\int_{q<M_s}\frac{d^4q}{(2\pi)^4}A^2_{\mathrm{Born}}\frac{1}{(P/2-q)^2}\frac{1}{(P/2+q)^2} = \\ &\equiv A^2_{\mathrm{Born}}\cdot X, \quad \text{with } X \approx \frac{1}{32\pi^2}(\ln\frac{4M_s^2}{s} + i\pi). \end{aligned} \tag{5.38}$$

We note here in particular that the result is a constant, independent of the momentum transfer k. Therefore also the one-loop amplitude can be effectively regarded as a contact term with a cut-off when $k > M_s$. Consequently the two-loop diagram in fig. 5.5b can be calculated in the same way as the one-loop diagram, and the result is

$$A_{2-\mathrm{loop}} = A_{1-\mathrm{loop}}\cdot A_{\mathrm{Born}}X = A_{\mathrm{Born}}\cdot(A_{\mathrm{Born}}X)^2. \tag{5.39}$$

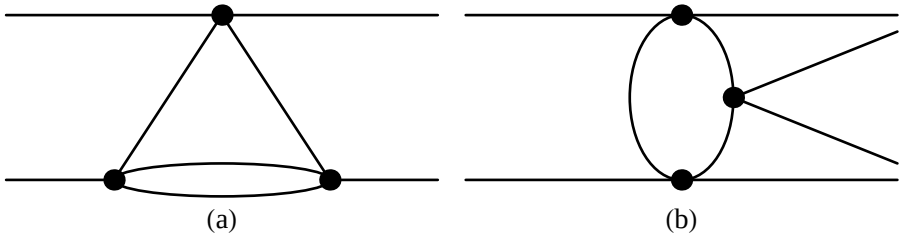

Figure 5.6: (a) An example of a non-ladder diagram contributing to the elastic cross section in region 5 in fig. 5.3. (b) An example of a diagram contributing to the inelastic cross section in region 5 in fig. 5.3.

In the same way we can calculate ladder diagrams with more loops. Summing all ladders we obtain

$$A_{\text{ladder}} = A_{\text{Born}}\,(1 + A_{\text{Born}}X + (A_{\text{Born}}X)^2 + \dots\,) = \frac{A_{\text{Born}}}{1 - A_{\text{Born}}X}. \qquad (5.40)$$

We see that instead of the exponent in the eikonal regime (where forward scattering dominates) we here obtain a geometric series from ladder type contributions. The importance of higher order corrections is now determined by the quantity $A_{\text{Born}}\,X$. When $|A_{\text{Born}}\,X| \ll 1$ the Born term dominates. This corresponds to region 3 in fig. 5.3.

When instead $|A_{\text{Born}}\,X| > 1$, we expect different results depending on whether it is the real or the imaginary part which dominates. When $\ln(4M_s^2/s) < \pi$, the imaginary part dominates the loop integral in eq. (5.38). Thus this diagram is dominated by real intermediate states i in fig. 5.1a, and the ladder diagrams in fig. 5.1b or fig. 5.5b should be important higher order corrections. This corresponds to region 4 in fig. 5.3.

When $\ln(4M_s^2/s) > \pi$ (region 5 in fig. 5.3) the real part dominates the loop integral. This implies that inelastic scattering and virtual intermediate states are essential. We then expect important contributions from more complicated, non-ladder, diagrams, like the examples shown in fig. 5.6. For this reason we do not expect the result in eq. (5.40) to be representative for a sum of all higher order corrections in this kinematical region.

5.6 Cross sections

Below we successively discuss the cross sections obtained in the five different regions in fig. 5.3.

5.6.1 Region 1, $s > M_s^2$ and $|\chi(b_d)| > 1$

In this region $s > M_s^2$ and $|\chi(b_d)| > 1$. As discussed in section 5.5.1 the scattering is suppressed for $-t > M_s^2$. The first constraint therefore means that the cross section is dominated by small angle scattering, the imaginary part dominates the one-loop contribution, and the eikonal $\chi(b)$ exponentiates. The cross section is then given by

$$\sigma = \int d^2\bar{b}_\perp \, 2Re(1 - e^{i\chi(\bar{b}_\perp)}). \tag{5.41}$$

The effect of the constraint $|\chi(b_d)| > 1$ was illustrated in fig. 5.4a. It implies that $b_d < b_c$, and that the approximation $\chi \approx -(b_c/b)^n$ in eq. (5.31) is relevant for all $b > b_c$. In particular this means that, for $b > b_c\,(> b_d)$, we have $|\chi| < 1$ and $2Re(1 - e^{i\chi(\bar{b}_\perp)}) \approx \chi^2$. For central collisions, where $b < b_c$, higher order loop corrections are important to satisfy unitarity. Here $|\chi|$ is larger than 1 and rapidly varying, the exponent in eq. (5.41) is oscillating, and therefore

$$\left\langle \, 2Re(1 - e^{i\chi(\bar{b}_\perp)}) \, \right\rangle \approx 2. \tag{5.42}$$

(For $b < b_d$ the variation in χ is only logarithmic, and therefore small in *relative* magnitude. As χ is very large, the variation may still be large in *absolute* magnitude and such that eq. (5.42) is valid also here.) Inserting these results into eq. (5.41), we get (for $n \geq 2$) the following result for the total cross section:

$$\sigma \approx \int_0^{b_c} d^2b \cdot 2 + \int_{b_c}^{\infty} d^2b \left(\frac{b_c}{b}\right)^{2n} = \pi b_c^2 (2 + \frac{1}{n-1}) = 2\pi\, b_c^2\, \frac{n - 1/2}{n-1}. \tag{5.43}$$

When s is increased, σ grows proportional to $b_c^2 \propto s^{2/n}$. We note that the cross section is dominated by central collisions with $b < b_c$ (especially for large n), with only a small contribution from larger impact parameters. Integrating the constant 1 in the parenthesis in eq. (5.35) between 0 and b_c gives a dominant forward peak, with oscillations at larger angles. The amplitude for these oscillations falls off proportional to $1/k^{3/2}$, corresponding to $d\sigma/dt \propto 1/k^3$ for the cross section.

For large k the dominant contribution in eq. (5.35) comes from the term $e^{i\chi}$ and a small range of b-values around b_s, where

$$b_s = b_c \left(\frac{n}{kb_c}\right)^{\frac{1}{n+1}}. \tag{5.44}$$

For these b-values the frequencies of the exponents $e^{i\overline{k}\cdot\overline{b}}$ and $e^{i\chi(\overline{b})}$ in eq. (5.35) oscillate in phase, which gives an enhanced contribution. Using the saddle-point approximation we get from this contribution (apart from logarithmic

corrections) a cross section which falls off like $d\sigma/dt \propto 1/t^{\frac{n+2}{n+1}}$. This contribution is dominating for $k > n/b_c$, where $|\chi(b_s)| > 1$. As pointed out in [4] it corresponds to classical scattering in a $1/r^{n+1}$-potential. For small scattering angles θ we have for a non-relativistic particle with mass m_1 moving with constant speed v and momentum $p = m_1 v$ in the potential of a mass m_2

$$\begin{aligned}\theta \approx \frac{|\bar{p}_\perp|}{|\overline{p}|} &= \frac{1}{|\overline{p}|}\int_{-\infty}^{\infty} dt F_\perp(r) \qquad (5.45)\\ &= -G_{N(4)} R^n S_n \Gamma(n) \frac{m_1 m_2}{m_1 v}\int_{-\infty}^{\infty}\frac{dr}{v}\frac{d}{db}\left(\frac{1}{\sqrt{r^2+b^2}}\right)^{n+1}\\ &= \frac{n(2\sqrt{\pi})^n\Gamma(\frac{n}{2})}{8\pi v^2}\frac{m_2}{M_D^{n+2}}\frac{1}{b^{n+1}}.\end{aligned}$$

From this we see that if $m_1 = s/(4m_2)$

$$b_{\text{nonrel}} = b_c\left(\frac{n}{4vpb_c}\right)^{\frac{1}{n+1}} \qquad (5.46)$$

agreeing parametrically with eq. (5.44). (A numerical difference is expected since eq. (5.44) is ultra-relativistic whereas eq. (5.46) is a non-relativistic result.) This behavior is discussed in more detail in [4], and we note that in this region, where s is much larger than both M_s^2 and s_{cd}, our result is consistent with the result of this reference. A necessary condition is, however, that $\sqrt{s}$, M_D, and M_s have values such that $b_s > b_d = 1/M_s$, which for fixed k-value gives a minimum value for M_s. If this relation is not satisfied, the phase variation in $\exp(i\chi)$ is given by eq. (5.32) rather than eq. (5.31), and therefore we do not get the phase coherence in the integral in eq. (5.35).

5.6.2 Region 2, $s > M_s^2$ and $|\chi(b_d)| < 1$

In region 2, s is larger than M_s^2 but smaller than s_{cd}, and therefore $b_d > b_c$. A typical example is illustrated in fig. 5.4b. We see here that $|\chi|$ is small compared to 1, apart from the logarithmic peak for very small b. The influence of the small b peak is also suppressed by a phase space factor proportional to $b\,db$. The cross section is therefore well approximated by the Born amplitude.

The largest contributions to the cross section come from b-values in the neighborhood of b_d; for larger b, $|\chi|$ falls off $\propto (b_c/b)^n$, and for smaller b the scattering is limited by the smaller phase space $\sim b\,db$. These b-values are just in the transition region between the two asymptotic forms in eqs. (5.31, 5.32). To get a good estimate of the cross section we should therefore use the exact expression for χ in eq. (5.28). For an order of magnitude estimate we may, however, approximate χ by the asymptotic result $\chi \approx -(b_c/b)^n$ for $b > b_d$, and

by a constant $= -(b_c/b_d)^n$ for all $b < b_d$. This gives the following qualitative estimate for the total cross section:

$$\sigma \sim \int_0^{b_d} d^2b \left(\frac{b_c}{b_d}\right)^{2n} + \int_{b_d}^{\infty} d^2b \left(\frac{b_c}{b}\right)^{2n} = \pi \frac{b_c^{2n}}{b_d^{2n-2}} \frac{n}{n-1}. \tag{5.47}$$

As $b_c \sim (s/M_D^{n+2})^{1/n}$, and $b_d = 1/M_s$, we note that the cross section grows $\propto s^2 M_s^{2n-2}/M_D^{2n+4}$. Thus, although the cross section is comparatively small in this region, it has a stronger growth rate $\propto s^2$ than in region 1.

For the differential cross section, we note that the t-channel Born amplitude is proportional to $1/k^2$ for $-k^2 \gg M_s^2$. This implies that the cross section has a forward peak. It corresponds to scattering at distances small compared to $1/M_s$, in the $1/r$ potential from eq. (5.26). There is however no forward divergence since the growth is softened at $-k^2 \sim M_s^2$, i.e. at distances comparable to the brane thickness.

5.6.3 Region 3, $s < M_s^2$ and $|A_{\text{Born}}X| < 1$

In region 3 the cross section is also dominated by the Born amplitude. But in this case the scattering is almost isotropic (apart from spin dependences) as the factor $-k^2$ in the propagator is small compared to the heavier and most important KK modes. This implies that we may also have important contributions from u- and s-channel exchanges. For identical particles, the u-channel contribution has the same magnitude as that from t-channel.

5.6.4 Region 4, $s < M_s^2$, $|A_{\text{Born}}X| > 1$ and $\mathbf{Im}(X) > \mathbf{Re}(X)$

The one-loop t-type contribution in fig. 5.5a, is dominated by the imaginary part, originating from real intermediate states. If loop diagrams of this type dominate, the all-loop amplitude is approximated by the geometric sum in eq. (5.38). As in region 3, the result is then approximately isotropic, but here higher order corrections give some suppression compared to the Born approximation. For identical particles the u-type ladder is identical to the t-type ladder and hence equally important. For particle-antiparticle scattering s-channel contributions have to be considered.

5.6.5 Region 5, $s < M_s^2$, $|A_{\text{Born}}X| > 1$ and $\mathbf{Im}(X) < \mathbf{Re}(X)$

In this region the one-loop diagram has a dominant real part. This implies that virtual intermediate states and inelastic reactions are important. Therefore non-ladder diagrams are expected to give large contributions, and we showed two examples in fig. 5.6. This region is consequently much more complicated than the other kinematical regions. It corresponds to situations where the

effective cut-off M_s is large ("narrow brane" or strong "brane tension") and the energy is in an intermediate range. From fig. 5.3 we see that for, e.g. $n = 3$, M_s must be larger than 5 M_D. In this paper we will not make any specific predictions for what might be expected in this kinematic region.

5.7 Conclusions

In the ADD model it is assumed that standard model particles live on a 4-dimensional brane, embedded in a $(4 + n)$-dimensional space with n compactified dimensions. In these only the gravitational field is allowed to propagate. If the brane is infinitely thin and infinitely rigid, the exchange of very massive Kaluza–Klein modes represents a contact interaction of infinite strength between the standard model particles. This is not physically acceptable and different ideas have been proposed to regularize the scattering process.

If the brane has a finite width, or if it is not infinitely well localized, the exchange of KK modes will be suppressed for KK wavelengths shorter than the width of the brane, or the size of its fluctuations. This will therefore give an effective cut-off (denoted M_s) for high KK masses, which does not have to be of the same magnitude as the fundamental Planck mass M_D.

In this paper we have studied the effect of such a cut-off on the scattering of standard model particles at various energies. We find that several troublesome infinities and divergencies are removed. The scattering process depends on three different energy scales, the collision energy $\sqrt{s}$, the fundamental Planck scale M_D, and the cut-off scale M_s. The Planck scale, $M_D = (8\pi R^n G_{N(4)})^{-1/(n+2)}$, depends on the compactification radius R of the extra dimensions and the magnitude of Newton's constant, while the effective cut-off depends on the width of the brane, $M_s \sim$ (brane thickness)$^{-1}$, or the fluctuations in its position. These scales are thus not automatically related. Clearly the compactification scale R must be larger than the brane width $1/M_s$.

Depending on the relative magnitude between these scales, we have here studied five different kinematical regions with different dynamical behavior. In one region (region 1 in fig. 5.3), the scattering is dominated by small angles, and the eikonal approximation is applicable. Here we recognize classical scattering in a $1/r^{n+1}$ potential and the results of Giudice-Rattazzi-Wells [4]. In two other regions (2 and 3 in fig. 5.3) the Born approximation is applicable. In one of these (region 2) forward scattering dominates, and corresponds to scattering in a $1/r$ potential, but with a coupling enhanced by a factor proportional to $(\frac{\text{compactification radius}}{\text{brane width}})^n$ compared to scattering in the ordinary $1/r$ Newtonian large distance potential. In the other Born region (region 3) the scattering is approximately isotropic, as expected in [5,6]. In a fourth region the exponentiation from ladder-type diagrams in the eikonal region is replaced by a geometric sum. The scattering is expected to be mostly elastic since on-shell intermedi-

ate states dominate, but approximately isotropic. In the last region inelastic processes and non-ladder loop diagrams are important and make predictions very difficult. The boundaries between the different regions are expressed in the three mass scales involved, as illustrated in fig. 5.3.

Acknowledgments

We thank Leif Lönnblad and Johan Bijnens for useful discussions.

References

[1] N. Arkani-Hamed, S. Dimopoulos, and G. R. Dvali *Phys. Lett.* **B429** (1998) 263–272, hep-ph/9803315.

[2] N. Arkani-Hamed, S. Dimopoulos, and G. R. Dvali *Phys. Rev.* **D59** (1999) 086004, hep-ph/9807344.

[3] I. Antoniadis, N. Arkani-Hamed, S. Dimopoulos, and G. R. Dvali *Phys. Lett.* **B436** (1998) 257–263, hep-ph/9804398.

[4] G. F. Giudice, R. Rattazzi, and J. D. Wells *Nucl. Phys.* **B630** (2002) 293–325, hep-ph/0112161.

[5] T. Han, J. D. Lykken, and R.-J. Zhang *Phys. Rev.* **D59** (1999) 105006, hep-ph/9811350.

[6] G. F. Giudice, R. Rattazzi, and J. D. Wells *Nucl. Phys.* **B544** (1999) 3–38, hep-ph/9811291.

[7] G. F. Giudice and A. Strumia *Nucl. Phys.* **B663** (2003) 377–393, hep-ph/0301232.

[8] D. Atwood, S. Bar-Shalom, and A. Soni *Phys. Rev.* **D62** (2000) 056008, hep-ph/9911231.

[9] R. I. Glauber, *Lectures in Theoretical Physics*. Interscience Publisher, NY, 1959.

[10] R. Blankenbecler and M. L. Goldberger *Phys. Rev.* **126** (Apr, 1962) 766–786.

[11] R. C. Arnold *Phys. Rev.* **153** (Jan, 1967) 1523–1546.

[12] R. Emparan, G. T. Horowitz, and R. C. Myers *Phys. Rev. Lett.* **85** (2000) 499–502, hep-th/0003118.

[13] S. Dimopoulos and G. Landsberg *Phys. Rev. Lett.* **87** (2001) 161602, hep-ph/0106295.

[14] S. B. Giddings and S. Thomas *Phys. Rev.* **D65** (2002) 056010, hep-ph/0106219.

[15] P. Kanti *Int. J. Mod. Phys.* **A19** (2004) 4899–4951, hep-ph/0402168.

[16] L. Lönnblad, M. Sjodahl, and T. Akesson *JHEP* **09** (2005) 019, hep-ph/0505181.

[17] C. M. Harris and P. Kanti *JHEP* **10** (2003) 014, hep-ph/0309054.

[18] M. Bando, T. Kugo, T. Noguchi, and K. Yoshioka *Phys. Rev. Lett.* **83** (1999) 3601–3604, hep-ph/9906549.

[19] T. Kugo and K. Yoshioka *Nucl. Phys.* **B594** (2001) 301–328, hep-ph/9912496.

[20] M. Sjodahl hep-ph/0602138.

Classical and Non-Classical ADD Phenomenology with High-$E_\perp$ Jet Observables at Collider Experiments

Paper VI

LU TP 06-29
August 2006

Classical and Non-Classical ADD Phenomenology with High-$E_\perp$ Jet Observables at Collider Experiments

Leif Lönnblad [1]
and
Malin Sjödahl[2]
Department of Theoretical Physics, Lund University,
Sölvegatan 14A, S-223 62 Lund, Sweden

Submitted to JHEP

Abstract
We use the results from a recent investigation of hard parton–parton gravitational scattering in the ADD scenario to make semi-quantitative predictions for a few standard high-$E_\perp$ jet observables at the LHC. By implementing these gravitational scattering results in the PYTHIA event generator and combining it with the CHARYBDIS generator for black holes, we investigate the effects of large extra dimensions and find that, depending on the width of the brane, the relative importance of gravitational scattering and black hole production may change significantly. For the cases where gravitational scatterings are important we discuss how to distinguish gravitational scattering from standard QCD partonic scatterings. In particular we point out that the universal colorlessness of elastic gravitational scattering implies fewer particles between the hard jets, and that this can be used in order to distinguish an increased jet activity induced by gravitational scattering from an increased jet activity induced by eg. super-symmetric extensions where the interaction is colorful.

[1]Leif.Lonnblad@thep.lu.se
[2]Malin.Sjodahl@thep.lu.se

6.1 Introduction

The most exotic, and by far most discussed collider signal of large extra dimensions in the ADD scenario [1–3] is the copiously produced extra dimensional black holes [4–7]. While these are expected to come with large cross sections and characteristic signals at the LHC for a "natural" Planck scale of around 1 TeV, both cross section and signals suffer severely from uncertainties associated with quantum gravity. This provides a wonderful chance to probe quantum gravity, but from the point of view of verifying the scenario it is not ideal. It is therfore worth looking for processes which involve fewer uncertainties than decaying black holes.

Other important ADD processes involve Kaluza–Klein modes, either the production of real ones, or the exchange of virtual ones in gravitational scattering of hard partons. The signal for the former involves a large missing transverse momentum and will be difficult to distinguish from eg. the production of stable super-symmetric particles in some SUSY extensions of the standard model. The later will show up as an increase of the jet cross sections at high energies and may, if this increase is is small, be difficult to distinguish from other beyond-the-standard-model effects.

In a previous paper [8] we investigated an alternative signal for the ADD scenario, namely the disappearance of the high-$E_\perp$ jet cross section due to the formation of black holes. However, in that paper we neglected the contribution from hard gravitational scattering.

Lately a coherent picture of gravitational scattering in the ADD model, at both low and high energies, was presented in [9]. In this paper we investigate the phenomenological consequences. Again, we will concentrate on standard jet observables to see how they are affected by the existence of large extra dimensions, using different choices of the model parameters. We will try to give a complete semi-quantitative description of the observables ranging from the region of perturbative gravitational scattering in the low-energy end to the domain of classical (non-quantum gravitational) black holes for energies above the Planck scale.

While the LHC should easily discover large extra dimensions for the most natural choices of Planck masses and number of extra dimensions, we find situations where the only signal could be a slight increase of the high-$E_\perp$ jet cross section at high energies from gravitational scattering. We therefore discuss the possibility of distinguish such scatterings from standard QCD events by studying the different color topologies involved. We also suggest that such a procedure could be used at the Tevatron to see if an increase of the high-$E_\perp$ jet cross section there could be the result of the onset of subplanckian gravitational scattering.

This paper is organized as follows. After a brief introduction to the ADD scenario in section 6.2, we summarize in section 6.3 the description of gravita-

tional scatterings developed in [9]. We then go on to discuss the production and decay of black holes in section 6.4 and, in section 6.5, we present our results before discussing our conclusions in section 6.6.

6.2 Basics of ADD

The so called ADD scenario, invented in 1998 by Arkani-Hamed, Dvali and Dimopoulos [1,2], aims at explaining the hierarchy problem, i.e. why the observed Planck scale at 10^{19} GeV is so large compared to the masses of the standard model particles. This is done by introducing a number, n, of extra dimensions in which only gravity is allowed to propagate.

In order to explain why these dimensions have not yet been observed, it is assumed that they are compactified with some (common) compactification radius R[1] and that no gauge fields are allowed to propagate in the extra dimensions. Gravity, on the other hand is, and this renders the form of Newton's law at distances, r, much smaller than the compactification radius

$$\frac{V(r)}{m_1 m_2} = -\frac{S_n \Gamma(n)}{M_{\rm P}^{n+2}(2\pi)^n}\frac{1}{r^{n+1}}. \tag{6.1}$$

Here $M_{\rm P}$ is the fundamental Planck scale, $S_n = 2\pi^{n/2}/\Gamma(n/2)$ is the surface of a unit sphere in n dimensions and $\Gamma(n)$ is the Euler Gamma function. At distances large compared to the compactification radius we must recover the normal 3+1-dimensional form of Newton's law

$$\frac{V(r)}{m_1 m_2} = -G_{N(4)}\frac{1}{r}. \tag{6.2}$$

Expressing Newton's constant in terms of the observed (3+1)-dimensional Planck scale, $G_{N(4)} \sim 1/M_{\rm P4}^2$, then gives the relation $M_{\rm P4}^2 \sim M_{\rm P}^{n+2}R^n$ between the fundamental Planck scale $M_{\rm P}$ and the observed 4-dimensional Planck scale, which explains how the fundamental Planck scale could be (almost) of the same order as the weak scale, but the observed effective Planck scale, $M_{\rm P4}$, many orders of magnitude larger.

However, this also implies that gravity should be very strong at small distances which opens up for the possibility of observing gravitational scattering and black holes at collider experiments.

6.3 Gravitational scattering in ADD scenario

Although the field theory of gravity is ultimately divergent also in more than 4 dimensions, an effective low-energy theory can be constructed by a perturbative

[1]We use R to denote the compactification radius rather than the compactification circumference (see the appendix for a discussion on conventions).

treatment of the metric in the limit where the metric perturbation is small. A Lagrangian can be derived and Feynman diagrams can be constructed from it. This is done in [10,11]. Since the extra dimensions are compactified, momentum occurs in each direction as multiples of some ground frequency, ie. as Kaluza–Klein modes.

In a gravitational event an outgoing Kaluza–Klein (KK) mode will have some (quantized) momentum in the extra dimensions, which enters in the Lagrangian as a mass term. But the KK modes can also occur as intermediate states in which case they have to be properly summed or, taking the continuum limit, integrated over. This gives rise to the integral

$$\sum_{\overline{m}_{\overline{l}}} \frac{1}{-m_{\overline{l}}^2 + k^2} \approx S_n R^n \int \frac{m^{n-1}}{-m^2 + k^2} dm. \tag{6.3}$$

Here $\overline{l}$ enumerates the allowed momenta, $m_{\overline{l}}$, in the extra dimensions, m is the absolute value of $m_{\overline{l}}$, and k^2 is the momentum squared of the $3+1$-dimensional part of the propagator. Note that this sum over KK states does imply momentum non-conservation for momenta transverse to the brane where the standard-model fields live, but this is not a complete surprise since translational invariance is broken in the bulk by the presence of the brane.

6.3.1 Dealing with divergences

What is worrying though, is that the field theory seems to contain divergences already at the tree level. However, the divergences dissappear when imposing the requirement that the standard model particles live on a brane, either directly by assuming a narrow distribution of the standard model fields into the extra dimensions [9, 12], or by a introducing a "brane tension" [13, 14]. Both these methods gives physical effective cut-offs for the momentum (mass) of the KK modes. For example, a Gaussian extension $e^{-m^2/(2M_s^2)}$ of the standard model field densities into the bulk gives an "effective propagator" [9]

$$D(k^2) = R^n S_n \int \frac{dm\, m^{n-1}}{k^2 - m^2} e^{-m^2/M_s^2} \tag{6.4}$$

for the exchange of KK modes with four-momentum exchange k^2. (This object, $D(k^2)$, is here sloppily called a propagator, despite the fact that the multiplicative Lorentz structure is not taken into account.)

For momentum exchange small compared to M_s, the standard model momentum k in the propagator is irrelevant (for most m in the integral), such that s-, t-, and u-channels are equally efficient and the scattering is fairly isotropic.

For $\sqrt{k^2} \gg M_s$ on the other hand, the interaction is dominated by forward scattering via the t-channel, and an all-order eikonal calculation is necessary

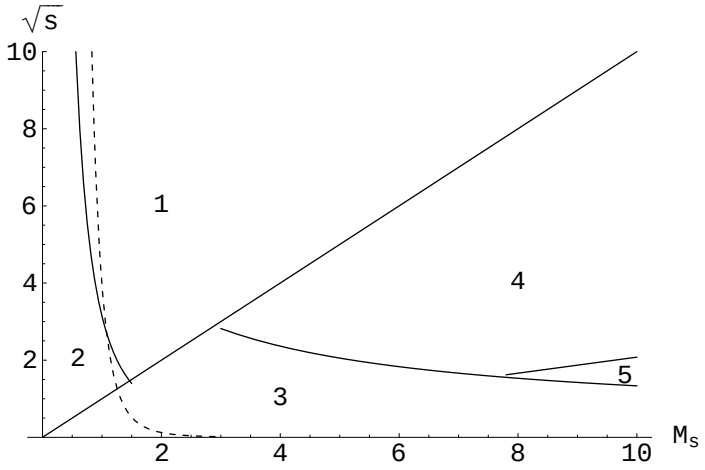

Figure 6.1: The $(\sqrt{s}, M_s)$-plane for $n = 4$ and $M_{\rm P} = 1$. The straight line separating region 1 and 4 is $\sqrt{s} = M_s$ while the straight line separating region 4 and 5 is the line where the real and imaginary parts in eq. (6.16) have equal magnitude. The power-like solid curve separating region 1 and 2 is $\sqrt{s_{cd}}$ from eq. (6.12) as a function of M_s and the line separating the regions 4 and 5 from region 3 is the line where $|A_{\rm Born}X| = 1$, see eq. (6.16). In the regions 1 and 2 $\sqrt{s}$ is larger than M_s, and, at least for $\sqrt{s} \gg M_s$, the eikonal approximation is correct. In region 1 the eikonal is, depending on b, either large compared to 1 or given by eq. (6.10). In region 2 on the other hand the b-range where $|\chi|$ is small includes a region where it is described by eq. (6.11). In region 3 the correction corresponding to higher order loops is small, but in region 4 it is important and helps assuring unitarity. The dashed line indicates the minimal $\sqrt{s}$ (for a given M_s) at which the black hole radius eq. (6.21) is larger than the brane width. The plot visibly very similar for n=6.

to ensure unitarity [9, 15]. The stage is therefore set by three energy scales, the fundamental Planck mass, $M_{\rm P}$, the inverse brane width (brane tension), M_s, and the rest mass of the partonic scattering, $\sqrt{s}$, and the phenomenology depend on their relative magnitude. It is illuminating to fix one of these scales an study the different kinematical regions in the plan spanned by the other two. This is done in fig. 6.1 where the $(\sqrt{s}, M_s)$-plane is plotted for $M_{\rm P}$ fixed to 1 TeV.

Below we will successively describe the contribution from the t-, u-, and s-channels and the various regions in fig. 6.1.

6.3.2 t-channel

As argued in the above section, we expect t-channel contributions to dominate at energies high compared to M_s. Unitarity constraints does, however, imply that the Born approximation can not be valid for sufficiently high energies. In fact, as is argued in [15,16], a completely new phenomenon occurs for scattering in more than 3 spatial dimensions; namely the emergence of a length scale associated with the transition from the classical to the quantum domain.

Intuitively this can be understood by considering the ratios

$$\frac{\Delta\theta}{\theta} \text{ and } \frac{\Delta b}{b} \tag{6.5}$$

where θ is the scattering angle and b the impact parameter in a scattering experiment. In the classical domain these ratios are both much smaller than 1. Requiring the opposite, and approximating

$$\Delta\theta \sim \frac{\Delta q}{Mv} \sim \frac{\hbar}{Mv\Delta b} \text{ and } \theta \sim \frac{b}{Mv^2}\frac{dV(b)}{db} \tag{6.6}$$

for a non-relativistic particle with speed, v, mass, M, and transverse momentum, Δq, moving in a potential, V, one finds, for a Coulomb-like potential $V(b) = \alpha/b$, the condition $\alpha > \hbar v$. For coupling constants close to 1, this basically implies that the relativistic and quantum mechanical regions coincide. For a more general potential of the form $V(b) = \alpha/b^{n+1}$, assuming n to be positive (this is what Gausses law gives in 3+n spatial dimensions), the separation of the classical and quantum domain depends on the impact parameter, such that, the transition occurs at $b_c \sim [\alpha/\hbar v]^{(1/n)}$. For gravitational coupling with $\alpha = G_{4+n}MM$, this corresponds to $b_c \sim [G_{4+n}M^2/(v\hbar)]^{1/n}$ [15]. Scattering in the potential eq. (6.1) is therefore expected to be mainly classical only if the impact parameter b is smaller than b_c.

For $M_{\rm P} \sim 1$ TeV the parameters of this equation are such that we will see a transition between the classical and quantum domain at LHC, and a more careful calculation, summing up amplitudes from ladders of t-channel exchange in fig. 6.2 to all orders is necessary. This calculation was performed in [15] by simply ignoring the divergences corresponding to local contributions in eq. (6.3), and recently in [9] by a more careful analysis using the effective propagator eq. (6.4).

The parameter b_c also corresponds to the impact parameter where the eikonal scattering phase

$$\chi(b) \quad = \quad \frac{1}{2s}\int \frac{d^2\bar{k}_\perp}{(2\pi)^2}\, e^{-i\bar{k}_\perp \bar{b}_\perp} A_{\rm Born}(-\bar{k}_\perp^2) \tag{6.7}$$

becomes large compared to $\hbar$. This makes perfect sense, as b_c represents the impact parameter separating quantum mechanical and classical scattering.

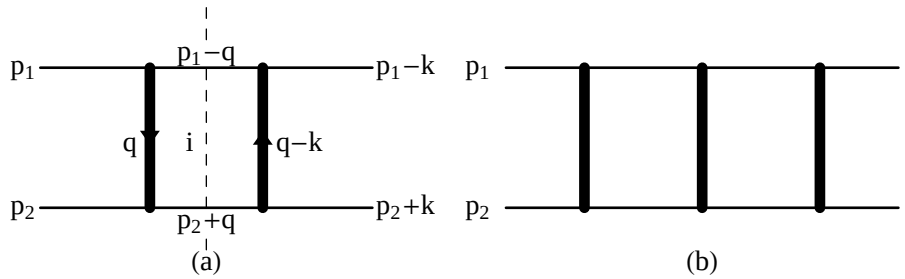

Figure 6.2: (a) The one loop contribution corresponding to exchange of two KK modes. The KK modes are drawn as thick lines and standard model particles as thin lines. (b) The two-loop contribution.

At least in the eikonal region, i.e. for small scattering angles, where there is no spin dependence, the Born amplitude can be written [9, 15]

$$A_{\rm Born}(k^2=t) = \frac{s^2}{2^{n-3}\pi^{n-1}M_{\rm P}^{n+2}}\,S_n\int_0^\infty \frac{dm\,m^{n-1}}{k^2-m^2}\,e^{-m^2/M_s^2} \tag{6.8}$$

where the suppression factor e^{-m^2/M_s^2} comes from implementing the requirement that the standard model particles live on a finite brane [9]. The same effect can be obtained by assuming a finite brane tension [13]. Computing the integrals in eq. (6.7) [9] then gives the result

$$\chi(b) = -\frac{sM_s^n}{(2\sqrt{\pi})^n M_{\rm P}^{n+2}}\Gamma(\frac{n}{2})U(\frac{n}{2},1,\frac{M_s^2b^2}{4}) \tag{6.9}$$

where the U-functions are confluent hyper-geometric functions of the second kind.

In the limit of large third argument, $M_sb \gg 1$ in U, ie. impact parameter much larger than the brane width, χ can be written

$$\chi(b) \approx -\left(\frac{b_c}{b}\right)^n \quad \text{for} \quad b_c \equiv \frac{1}{\sqrt{\pi}}\left[\frac{s\Gamma(n/2)}{M_{\rm P}^{n+2}}\right]^{1/n}. \tag{6.10}$$

At least if $b_c \gg 1/M_s$ the eikonal eq. (6.9) reaches 1 in the region where it is determined by eq. (6.10) and b_c is indeed the parameter associated with the transition from the quantum mechanical to the classical region. For M_s small compared to $M_{\rm P}$ the brane width is more important and there is an energy range where the impact parameter for which $|\chi|$ reaches 1, is given by the small argument limit in U, rather than the large argument limit,

$$\chi(b) \approx \frac{2s}{(2\sqrt{\pi})^n M_{\rm P}^2}\left(\frac{M_s}{M_{\rm P}}\right)^n\left(\ln(M_sb)+\frac{1}{2}\psi(\frac{n}{2})\right) \tag{6.11}$$

where $\psi(\frac{n}{2})$ is the digamma function. The transition between, $|\chi(b)| \approx 1$ described by eq. (6.11), and $|\chi(b)| \approx 1$ described by eq. (6.10), occurs roughly at the energy where $b_c = 1/M_s$, and the phenomenology will therefore differ in the regions $b_c > 1/M_s$ and $b_c < 1/M_s$. Solving $b_c = 1/M_s$ we find

$$s_{cd} = \frac{M_{\rm P}^{n+2}\pi^{n/2}}{M_s^n \Gamma(\frac{n}{2})} \tag{6.12}$$

this is the line separating region 1 and 2 in fig. 6.1. For $t \gg M_s^2$ the all order eikonal amplitude is given by

$$A_{\rm eik}(k^2) = -2is \int d^2\bar{b}_\perp e^{i\bar{k}_\perp \cdot \bar{b}_\perp}(e^{i\chi} - 1). \tag{6.13}$$

When $|\chi|$ is large compared to 1 which, for $b_c \gg 1/M_s$, happens for $b < b_c$, the exponentiation in eq. (6.13) is important while for larger b the eikonal amplitude is approximated by the Born term.

For $b_c < 1/M_s$, region 2 in fig. 6.1, $|\chi|$ is smaller than 1 except for very small impact parameters,

$$b < \frac{1}{M_s} \exp\left(-\frac{(2\sqrt{\pi})^n M_{\rm P}^{n+2}}{2sM_s^n}\right), \tag{6.14}$$

found by ignoring the digamma function in eq. (6.11). In the whole of region 1 and 2 for $t \gg M_s^2$ the gravitational cross section is obtained from the all order eikonal amplitude in eq. (6.13) (although higher order corrections are only important region 1). It is given by

$$\frac{d\sigma_{\rm eik}}{dt} = \frac{1}{16\pi s^2}|A_{\rm eik}|^2. \tag{6.15}$$

If, on the other hand, $\sqrt{s} \ll M_s$, such that $\sqrt{-t}$ necessarily is small compared to M_s, the amplitude is (apart from large angle spin dependences) fairly isotropic. The ladder-type diagrams in fig. 6.2 will effectively turn into ϕ^4 interactions as in fig. 6.3.

Since the coupling grows with energy, higher order corrections will for some s become necessary to ensure unitarity. Summing up all contributions of the type in fig. 6.3, a geometric series is found [9] which helps unitarizing the cross section. For the 1-loop contribution we have, with $P = p_1 + p_2$ as in fig. 6.3,

$$\begin{aligned} A_{1-\rm loop} &= \frac{-i}{2}\int_{q<M_s} \frac{d^4q}{(2\pi)^4} A_{\rm Born}^2 \frac{1}{(P/2-q)^2}\frac{1}{(P/2+q)^2} = \\ &\equiv A_{\rm Born}^2 \cdot X \text{ with } X \approx \frac{1}{32\pi^2}(\ln\frac{M_s^2}{s/4} + i\pi) \end{aligned} \tag{6.16}$$

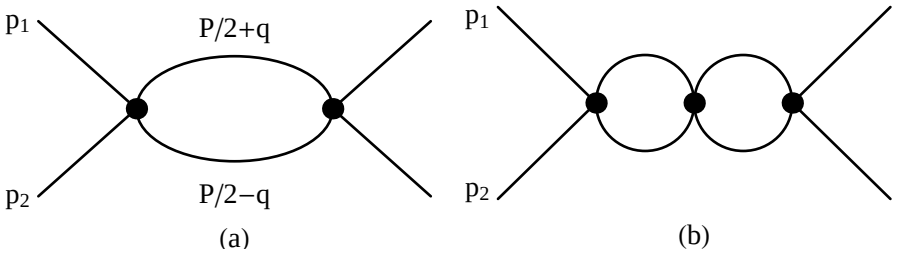

Figure 6.3: When the exchanged momentum is small compared to M_s, the KK propagator are effectively replaced by vertex factors. The diagrams in fig. 6.2 can then be drawn as above with only standard model particle lines.

and higher loop corrections give similar results. Summing all ladders we obtain

$$A_{\text{ladders}} = A_{\text{Born}}\left(1 + A_{\text{Born}}X + (A_{\text{Born}}X)^2 + \dots\right) = \frac{A_{\text{Born}}}{1 - A_{\text{Born}}X}. \quad (6.17)$$

Thus loop contributions of this type helps unitarizing the cross section in region 4 in fig. 6.1, defined to be the region where $\sqrt{s} < M_s$, but on-shell intermediate states in fig. 6.3 dominate. While we can not prove that these are the most important contributions, it seems likely as long as the cross section is dominated by on-shell states. In region 5 in fig. 6.1 this is no longer true since here the imaginary part in eq. (6.16) is larger than the real part. The simulations performed in this paper are in the phase space region 1, 2, 3 and 4 in fig. 6.1, and we use eq. (6.16) to unitarize the cross section in regions 3 and 4 (although it's not important in region 3).

6.3.3 u-channel

In the regions 1 and 2, the u-channel contribution is small compared to forward t-channel scattering. In the regions 3 and 4, corresponding to $\sqrt{s} < M_s$, it is, however, of the same order of magnitude. In fact there is no difference between the u and t-channel in fig. 6.3, implying that u-channel contributions run into problems with unitarity at the same energy as t-channel contributions, and the result eq. (6.16) can be used also for the u-type ladders.

The relevance of the u-channel ladders contribution is, however, significantly lowered by the fact that interaction among similar partons is suppressed at LHC. To get a handle on the importance of u-channel contribution, assume that only valence quarks contribute to the cross section. This is a reasonable assumption at sufficiently high momentum fractions and also, it will give an upper limit. The probability for the colliding partons to have similar flavor,

spin and color is then approximately 1/10. *Assuming* that the t-channel ladders for scattering of particles with momenta p_1 and p_2 to momenta p_3 and p_4 have been calculated for all momentum transfers to be $A_{ladders}(p_1p_2 \to p_3p_4)$, the total amplitude, taking both t- and u-channel contributions into account, would be $A_{u+t} = A_{ladders}(p_1p_2 \to p_3p_4) + A_{ladders}(p_1p_2 \to p_4p_3)$ for scattering of identical particles. We consider for simplicity maximal constructive interference, giving us $A_{u+t} = 2A_{ladders}(p_1p_2 \to p_3p_4)$. The ratio of the average extra cross section for both the t- and u-ladders compared to the pure t-ladders cross section would then be something like $2^2/10$. This is a significant but not critical contribution, and it is an overestimate.

6.3.4 s-channel

For $s \ll M_s^2$, the factor $k^2 = s$ in eq. (6.8) is insignificant compared to most contributing KK masses and gives an amplitude similar to the t- and u-channels. There is, however, one complication. Due to the relative difference in sign between $k^2 = s$ and m^2 in eq. (6.8) KK modes can be produced on shell.

From the point of view of inclusive observables, these s-channel on-shell Kaluza–Klein states are, however, unimportant. The width of a *single* KK mode with mass m to decay into two standard model particles of energy $E/2$ is $\sim m^3 G_{N(4)}$ giving lifetimes of order 1000 seconds [11]. These KK modes will leave the detectors unseen.

6.3.5 Phenomenology of low energy gravitational scattering

As already mentioned section 6.3.1, a gravitational scattering where the Kaluza-Klein mode is not in the outgoing state, comes with a momentum cut-off from the width of the brane, or from fluctuations of the brane. In the low-energy region, 3 in fig. 6.1, where the born approximation is applicable, a cut-off dependent amplitude can be used for describing the interaction. From the point of view of perturbative gravitational scattering with internal KK modes only, this does not result in any extra parameters to describe the interaction. Instead it suffice to replace the Planck scale $M_{\rm P}$ by an effective Planck scale according to

$$M_{\rm eff} = \frac{1}{2}\left(\frac{(n-2)2^n\pi^{\frac{n-2}{2}}M_{\rm P}^{n+2}}{M_s^{n-2}}\right)^{\frac{1}{4}} \tag{6.18}$$

such that the Born amplitude, eq. (6.8), (neglecting spins) can be written

$$A_{\rm Born} = -\frac{s^2}{M_{\rm eff}^4}, \tag{6.19}$$

after integration over m, neglecting $k^2 = t$, u or s. In this kinematical region, gravitational scattering in the ADD model is a well behaved effective field theory depending on only one free parameter, M_{eff}. The low-energy spin dependent footprint of the ADD scenario for *any* number of extra dimensions can then be written

$$\frac{d\sigma}{dt} = \frac{k_s}{s}\left[\frac{\pi\alpha_s^2}{s}f(z) - \frac{s\alpha_s}{M_{\text{eff}}^4}g(z) + \frac{s^3}{\pi M_{\text{eff}}^8}h(z)\right] \tag{6.20}$$

where α_s is the strong coupling constant and k_s, $g(z)$, $h(z)$ and $f(z)$ are process dependent functions taking spin-dependence into account given in [17].

Gravitational scattering differ from standard-model and most beyond-standard-model processes in several ways. The experimentally most striking is probably that it increases with increasing energy. As the experimental situation stands today this is, however, badly overcompensated by the decreasing parton distribution functions for high momentum factions. The interaction is mediated by the large number of Kaluza–Klein modes, implying that the cross section will not have a single resonance structure, as opposed to cross section signatures of most other beyond-standard-model particles. Due to the different spin dependence of gravitational scattering the angular distribution will also differ.

We will here consider another difference, namely that contrary to the main contribution to inclusive cross sections, both in the standard model and in super-symmetric extensions, the gravitational interaction is colorless. As we shall see, this implies noticeable differences in particle multiplicity outside the jets.

6.4 Black holes in ADD scenario

Black holes with mass large compared to the fundamental Planck scale, but with radius small compared to the compactification radius are expected to behave much like extra dimensional versions of astronomical 3+1-dimensional black holes. The Schwarzschild radius is given by

$$r_{\text{Sch}} = \frac{1}{\sqrt{\pi}M_{\text{P}}}\left[\frac{M_{\text{BH}}}{M_{\text{P}}}\frac{8\Gamma(\frac{n+3}{2})}{n+2}\right]^{\frac{1}{n+1}} \tag{6.21}$$

and the temperature is given by [18]

$$T = \frac{n+1}{4\pi r_{\text{Sch}}}. \tag{6.22}$$

Note that small black holes are hotter.

A major difference between black holes in the ADD scenario and ordinary 3-dimensional black holes is that ADD black holes do not radiate gauge fields into most of phase space, since only gravity is allowed to propagate in the extra dimensions. One may believe that this would lead to almost no radiation on the brane (where gauge fields and, hence, also we live) as the bulk phase space is much larger. However, it has been shown that this is not necessarily the case [4].

Since we are considering the non-idealized situation of a finite brane width we must also consider the implications of this on black hole production. In particular, a natural requirement is that the brane is not more extended than the black hole, leading to the condition $r_{\rm Sch} < 1/M_b$ for the formation of black holes. As we will see this prevents black holes from appearing at the LHC for sufficiently small M_s.

On the other hand, if M_s is large, we may, with increasing $\sqrt{s}$, go directly from the Born region 3 in fig. 6.1 to black hole production. This should be worrying since the black holes are treated semi-classically but the gravitational scattering in region 3 is purely quantum mechanical. It is reasonable that the black holes should start behaving classically when the Compton wave length is of the same order as the black hole radius, but it would have been more comforting to only study black hole production in region 1 in fig. 6.1, where the gravitational scattering is mainly classical already at lower energies. This represents a genuine quantum gravity uncertainty.

Already at a classical level the cross section for black hole creation is subject to significant uncertainties. This is basically due the fact that it does not suffice to consider the colliding objects, but in addition the curvature of space-time far outside the black hole needs to be calculated. Classical numerical simulations for black hole formation in extra dimensions have been preformed in [19, 20] with the result that the geometric cross section, πr^2, should be multiplied with a factor $\sim 0.7 - 3$, increasing with the number of extra dimensions. For this paper we have, however, chosen to keep the constant at 1.

As the black holes considered here are formed from partons inside the protons there is also an uncertainty from the usage of parton distribution functions for an essentially non-perturbative process [21] . (A discussion about the effects of quantum fluctuations based on wave packages can be found in [22, 23].)

Then there is the question of the onset of black hole production. It can be argued that no black holes should be formed below (roughly) the Planck scale as the uncertainty principle would forbid sufficient localization of the partons. But precisely when does black holes begin to form?

We consider first the condition that the black holes have to be well localized in our ordinary dimension. Looking at the momenta of the incoming partons in their combined rest frame it is reasonable to require that their wavelength, $\lambda_l \propto 2/\sqrt{s}$, is less than $r_{\rm Sch}$. The corresponding requirement in the transverse

direction gives the requirement: $\lambda_\perp \propto 1/p_T < r_{\rm Sch}$. Clearly one can argue about the proportionality constant. We have chosen

$$M_{\rm min} = 2/r_{\rm Sch}(M_{\rm min}). \tag{6.23}$$

Combining this with the expression for the Schwarzschild radius eq. (6.21) we get

$$M_{\rm min} = M_{\rm P}\left[\frac{(2\sqrt{\pi})^{n+1}(n+2)}{8\Gamma(\frac{n+3}{2})}\right]^{\frac{1}{n+2}}. \tag{6.24}$$

Numerically the value of $M_{\rm min}$ is then approximately twice the Planck mass.

As we consider a finite brane width we must add the condition $r_{\rm Sch} > 1/M_s$, leading to the minimal mass

$$M_{\rm min2} = \frac{M_{\rm P}^{n+2}(2+n)\pi^{\frac{n+1}{2}}}{8\Gamma\left[\frac{3+n}{2}\right]M_s^{1+n}}. \tag{6.25}$$

Again one can argue about the proportionality constant. While we take into account the effects of a finite brane, we do not consider the dynamics governing the brane, and possibly describing its width, although this may have significant effects on the spectra observed [24, 25].

Once a black hole has formed it is believed to lose most of its geometric asymmetries in a short period referred to as the balding phase. This phase leaves a black hole whose only geometric asymmetry can be described by one angular momentum parameter. However, it turns out that this angular momentum tends to be lost rather quickly via Hawking radiation, such that the black hole (apart from gauge charges) can be described by the Schwarzschild metric.

Neglecting the gauge charges, which in the case of electromagnetism has been shown to have a modest influence [26], the disappearance of the black hole would be well described by Hawking radiation if the black hole was much heavier than the Planck mass, and if no brane effects, such as the black hole recoiling of the brane [27, 28], or interacting with the brane [24, 25] is taken into account. The problem is that most collider-produced black holes will not be much heavier than the Planck.

For a hole which is not heavy compared to the Planck mass one cannot treat the metric as a static background for the emitted quanta, the back-reaction of the quanta to the metric should be taken into account and this is not done in the derivation of the Hawking radiation [29]. Also, at some point, the lifetime of the black hole becomes shorter than its radius. This makes it difficult to talk about a thermalized black hole.

Considering all of this, it should not come as a surprise if black holes where observed with spectra which differs significantly from that expected from eq. (6.22).

6.5 Results

We have used the amplitudes for gravitational scattering for the different regions in fig. 6.1 presented above to reweight the standard QCD $2 \to 2$ scatterings in the PYTHIA (version 6.2 [30]) event generator. In the regions 1 and 2 we have used the (elastic spin-independent t-type) all order eikonal cross section from eq. (6.7) and eq. (6.13). In the regions 3 and 4 we have used the spin dependent Born amplitude [31] corresponding to eq. (6.20), and higher order corrections according to eq. (6.17). In region 3 the higher order corrections are small, but in region 4 they are essential. In the case of particle-antiparticle scattering, such that the scattering can be mediated via the s-channel, we have "unitarized" also the s-channel contribution in region 4 (and 3) using eq. (6.17), despite that fact the the s-type ladders, diagrams in fig. 6.3 rotated by $\pi/2$ do not have on-shell intermediate standard model particles. There are thus several fundamental uncertainties associated with gravitational scattering in region 4. First, we use the spin dependent Born amplitude, but we do not take spin dependence consistently into account in eq. (6.17) since we use the same $A_{\text{Born}}(t)$ everywhere in all ladders. Second, we suppress s-type contributions in the same way as u- and t-type. (Note that we call the ladders in fig. 6.2 and fig. 6.3 t-type, sometimes these diagrams are referred to as s-channel, since the resummation is in s.)

The different treatments in the various regions means that we could expect a discontinuous transition when $\sqrt{s}$ is increased, such that we cross the line $\sqrt{s} = M_s$ in fig. 6.1. As long as the Born approximation is applicable (regions 2 and 3), this transition just corresponds to starting neglecting spin-dependence in region 2. If the transition is between region 4 and 1, the situation is, however, worse due to fundamental uncertainties associated with region 4.

For each generated $2 \to 2$ scattering we also change the color flow between the scattered partons with a probability $\sigma_{\text{ADD}}/(\sigma_{\text{ADD}} + \sigma_{\text{QCD}})$ to reflect the colorless nature of the graviton exchange. The resulting partonic state is then allowed to evolve a QCD cascade and is finally hadronized to produce fully simulated hadron-level events. Where relevant, we have also added multiple soft and semi-hard QCD scatterings to simulate the underlying event according to the model implemented in PYTHIA [32].

In addition, we have used the CHARYBDIS [33] program to simulate the production and decay of black holes as described in section 6.4. To ensure that the energy is sufficiently localized, in our ordinary dimensions and in the extra dimensions, we have required a minimal black hole mass according to eq. (6.24) and eq. (6.25). We also use the Schwarzschild radius to cut off any QCD and gravitational $2 \to 2$ scatterings for large enough masses and transverse momenta as discussed in [8].

We limit our investigation to two standard inclusive high-$E_\perp$ jet observables, namely the $E_\perp$-spectrum of the highest-$E_\perp$ jet in an event, and the

$M_{\rm eff}$	n	$M_s/M_{\rm P}$	$M_{\rm P}$	M_s
1.0	4	$\frac{1}{2}$	0.45	0.22
1.0	4	1	0.63	0.63
1.0	4	2	0.89	1.79
1.0	4	4	1.26	5.05
1.0	6	2	0.56	1.13
0.7	4	4	0.88	3.54
4.0	4	4	5.05	20.21

Table 6.1: The different values of $M_{\rm eff}$, number of extra dimensions, n, and the ratio of $M_s/M_{\rm P}$ used in the simulations together with the resulting approximative values of $M_{\rm P}$ and M_s. The masses are all given in units of TeV.

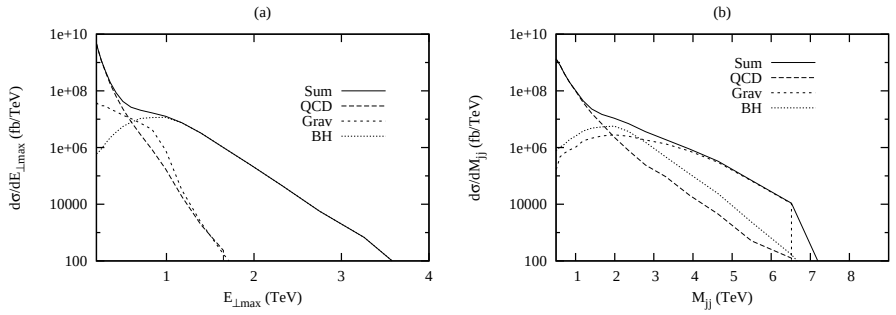

Figure 6.4: (a) The $E_\perp$-spectrum of the highest $E_\perp$ jet in an event, and (b) the invariant mass spectrum of the two highest $E_\perp$ jets in an event at the LHC. In both cases $M_{\rm eff} = 1$ TeV with 4 extra dimensions and $M_s/M_{\rm P} = 2$ ($M_{\rm P} \approx 0.9$ TeV, $M_s \approx 1.8$ TeV). The long-dashed lines are the contribution from QCD scatterings, short-dashed lines the contribution from gravitational scatterings, dotted lines the contribution from the decay of black holes and full lines the sum of all contributions.

distribution in invariant mass, M_{jj}, of the two highest-$E_\perp$ jets in an event. As high-$E_\perp$ jets will be a part of almost any signal of new physics at the LHC, such observables will be measured early on after the start of the experiments and it is also where one would expect gravitational scatterings to contribute. We use a simple cone algorithm[2] with a code radius of 0.7, assuming a calorimeter covering the pseudo-rapidity interval, $|\eta| < 2.5$, and requiring a minimum $E_\perp$ of 100 GeV for the resulting jets. We have checked that our results do not depend much on the algorithm chosen.

[2]The `GETJET` algorithm originally written by Frank Paige.

In fig. 6.4 we show generated the $E_{\perp\max}$ and M_{jj} distributions at the LHC for the case of four extra dimensions, $M_{\text{eff}} = 1$ TeV and $M_s/M_{\text{P}} = 2$ (see table 6.1 for the resulting values of M_{P} and M_s). In the $E_{\perp\max}$ spectra we find that the cross section is dominated by QCD scatterings at low $E_\perp$as expected, followed by an intermediate region where gravitational scattering becomes important before black-hole production starts dominating the cross section at large $E_\perp$. For the M_{jj}-spectrum, the situation is different, and the gravitational scatterings dominates at large masses.

Modulo effects of the parton densities we expect both gravitational scattering and black-hole production to increase with energy. For black holes one may naively not necessarily expect to find high-$E_\perp$ jets, as energetic quanta are Boltzmann suppressed in the Hawking radiation. However, it turns out that the large cross section for a black hole to form at high s, multiplied with the small probability for the Black hole to radiate extremely energetic quanta, may dominate over the non-black hole cross section for rather large transverse momenta [8]. (Even if well localized QCD and gravitational scattering events are not suppressed due to black hole production.) These extremely energetic quanta do, however, not obey the semiclassical approximation in the Hawking radiation derivation, and are therefore associated with large uncertainties.

For large $E_\perp$, however, the gravitational scattering events, just as the QCD ones, will be localized inside the Schwarzschild radius and will collapse into a black hole.

In fig. 6.5 we show the M_{jj}-distribution of gravitational scatterings only, divided into the contributions from the different regions in fig. 6.1. Keeping $M_{\text{eff}} = 1$ TeV and the number of extra dimensions (4) fixed, we vary M_s/M_{P} and find that the contribution from region 1 dominates except in the low-mass regions below M_s. The transitions between the regions are not sharp, mainly due to the smearing introduced by shower, hadronization and the jet reconstruction. This smearing hides the fact that the transition between $\sqrt{s} > M_s$ and $\sqrt{s} < M_s$ is discontinuous in the distribution of the generated s. In the case this transition occurs between region 2 and 3, where the Born approximation is applicable, the discontinuity is not even visible in the generated s-distribution. If the transition occurs between region 4 and 1, a discontinuity can, however, be seen.

We note in table 6.1 that, although M_{eff} is kept fixed, giving the same amount of gravitational scattering at $\sqrt{s} \ll M_s$, increasing the ratio M_s/M_{P} will increase *both* M_s and M_{P}. And since black-hole production depends of M_{P} and M_s differently via eqs. (6.21), (6.23) and (6.25), we can vary the relative importance of gravitational scattering and black-hole production by varying M_s/M_{P}. Hence we see in fig. 6.6a that lowering M_s/M_{P} to 1, the gravitational scattering will never give a sizeable contribution to the $E_{\perp\max}$-distribution, while increasing the ratio to 4 (fig. 6.6b) results in the gravitational scattering

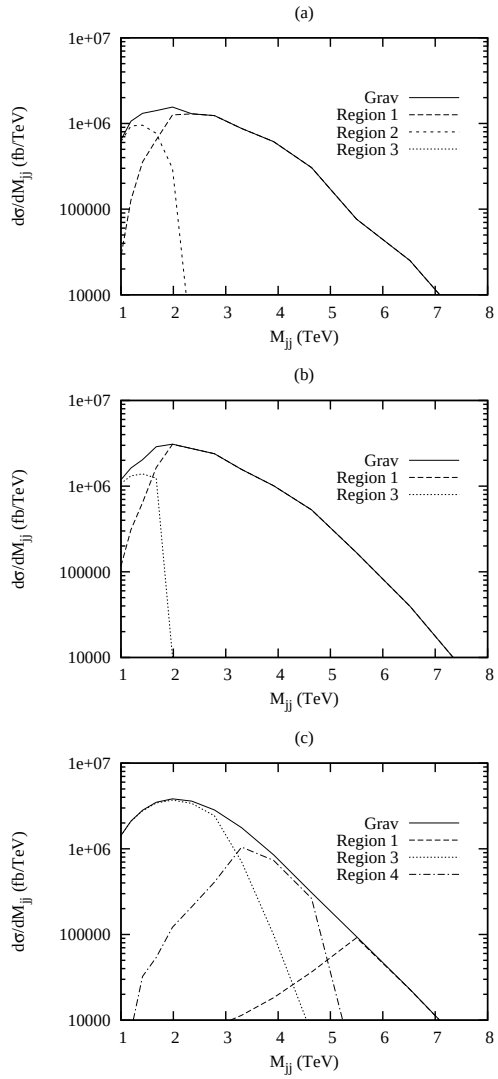

Figure 6.5: The contribution of different regions in figure 6.1 to the di-jet mass spectrum from gravitational scatterings at the LHC with $M_{\rm eff} = 1$ TeV, 4 extra dimensions and $M_s/M_{\rm P} = 1$ (a), 2 (b) and 4 (c). In all cases the full line is the sum of all contributions and the contributions from regions 1, 2, 3 and 4 is given by the long-dashed, short-dashed, dotted and dash-dotted lines respectively.

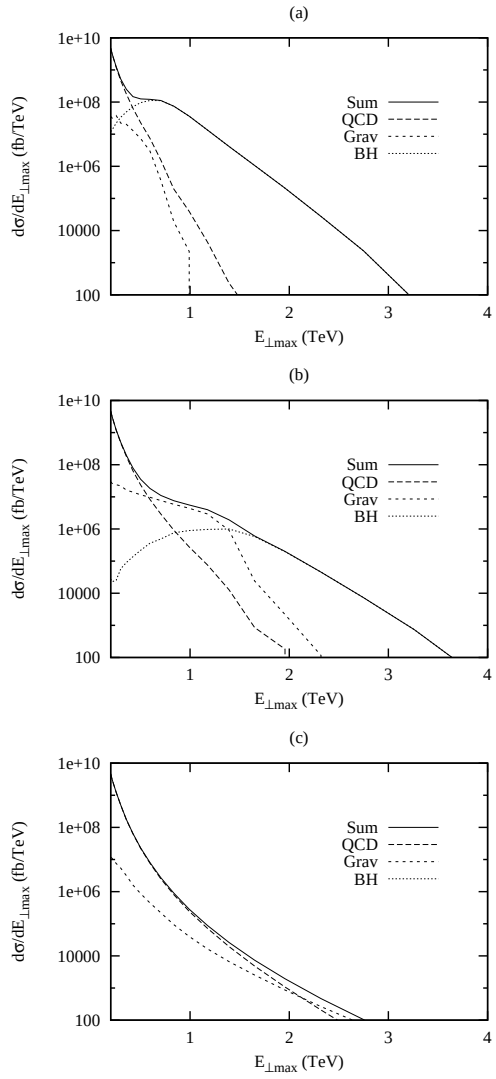

Figure 6.6: The same as fig. 6.4a, but with $M_s/M_{\rm P} = 1$ (a), 4 (b) and 0.5 (c).

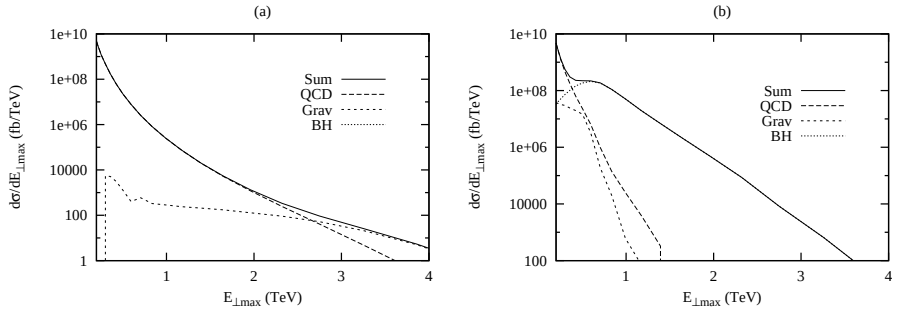

Figure 6.7: The same as fig. 6.4a, but with (a) 4 extra dimensions, $M_{\rm eff} = 4$ TeV, $M_s/M_{\rm P} = 4$ and (b) 6 extra dimensions, $M_{\rm eff} = 1$ TeV, $M_s/M_{\rm P} = 2$.

dominating the cross section further out in $E_\perp$ as compared to fig. 6.4a. In fig. 6.6c we decrease the ratio even further to 0.5 which results in a brane thickness so large that black holes can never be formed at the LHC, and the only indication of the presence of extra dimensions in the $E_\perp$-spectrum is a slight increase in the cross section for large $E_{\perp\rm max}$.

A similar effect can be obtained by increasing the effective mass, while keeping the ratio M_s/M_p fixed, hence increasing both $M_{\rm P}$ and M_s. This is done in fig. 6.7a and, again, the only visible effect of the extra dimensions is from gravitational scattering in the high-$E_\perp$ region. On the other hand we see in fig. 6.7b how increasing the number of extra dimensions to 6, keeping $M_{\rm eff} = 1$ TeV, gives a negligible contribution from gravitational scattering to the $E_{\perp\rm max}$-distribution, which instead is completely dominated by the decay of black holes.

If large extra dimensions exist, one would hope that the scales are such that they would be easily discovered at the LHC by, eg. the striking signature of a decaying black hole. However, it is easy to see how nature could conspire, such that the only signal would be a slight increase of the high-$E_\perp$ jet cross section. There are, of course, other signals, such as the production of real gravitons, showing up as large missing transverse momenta. But such signals could also be the result of other possible beyond-the-standard-model scenarios. In any case, it would be desirable to be able to distinguish gravitational scatterings from standard QCD events. One obvious difference is that the exchange of a graviton is colorless in contrast to a QCD scattering. This will necessarily give rise to a different color topology in gravitational events as compared to QCD ones. In particular one would expect the appearance of so-called rapidity gaps between the jets in gravitational scattering events. Although these gaps may be filled by secondary soft and semi-hard QCD scatterings, one may still expect a lower activity between the jets in such events.

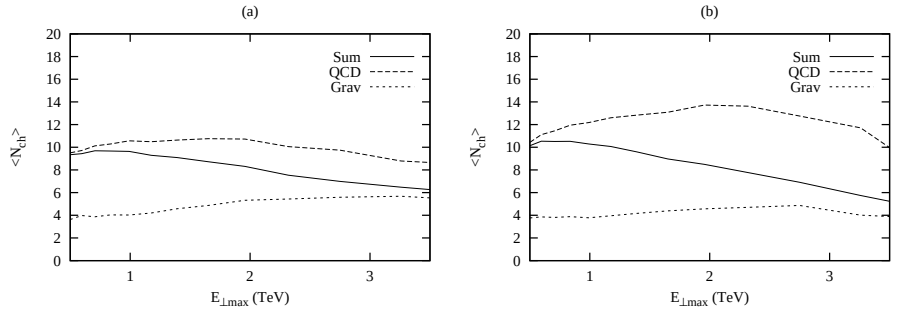

Figure 6.8: The average number of charged particles outside the jet-cones in the central rapidity unit between the two hardest jets in events corresponding to fig. 6.6c. The full line is for all events while the long-dashed and short-dashed are for QCD and gravitational scatterings respectively. In (b) only events with a minimum pseudo-rapidity difference of one unit between the two highest $E_\perp$ jets are included, while in (a) there is no such requirement.

In fig. 6.8a we show the average number of charged particles with a transverse momentum above 0.5 GeV outside the jet cones in the middle unit of pseudo-rapidity between the two hardest jets as a function of $E_{\perp\max}$. Hence, we count only charged particles, c, with

$$\begin{aligned} p_{\perp c} &> 0.5 \text{ GeV}, \\ \Delta R_{c1}, \Delta R_{c2} &> 0.7 \text{ and} \\ \left| \eta_c - \frac{\eta_1 + \eta_2}{2} \right| &< 0.5, \end{aligned} \tag{6.26}$$

where η_c and η_i are the pseudo rapidities of the particle and (the center of) jet i respectively and ΔR_{ci} is the distance between the particle and jet i in the pseudo-rapidity–azimuth-angle (η, ϕ) plane. In this simulation we have included multiple interactions in PYTHIA to simulate the underlying event.[3] We see that the expectation from QCD events is around 10 particles, while for gravitational scatterings the average is around 5. With sufficient statistics it could therefore be possible to observe the decrease in the number of charge particles with increasing $E_{\perp\max}$ as gravitational scatterings starts to dominate. In fig. 6.8a we have not required a large rapidity separation between the jets. Doing so would increase the effect, as shown in fig. 6.8b, but on the other hand the statistics would decrease.

We note that the absolute numbers in fig. 6.8 is very sensitive to the modeling of the underlying event, which is very difficult to predict for the LHC. The

[3]Using parameter settings according to the so-called Tune-A by Rick Field [34].

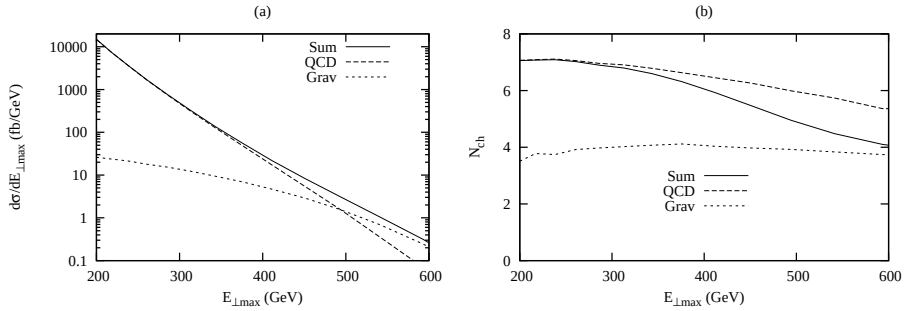

Figure 6.9: (a) The $E_\perp$-spectrum of the highest $E_\perp$ jet in an event, and (b) The average number of charged particles outside the jet-cones in the central rapidity unit between the two hardest jets at the Tevatron for $M_{\rm eff} = 700$ GeV, $M_s/M_{\rm P} = 4$ and 4 extra dimensions. The full line is for all event while the long-dashed and short-dashed are for QCD and gravitational scatterings respectively.

underlying event should, however, give the same contribution to both scattering types, and the difference between the two should be fairly well predicted by PYTHIA.

At the Tevatron there was an indication of an excess of the cross section for very high $E_\perp$ jets as compared to the QCD prediction [35, 36]. Although a re-evaluation of the uncertainties due to the parton density parameterizations used in the QCD calculations has brought this excess within the limits of the statistical and systematical errors, it is still intriguing that such an excess could be the signal of the onset of gravitational scattering due to the presence of large extra dimensions.

In fig. 6.9a we show our prediction for the $E_{\perp\rm max}$ distribution for $n = 4$, $M_{\rm eff} = 700$ GeV and $M_s/M_{\rm P} = 4$ at the Tevatron. The parameters were chosen so that the excess above standard QCD production is approximately within the statistical and systematical uncertainties of the corresponding Tevatron measurement. In fig. 6.9b we then show the average number of charged particles outside the cones (same as in fig. 6.8, but counting charged particles with transverse momenta down to 0.25 GeV). The decrease in the region where gravitational scatterings become important is significant, although it may be difficult to get enough statistics to measure it even for Run-II at the Tevatron. However, it is not completely inconceivable that by finding a more sensitive observable of the color structure, we could be able to see the first indication of large extra dimensions already at the Tevatron, before LHC is switched on.

6.6 Conclusions

We have studied gravitational scattering and black hole production at the LHC and the Tevatron in the ADD scenario assuming that brane on which the standard model fields live have a finite width. We found that the relative importance of gravitational scattering and black hole production is sensitive to this width, and that for large widths the extension of the standard model particle fields into the bulk, may prevent black holes from forming since the energy may not be sufficiently localized within the black hole radius.

A wide brane corresponds to a low cut-off for virtual Kaluza–Klein modes (the brane width and the KK cut-off, M_s, are inversely related via a Fourier transform [9]) and therefore results in weaker gravitational interaction in the non-classical regions. It is thus possible for nature to conspire, by choosing a low M_s, such that neither much gravitational scattering or black holes is observed at the LHC. In this case processes involving the production of on-shell KK modes resulting in missing $E_\perp$ may become important observables.

In our simulations we have used values of $M_{\rm P}$, M_s and the number of extra dimensions, n, which we believe have not yet been excluded by experiments (see eg. [37, 38] for recent reviews). Most of these limits are only relevant to $M_{\rm P}$ but restrictions on M_s could be obtained by considering processes involving both virtual and real KK modes.

In the case of low M_s, only a weak increase in the jet spectra could be observed at LHC, and the signal of missing $E_\perp$ could be the result of SUSY. We point out that the colorless nature of gravitational scattering could be a way of distinguishing gravity induced events from other beyond-standard-model extensions. In fact this method could be used to indicate if an excess of jet activity at high transverse energies at the Tevatron is a result of gravitational scattering.

6.A Appendix

There are at least four definitions of the Planck mass. Often one have to understand which definition an author uses by the relation of the Planck mass to the 4-dimensional Newton's constant $G_{N(4)}$ or to the Schwarzschild radius of a black hole. The process of hunting down constants is further complicated by the use of different definitions of the compactification radius, many authors [10] mean by the compactification radius rather the compactification circumference, here denoted L, whereas others really mean the radius, $R = L/(2\pi)$. In order to simplify comparison between the different conventions we here state the relations between the Planck masses $M_{\rm P}$ (used here) and in [33], M_D used in [11, 15], M_G, M_S used in [10] and the 4-dimensional Newton's constant $G_{N(4)}$, the relation between the Planck masses and Schwarzschild radius, and

the relations of the Planck masses to each other.

$$M_D^{2+n} = \frac{1}{8\pi R^n G_{N(4)}} \tag{6.27}$$

$$M_{\rm P}^{2+n} = \frac{1}{L^n G_{N(4)}} \tag{6.28}$$

$$M_G^{2+n} = \frac{2^{n-2}\pi^{n-1}}{L^n G_{N(4)}} \tag{6.29}$$

$$M_S^{2+n} = \frac{\Gamma\left(\frac{n}{2}\right)\pi^{n/2}}{2^{1-n}L^n G_{N(4)}} \tag{6.30}$$

$$r_{\rm Sch} = \frac{1}{M_D}\left[\frac{M_{BH}}{M_D}\right]^{\frac{1}{n+1}}\left[\frac{2^n\pi^{\frac{n-3}{2}}\Gamma\left(\frac{n+3}{2}\right)}{n+2}\right]^{\frac{1}{n+1}} \tag{6.31}$$

$$r_{\rm Sch} = \frac{1}{\sqrt{\pi}M_{\rm P}}\left[\frac{M_{BH}}{M_{\rm P}}\right]^{\frac{1}{n+1}}\left[\frac{8\Gamma\left(\frac{n+3}{2}\right)}{n+2}\right]^{\frac{1}{n+1}} \tag{6.32}$$

$$r_{\rm Sch} = \frac{2}{M_G}\left[\frac{M_{BH}}{M_G}\right]^{\frac{1}{n+1}}\left[\frac{\pi^{\frac{n-3}{2}}\Gamma\left(\frac{n+3}{2}\right)}{n+2}\right]^{\frac{1}{n+1}} \tag{6.33}$$

$$r_{\rm Sch} = \frac{1}{M_S}\left[\frac{M_{BH}}{M_S}\right]^{\frac{1}{n+1}}\left[\frac{2^{2+n}\Gamma\left(\frac{n+3}{2}\right)\Gamma\left(\frac{n}{2}\right)}{\sqrt{\pi}(n+2)}\right]^{\frac{1}{n+1}} \tag{6.34}$$

$$\begin{aligned} M_{\rm P} &= 2^{\frac{3-n}{2+n}}\pi^{\frac{1-n}{2+n}}M_D \\ &= 2^{\frac{2-n}{2+n}}\pi^{\frac{1-n}{2+n}}M_G \\ &= 2^{\frac{1-n}{2+n}}\pi^{\frac{-n}{4+2n}}\Gamma\left(\frac{n}{2}\right)^{\frac{-1}{2+n}}M_S \end{aligned} \tag{6.35}$$

References

[1] N. Arkani-Hamed, S. Dimopoulos, and G. R. Dvali *Phys. Lett.* **B429** (1998) 263–272, hep-ph/9803315.

[2] N. Arkani-Hamed, S. Dimopoulos, and G. R. Dvali *Phys. Rev.* **D59** (1999) 086004, hep-ph/9807344.

[3] I. Antoniadis, N. Arkani-Hamed, S. Dimopoulos, and G. R. Dvali *Phys. Lett.* **B436** (1998) 257–263, hep-ph/9804398.

[4] R. Emparan, G. T. Horowitz, and R. C. Myers *Phys. Rev. Lett.* **85** (2000) 499–502, hep-th/0003118.

[5] S. Dimopoulos and G. Landsberg *Phys. Rev. Lett.* **87** (2001) 161602, hep-ph/0106295.

[6] S. B. Giddings and S. Thomas *Phys. Rev.* **D65** (2002) 056010, hep-ph/0106219.

[7] P. Kanti *Int. J. Mod. Phys.* **A19** (2004) 4899–4951, hep-ph/0402168.

[8] L. Lönnblad, M. Sjodahl, and T. Akesson *JHEP* **09** (2005) 019, hep-ph/0505181.

[9] M. Sjodahl and G. Gustafson hep-ph/0608080.

[10] T. Han, J. D. Lykken, and R.-J. Zhang *Phys. Rev.* **D59** (1999) 105006, hep-ph/9811350.

[11] G. F. Giudice, R. Rattazzi, and J. D. Wells *Nucl. Phys.* **B544** (1999) 3–38, hep-ph/9811291.

[12] M. Sjodahl hep-ph/0602138.

[13] M. Bando, T. Kugo, T. Noguchi, and K. Yoshioka *Phys. Rev. Lett.* **83** (1999) 3601–3604, hep-ph/9906549.

[14] T. Kugo and K. Yoshioka *Nucl. Phys.* **B594** (2001) 301–328, hep-ph/9912496.

[15] G. F. Giudice, R. Rattazzi, and J. D. Wells *Nucl. Phys.* **B630** (2002) 293–325, hep-ph/0112161.

[16] L. D. Landau and E. M. Lifshitz. BERLIN, GERMANY: AKADEMIE-VERL. (1974).

[17] D. Atwood, S. Bar-Shalom, and A. Soni *Phys. Rev.* **D62** (2000) 056008, hep-ph/9911231.

[18] R. C. Myers and M. J. Perry *Ann. Phys.* **172** (1986) 304.

[19] H. Yoshino and Y. Nambu *Phys. Rev.* **D67** (2003) 024009, gr-qc/0209003.

[20] H. Yoshino and V. S. Rychkov hep-th/0503171.

[21] C. M. Harris *et al.* hep-ph/0411022.

[22] S. B. Giddings and V. S. Rychkov *Phys. Rev.* **D70** (2004) 104026, hep-th/0409131.

[23] V. S. Rychkov hep-th/0410041.

[24] V. P. Frolov, D. V. Fursaev, and D. Stojkovic *JHEP* **06** (2004) 057, gr-qc/0403002.

[25] V. P. Frolov, D. V. Fursaev, and D. Stojkovic *Class. Quant. Grav.* **21** (2004) 3483–3498, gr-qc/0403054.

[26] D. N. Page *Phys. Rev.* **D16** (1977) 2402–2411.

[27] V. P. Frolov and D. Stojkovic *Phys. Rev. Lett* **89** (2002) 151302, hep-th/0208102.

[28] V. P. Frolov and D. Stojkovic *Phys. Rev.* **D66** (2002) 084002, hep-th/0206046.

[29] S. W. Hawking *Commun. Math. Phys.* **43** (1975) 199–220.

[30] T. Sjöstrand, L. Lönnblad, and S. Mrenna, "PYTHIA 6.2: Physics and manual," arXiv:hep-ph/0108264.

[31] G. F. Giudice, T. Plehn, and A. Strumia *Nucl. Phys.* **B706** (2005) 455–483, hep-ph/0408320.

[32] T. Sjostrand and M. van Zijl *Phys. Rev.* **D36** (1987) 2019.

[33] C. M. Harris, P. Richardson, and B. R. Webber *JHEP* **08** (2003) 033, hep-ph/0307305.

[34] R. Field, "Min-Bias and the Underlying Event at the Tevatron and the LHC." http://www.phys.ufl.edu/∼rfield/cdf/FNAL_Workshop_10-4-02.pdf. Talk presented at the Fermilab ME/MC Tuning Workshop, October 4, 2002.

[35] **CDF** Collaboration, F. Abe *et al. Phys. Rev. Lett.* **77** (1996) 438–443, hep-ex/9601008.

[36] **CDF** Collaboration, A. A. Affolder *et al. Phys. Rev.* **D64** (2001) 032001, hep-ph/0102074.

[37] W.-M. Yao *et al. Journal of Physics G* **33** (2006) 1.

[38] **CDF** Collaboration, A. Abulencia *et al.* hep-ex/0605101.